UNIVERSITY OF GOTHENBURG

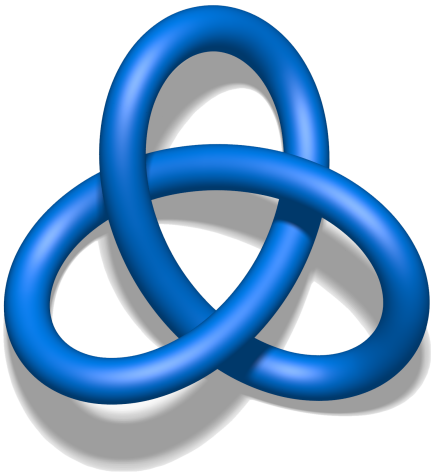

Topological Band Theory, An Overview

Theoretical Physics Master Thesis

Author:
Jens Roderus

Supervisor:
Mariana Malard

Department of Physics
UNIVERSITY OF GOTHENBURG
Gothenburg, Sweden, 2018

Abstract

Topological insulators, superconductors and semi-metals are states of matter with unique features such as quantized macroscopic observables and robust, gapless edge states. These states can not be explained by standard quantum mechanics, but require also the framework of topology to be properly characterized. Topology is a branch of mathematics having to do with properties that are conserved under continuous deformations of spaces. This review presents some of the ways in which topology and condensed matter physics come together, with a focus on non-interacting models which can be described with a band theory approach. Furthermore, the focus is on insulating systems but the discussions may sometimes be applied to superconductors and semi-metals. The field of topological phases of matter is not all together new, yet it lacks elementary introductions to newcomers. This review is meant for those with basic condensed matter physics background and aims at providing a self-consistent overview of the central concepts in the field of topological matter.

The structure of the review is as follows: In Chapter 1, a brief historical background is given. Also, a basic introduction to topology is presented, with focus on how it is used in condensed matter physics. Following this, Chapter 2 introduces three important discrete symmetries which are key in characterizing topological phases of matter. In particular, the effect that these symmetries have on a general Bloch Hamiltonian is shown. In Chapter 3, the effect of discrete symmetries on certain models is investigated. The well-known Su-Schrieffer-Heeger model is discussed because it is the simplest models known to exhibit a topological phase and a topological invariant. Chapter 4 broadens the discussion of this topological invariant which is a winding number. Chapter 5 introduces the geometric phase (Berry phase) which is used to describe another topological invariant, the Chern number, the subject of Chapter 6. There the alternative interpretations of the Chern number are discussed. Afterwards, in Chapter 7, the quantum Hall effect is presented. Following this, a general classification scheme for topological phases of fermionic, non-interacting systems will be presented in Chapter 8. It will be shown how it can be determined whether a system could possibly host a topological phase or not based on the symmetries of the Hamiltonian. Chapter 9 focuses on the concepts pertaining to the physics of the gapless edge states which appear between the interface of a (non-interacting) topological insulator and a topologically trivially insulator. Among the concepts discussed here is the bulk-boundary correspondence and topological protection. Lastly, Chapter 10 contains a brief recap of what has been established in the review and some conclusionary remarks.

Acknowledgements

It has been somewhat of a dream come true for me to have been able to take on such an inspiring master's project. I would like to express my sincere appreciation to my supervisor, Mariana Malard, who was immediately on board with this project. She taught me countless things in this subject with which I was previously unfamiliar. Together we tackled numerous questions by many fruitful discussions. Under her guidance I was able to grow as scientist and to fully immerse myself into the subject.

I also want to thank the people at the *Soliden* building of Chalmers university who are working with topology. Thank you for letting me ask questions and keep a conversation.

My warmest thank you goes out to my former class mates who I kept dialogues with during the project. Lastly I want to thank my family and relatives.

Contents

1 What is a Topological Phase?

One of the most fundamental goals in condensed matter physics is the characterization of states of matter. Topological insulators, superconductors and semi-metals are phases of matter with unique properties. Contrary to phases of matter which may be described within the framework of Landau's theory, topological materials can not be characterized only with symmetries and an order parameter; they require concepts of topology. Before going into the proper description of such phases in later chapters, a brief historical introduction is given and the basic notions of topology and its role in condensed matter physics is presented.

1.1 Historical Introduction

In 1980, von Klitzing *et al.* [1] discovered the *quantum Hall effect* (see Chapter 7). They measured a quantized conductivity (Hall conductivity) in units of fundamental constants e^2/h, with e being the elementary charge and h being Planck's constant. The effect was measured in a two-dimensional electron system at very low temperatures with a strong external magnetic field and a transverse electric field. The remarkable thing about the measurements is that they are independent of the geometry and imperfections of the sample, a general property of topological insulators. The quantization has been confirmed [2] with an uncertainty of 3.3 parts in 10^9. The robustness of measurements to such a degree was unprecedented. Amongst other things, this allowed for an experimental determination of constants of nature to a remarkable accuracy.

The quantized Hall conductivity had been theorized [3] a few years earlier, in 1974, by Ando and Uemura. In 1982, Thouless, Kohomoto, Nightingale and den Nijs (TKNN) recognized (with the help of Barry Simon) the phenomenon as topological in addition to quantum mechanical. The integer appearing in the Hall conductivity was shown to be a *topological invariant*, namely a *Chern number* (see Chapter 6). The Chern number that appears in the quantum Hall effect is often referred to as the *TKNN-invariant*. Following these events, it was shown by Halperin in 1982 [4] that the quantum Hall sheet hosts chiral (moving in one direction), gapless edge states at the interface between the sample and a vacuum, while the bulk remains insulating. It holds for all topological insulators that they have insulating bulks and conducting edges. Remarkably, the existence of the gapless edge modes can be characterized by topological invariants defined in the bulk. This is an example of the *bulk-boundary correspondence*, to be discussed in Chapter 9.

In 2016, half of the Nobel Prize in physics was awarded [5] to David Thouless, with the other half shared between Duncan Haldane and Michael Kosterlitz, for their contributions to the theoretical understanding of the interplay between topology and condensed matter physics.

The implications of these findings were manifold. The quantum Hall state corresponds to a new state of matter which is not characterized by the classical Landau paradigm of symmetry breaking. Classically, the properties of a system are governed by conservation laws and symmetries. For example, under the freezing of a liquid, the continuous translation invariance is broken, forming a solid with only discrete translation invariance. A more sophisticated example is given by a ferromagnet. Suppose that a two-dimensional model is described by spins arranged on a square lattice. In a paramagnetic phase, the spins are oriented randomly and this is characterized by a vanishing net magnetization and rotational symmetry. Upon lowering the temperature to a critical value, the paramagnet undergoes a phase transition into a ferromagnetic state where all spins are aligned parallel to each other. The net magnetization, which is an example of an order parameter, is non-zero and the rotational symmetry is broken. The change in symmetry and the order parameter signals a phase transition. The experimental verification of the quantum Hall effect exposed the incompleteness of the Landau paradigm because the associated phase transitions were not characterized by a change in symmetries or order parameters. Phase transitions like those occurring in the quantum Hall effect are instead topological in nature, hence the name *topological phase transition*.

A non-interacting topological phase always hosts gapless boundary modes which are robust against perturbations that preserve the minimal defining properties of the phase. This will be discussed more in-

depth in Chapter 9. The robustness of these states are experimentally interesting in many areas of research, like quantum computation. Essentially, what a quantum computer does is perform unitary transformations on a quantum state and measure the output. During this process, the noise level must be kept under a certain threshold. This task would be greatly facilitated if one could exploit the robustness of topologically protected states. Topological states of matter also has implications for spintronics. In the absence of a magnetic field, the *spin quantum Hall effect* hosts two different conducting channels at a given edge. The channels are spin separated such that spin up particles move in one direction and spin down particles move in the opposite direction. The spin quantum Hall effect was proposed [6, 7] by Kane and Mele in 2005. The proposal included a suggested model to realize the effect which was a graphene model with spin-orbit coupling. The spins are essentially locked to the momentum by the spin-orbit coupling. It turned out to be difficult to realize the spin quantum Hall effect in graphene due to the weak spin-orbit coupling. Shortly after, Bernevig, Hughes and Zhang predicted that the spin quantum Hall effect could be realized in HgTe quantum wells [8]. This was confirmed experimentally [9] by König *et al.* in 2007. It was theoretically understood at the time that the spin quantum Hall effect was a different type of topological phase from the quantum Hall effect because it was known to be characterized by a $\mathbb{Z}_2$-topological invariant. Meaning it could only take on two values, contrary to the Chern number which can theoretically take on any integer value.

Around the same time, people were extending the ideas to three-dimensional systems. Fu and Kane [10] predicted in 2006 that the $\mathrm{Bi}_{1-x}\mathrm{Sb}_x$ alloy was a three dimensional topological insulator. This was confirmed using angle-resolved photoemission spectroscopy of the surface states by Hsieh *et al.* [11] in 2008.

On a separate timeline the theory of topological superconductors had an interesting development in 1999 when Read and Green [12] considered such phases in two dimensions. At the same time Kitaev [13] considered a one-dimensional model of topological superconductors. Both models were spinless, break time reversal and host *Majorana zero modes* (see Section 9.3.1). One way to experimentally confirm topological superconductivity is to confirm the existence of Majorana zero modes, which, due to a number of experimental difficulties, has not yet been done without the shadow of a doubt.

The original discoveries of the quantum Hall effect and the spin quantum Hall effect triggered a surge of research in this new field of topological phases of matter. Following all these discoveries are more, topologically non-trivial findings, such as the *fractional quantum Hall effect.* For free systems, there is a classification scheme that allows one to predetermine whether a system could exhibit topologically non-trivial phases, see Chapter 8. Interacting systems are generally not as well understood due to the lack of classification and the difficulties of describing many-body interactions and greater experimental difficulties.

This review aims at providing a self-consistent and coherent overview of the basic theory of the field of topological matter, with a strict focus on non-interacting systems. Anyone who wishes to complement this review with a more widespread coverage of topics, including interacting systems[1], is referred to the book on quantum matter and quantum computations by T. D. Stanescu [14].

1.2 What is Topology?

It is often the case that there is a rich mathematical structure underlying the physical concepts that arise in the description of topological phases. Yet, some concepts can be explained by simpler physical reasoning. For example, the Chern invariant is described mathematically in the language of *fiber bundles* [15]. However, it can be understood physically in terms of the Berry phase. Likewise, the Berry phase is known mathematically as a holonomy [15]. But it is physically more favourable to interpret it as the overlap of neighbouring states (see Section 5.2.1). In this review, the physical interpretations are favoured and the mathematical underlying concepts are hinted towards.

[1]Interacting systems are not part of this review. To not leave the reader out in the cold a brief overview of topological phases of interacting systems is given in Appendix C. Pedagogically, this appendix is best read at the end of the review.

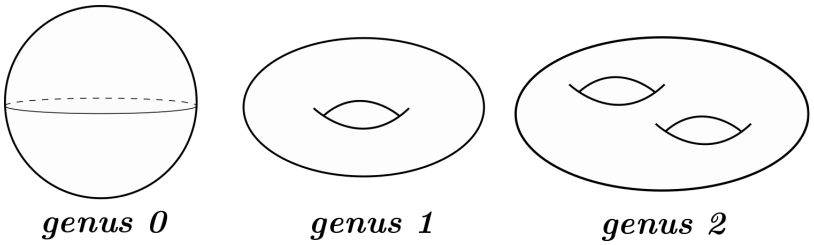

Figure 1.1: The genus of a surface is the number of holes it has and it can not be changed by a continuous deformation. Therefore the three surfaces in this figure are topologically inequivalent.

1.2.1 Topology in Mathematics

When delving deeper into the subject of topological phases, the mathematics become evermore important. With this in mind, a basic overview of the concepts of topology is given in this section. For a complete review of the mathematical concepts of topology which are relevant for physicists see [15].

Topology is the study of properties of objects which remain invariant under continuous deformations, that is, deformations where no cutting or tearing is allowed. For example, the number of holes, referred to as the *genus*, of a surface is a topological invariant, see Figure 1.1. A topological invariant is something that does not change under continuous deformations. To be more precise, the objects that are being deformed are *topological spaces*, which are defined out of open sets of some space. An open set in Euclidian 1-space, $\mathbb{R}$, is (a, b) as opposed to the closed set $[a, b]$.

Definition 1.1 (Topological space) *Let T be a collection of subsets of a set X. The pair (X, T) is a topological space if (1) The empty set, $\emptyset$ and X are in T; (2) Any union of elements from T is in T; (3) Any finite intersection of elements from T is in T*[2].

The collection T is referred to as a topology on the set X. An example of a topological space is given by $X_e = \{a, b, c, d\}$ and $T_e = \{a, b, \{a, b\}, \emptyset, X\}$. It is straightforward to confirm that (X_e, T_e) fulfills the conditions (1)-(3) in definition 1.1.

Next one would like to establish a way of determining whether there is an equivalence between different topological spaces. Consider two topological spaces (X_1, T_1) and (X_2, T_2), a function f between these topological spaces $f : X_1 \to X_2$, is *continuous* if for any open subset $O_2 \subset X_2$ the inverse image, $f^{-1}(O_2) \subset X_1$ is an open subset of X_1. A continuous function f with a continuous inverse is said to be a *homeomorphism* if it is a continuous *bijection* (one to one and onto) between X_1 and X_2. Any two topological spaces with a homemorphism are said to be homeomorphic and topologically equivalent. The homeomorphism preserves the topological structure (for example, topological invariants remain the same) [14] and defines an equivalence relation[3]. The resulting equivalence classes are comprised of all homeomorphic topological spaces.

From this one can go on to define objects such as fiber bundles in order to describe Chern numbers. However, because the focus of this review is on physical interpretations there is no need to go much deeper into the mathematical details of topology.

[2]There are different definitions of a topological space, for example, it can be constructed out of neighbourhoods [16].

[3]An equivalence relation between elements of a set is at the same time reflexive ($a = a$), symmetric ($a = b \Leftrightarrow b = a$) and transitive ($a = b,\ b = c \Rightarrow a = c$). All equivalent elements of a set, denoted by $\equiv$, belong to the same equivalence class. Hence if the elements of the set $X = \{a, b, c, d, e\}$ fulfill, $a \equiv b \equiv c \not\equiv d,\ d \equiv e$, then the set X has two equivalence classes $\{a, b, c\}$ and $\{d, e\}$.

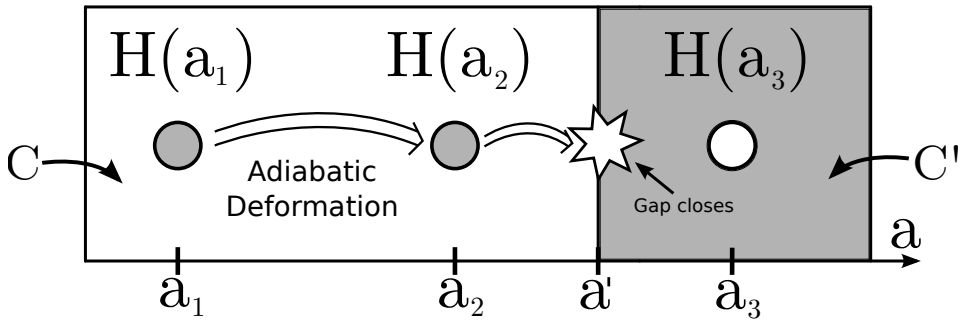

Figure 1.2: Phase diagram of a fictitious model. The parameter a of a Hamiltonian $H(a)$ can be adiabatically deformed from a_1 to a_2 thus connecting the Hamiltonians $H(a_1)$ with $H(a_2)$ which are then topologically equivalent. At $a = a'$ the band gap closes and thus no adiabatic deformation can go past a'. The system described by $H(a_3)$ is recognized as in a distinct topological phase from $H(a_1)$ or $H(a_2)$ and is therefore characterized by a different value of the topological invariant (C' and C respectively) of the model.

1.2.2 Topology in Physics

To characterize different phases of physical systems one must establish how to determine whether two systems are equivalent or not. The Hamiltonian of a system fully characterizes energy eigenstates and energy eigenvalues and hence it is said that, *if a Hamiltonian can be continuously deformed into another Hamiltonian by a deformation of its parameters, then the Hamiltonians are equivalent.* Importantly, it is assumed that the spectrum is gapped and the continuous deformation must never close this gap. The parameters of a Hamiltonian are for example hopping amplitudes and chemical potential and sometimes degrees of freedom like momentum can be considered parameters as well. Furthermore, the deformation may not change the symmetries of the Hamiltonian. With these constraints the continuous deformation is known as an *adiabatic deformation.* The details of adiabatic deformations will be discussed in Section 5.1.

The adiabatic deformations define an equivalence relation and the resulting equivalence classes are identified as topological phases. Loosely speaking, a phase of matter refers to a system with a distinct set of physical properties. Indeed, the topological phases as defined by these equivalence classes exhibit unusual physical properties like robust, gapless edge modes (see Chapter 9).

To distinguish between the different topological phases one defines topological invariants which are by construction known not to change under adiabatic deformations, see Figure 1.2. These topological invariants must be defined over the whole system and what is typically done is that all momentum degrees of freedom are integrated or summed over. Examples of such topological invariants are winding numbers (Chapter 4) or Chern numbers (Chapter 6). If, for a given Hamiltonian, it is possible to find different values of a topological invariant, in different regions of parameter space, then the model has different *topological phases* and the Hamiltonians describing the different phases can not be adiabatically deformed into one another.

Before constructing topological invariants in the later chapters, an introduction to the symmetries which must be preserved under adiabatic deformations is given.

2 The Symmetries S, T and C

Whether or not a system exhibits topological properties is largely dependent on the discrete symmetries of the system. There are three discrete symmetries of fundamental importance, *chiral symmetry* or *sublattice symmetry*, *time reversal symmetry* and *particle-hole symmetry*. This chapter introduces these discrete symmetries and the outcome of the first three sections is the effect that the symmetries have on the *Bloch Hamiltonian*, which is used to find the single-particle energies of a given system.

In the many-body language of *second quantization*, where the Hamiltonian, $\mathscr{H}$, is written in terms of creation and annihilation operators that act on a many-body Fock space, the three discrete operations are symmetries if they commute with the Hamiltonian [17, 18]

$$[\mathscr{S}, \mathscr{H}] = [\mathscr{T}, \mathscr{H}] = [\mathscr{C}, \mathscr{H}] = 0.$$

Here the symmetry operators that act on the second quantized Hamiltonian are given by $\mathscr{S}$ for chiral symmetry, $\mathscr{T}$ for time reversal symmetry and $\mathscr{C}$ for particle-hole symmetry. The Hamiltonian matrix $\mathcal{H}(k)$ with matrix elements $\mathcal{H}_{ij}(k)$ is defined for a non-interacting many-body theory by

$$\mathscr{H} = \sum_{k,i,j} c^\dagger_{k,i} \mathcal{H}_{ij}(k) c_{k,j}, \tag{2.1}$$

in terms of creation operators $c^\dagger_{k,i}$ and annihilation operators $c_{k,i}$ which create and remove particles with momentum k and internal degrees of freedom i respectively. $\mathcal{H}(k)$ *is known as the Bloch Hamiltonian* and it fully characterizes the single-particle energies of a non-interacting system which are obtained upon diagonalization. It is assumed that the system has translation invariant position degrees of freedom which have been Fourier transformed into momentum k. The creation and annihilation operators obey the *fundamental commutation relations* of whatever particle they describe. In this review, electrons are described on a translation invariant lattice. Electrons are fermions and thus the fundamental (anti)commutation relations are

$$\{c^\dagger_n, c^\dagger_m\} = 0, \tag{2.2a}$$
$$\{c_n, c_m\} = 0, \tag{2.2b}$$
$$\{c_n, c^\dagger_m\} = \delta_{nm}, \tag{2.2c}$$

for any type of indices n, m.

A non-interacting many-body Hamiltonian is the sum of single-particle Hamiltonians

$$\mathscr{H} = \sum_{n=1}^{N} H_n, \tag{2.3}$$

where N is the number of particles in the system. From the theory of second quantization it is known that the matrix elements in Eq. (2.1) are those of a single particle

$$\mathcal{H}_{ij}(k) = \langle k, i | H | k, j \rangle ,$$

where $|k, i\rangle$ is a single-particle state. The following notation is kept throughout the review

$$\begin{aligned}
\mathscr{H} &= \sum_{k,i,j} c^\dagger_{k,i} \mathcal{H}_{ij}(k) c_{k,j} \Rightarrow \text{Second quantized, many-body Hamiltonian operator,} \\
H &= \sum_{k,i,j} |k,i\rangle \, \mathcal{H}_{ij}(k) \, \langle k,j| \Rightarrow \text{Single-particle Hamiltonian operator,} \\
\mathcal{H}(k) &= \text{matrix with elements } \mathcal{H}_{ij}(k) \Rightarrow \text{Single-particle Hamiltonian matrix (Bloch Hamiltonian).}
\end{aligned} \tag{2.4}$$

The matrix elements of the second quantized Hamiltonian $\mathscr{H}$ and the single-particle Hamiltonian operator H of Eq. (2.4) are the same even though the operators are fundamentally different. The second quantized operator acts on a multi-particle Fock state while the single-particle operator acts on a single-particle state.

It is noted that single-particle operators do not necessarily obey the same invariance relations as the second quantized operators, see [17, 18] or Appendix A. In fact the single-particle chiral operator and the single-particle particle-hole operator anticommute with the single-particle Hamiltonian. The reason for this difference arises from the fact that the symmetry operations act non-trivially on the creation and annihilation operators which are present only in the second quantized Hamiltonian. In this chapter the focus is on single-particle operators because it provides an elementary way of finding the restriction imposed on the Bloch Hamiltonian and in turn, the spectrum of the system.

2.1 Chiral Symmetry S

If a system can be divided into two subsystems with no interactions or hoppings (bonds) within each subsystem, then the system has a *chiral symmetry*. As an example, consider a one dimensional lattice with two lattice sites per unit cell, call them A and B. The full chain is made up of a number of unit cells lying next to each other so that any A site, is surrounded by two B sites and vice versa. Including only hopping between adjacent lattice sites A and B (a nearest neighbour approximation) would make the system chiral symmetric where the subsystems in this case are the two sublattices made of A- and B-sites. Hence the alternative name *sublattice symmetry*.

2.1.1 Projection Operator

The chiral operator is best understood in terms of the *projection operator*

$$P_X = \sum_k \sum_{i \in X} |k,i\rangle \, \langle k,i| \, . \tag{2.5}$$

This is not the *identity operator* because the sum on i is over one subspace X, of the full Hilbert space. If the system is divided into two subsystems A and B, then $P_A + P_B$ becomes the resolution of identity. It is assumed that both subsystems are equally large, with r internal degrees of freedom making up each subsystems. Then all base kets can be assembled into a $2r-$dimensional *bipartite spinor*

$$|k\rangle = \Big(\underbrace{|k,1\rangle \ldots |k,r\rangle}_{\in A}, \underbrace{|k,r+1\rangle \ldots |k,2r\rangle}_{\in B} \Big) \, , \tag{2.6}$$

with the first r entries in Eq. (2.6) belonging to subsystem A and the remaining r entries belong to subsystem B. This spinor basis will be referred to as the *chiral basis*. These subsystems could be sublattices, or a spin up and spin down partition or some other partition that divides the Hilbert space in two equally big subspaces. The treatment here is general and the details of what makes up the subsystems are not specified.

Throughout this text, single-particle operators are denoted by M and their corresponding matrix representations are $\mathcal{M}$. An arbitrary operator can be written in terms of its matrix elements according to

$$M = \sum_{k,k',i,j} |k,i\rangle \, \mathcal{M}_{ij}(k,k') \, \langle k',j| \,, \text{ with } \mathcal{M}_{ij}(k,k') = \langle k,i|M|k',j\rangle$$

as was seen for the single-particle Hamiltonian operator in Eq. (2.4), with the latter being diagonal in k due to translation invariance. This is nothing other than inserting two resolutions of identity. The projection operator can thus be written

$$P_{A/B} = \sum_{k,k',i,j} |k,i\rangle \, \langle k,i| \, P_{A/B} \, |k',j\rangle \, \langle k',j| = \sum_{k,k',i,j} |k,i\rangle \, (\mathcal{P}_{A/B})_{ij}(k,k') \, \langle k',j| \,, \tag{2.7}$$

where A/B means A or B. The matrix elements are found by using Eq. (2.5),

$$(\mathcal{P}_{A/B})_{ij}(k,k') = \langle k,i| \, P_{A/B} \, |k',j\rangle = \sum_{q,l\in A/B} \langle k,i|q,l\rangle \, \langle q,l|k',j\rangle = \sum_{q,l\in A/B} \delta_{kq}\delta_{k'q}\delta_{il}\delta_{jl}.$$

The elements are independent of momentum and thus become

$$(\mathcal{P}_{A/B})_{ij} = \begin{cases} \delta_{ij}, & i \in A/B \\ 0, & \text{otherwise} \end{cases} \,. \tag{2.8}$$

The matrix $\mathcal{P}_{A/B}$ with matrix elements $(\mathcal{P}_{A/B})_{ij}$ is the matrix representation of the projection operator in the chiral basis. In this way, the ijth entry of the matrix $\mathcal{P}_{A/B}$ corresponds to the coefficient of $|k,i\rangle \, \langle k,j|$ in $P_{A/B}$. From Eqs. (2.6) and (2.8) the matrices are found to be

$$\mathcal{P}_A = \left(\begin{array}{c|c} \mathbb{1} & 0 \\ \hline 0 & 0 \end{array}\right)_{2r\times 2r}, \quad \mathcal{P}_B = \left(\begin{array}{c|c} 0 & 0 \\ \hline 0 & \mathbb{1} \end{array}\right)_{2r\times 2r}. \tag{2.9}$$

By using the matrix representation and the bipartite spinors Eq. (2.6) the projection operator can be expressed as

$$P_{A/B} = \sum_k |k\rangle \, \mathcal{P}_{A/B} \, \langle k| \,. \tag{2.10}$$

In the chiral basis, Eq. (2.6), the single-particle Hamiltonian operator becomes

$$H = \sum_k |k\rangle \, \mathcal{H}(k) \, \langle k| \,, \tag{2.11}$$

where $\mathcal{H}(k)$ is the Bloch Hamiltonian (matrix) with elements $\mathcal{H}_{ij}(k) = \langle k,i|H|k,j\rangle$.

For a generic Bloch Hamiltonian it holds that

$$\mathcal{H}(k) = \mathcal{P}_A\mathcal{H}(k)\mathcal{P}_A + \mathcal{P}_A\mathcal{H}(k)\mathcal{P}_B + \mathcal{P}_B\mathcal{H}(k)\mathcal{P}_A + \mathcal{P}_B\mathcal{H}(k)\mathcal{P}_B. \tag{2.12}$$

This can be seen by computing the following matrix element

$$[\mathcal{P}_{A/B}\mathcal{H}(k)\mathcal{P}_{A'/B'}]_{ij} = [\mathcal{P}_{A/B}\mathcal{H}(k)]_{il}[\mathcal{P}_{A'/B'}]_{lj} = \begin{cases} [\mathcal{P}_{A/B}\mathcal{H}(k)]_{ij}, & j \in A'/B' \\ 0, & \text{otherwise} \end{cases} \,,$$

where Eq. (2.8) was used and repeated indices are summed. Note that the second projection operator is labeled by A'/B' such that it can be either $\mathcal{P}_A$ or $\mathcal{P}_B$ independently of what the first projector is chosen to be. Using Eq. (2.8) once more, it is found that

$$[\mathcal{P}_{A/B}\mathcal{H}(k)\mathcal{P}_{A'/B'}]_{ij} = \begin{cases} \mathcal{H}_{ij}(k), & i \in A/B \text{ and } j \in A'/B' \\ 0, & \text{otherwise} \end{cases} . \tag{2.13}$$

This statement validates Eq. (2.12).

Consider now instead a chiral symmetric Hamiltonian. As defined before, chiral symmetry implies that there exists two subsystems, A and B, without any bonds inside themselves, i.e.,

$$\mathcal{H}_{ij}(k) = 0 \quad \text{if } i, j \in A \text{ or } i, j \in B.$$

A chiral symmetric Bloch Hamiltonian is off-diagonal in the chiral basis. Using Eq. (2.13), it follows that $\mathcal{P}_A\mathcal{H}(k)\mathcal{P}_A = \mathcal{P}_B\mathcal{H}(k)\mathcal{P}_B = 0$ and thus, Eq. (2.12) becomes

$$\mathcal{H}(k) = \mathcal{P}_A\mathcal{H}(k)\mathcal{P}_B + \mathcal{P}_B\mathcal{H}(k)\mathcal{P}_A. \tag{2.14}$$

With this understanding of the projection operator, the chiral operator can now be defined.

2.1.2 Chiral Operator

The chiral operator is defined as the *difference between the projections on the two subsystems* [19],

$$S = P_A - P_B. \tag{2.15}$$

Writing that

$$S = \sum_k |k\rangle \, \mathcal{S} \, \langle k| \tag{2.16}$$

and applying Eqs. (2.10) and (2.15) it follows that

$$\mathcal{S} = \mathcal{P}_A - \mathcal{P}_B = \sigma_z \otimes \mathbb{1}_{r\times r}, \tag{2.17}$$

where the last equality comes from Eq. (2.9). The matrix σ_z is the third Pauli matrix[4]. The chiral symmetry operator is trivially Hermitian because projectors are Hermitian. It is also equal to its inverse. To see this, first note that

$$P_{A/B}^2 = \sum_k \sum_{i\in A/B} \sum_{k'} \sum_{i'\in A/B} |k,i\rangle \langle k,i|k',i'\rangle \langle k',i'| = \sum_k \sum_{i\in A/B} |k,i\rangle \langle k,i| = P_{A/B}.$$

Secondly,

$$P_A P_B = \sum_k \sum_{i\in A} \sum_{k'} \sum_{i'\in B} |k,i\rangle \langle k,i|k',i'\rangle \langle k',i'| = 0$$

since the overlap $\langle k,i|k',i'\rangle$, with $i \in A$ and $i' \in B$, is zero because the two subsystems are disjoint. Generally then

$$P_A P_B = P_B P_A = 0.$$

[4]The Pauli matrices are given by $\sigma_x = \begin{pmatrix} 0 & 1 \\ 1 & 0 \end{pmatrix}$, $\sigma_y = \begin{pmatrix} 0 & -i \\ i & 0 \end{pmatrix}$, $\sigma_z = \begin{pmatrix} 1 & 0 \\ 0 & -1 \end{pmatrix}$. They are often accompanied by a fourth matrix, $\sigma_0 = \begin{pmatrix} 1 & 0 \\ 0 & 1 \end{pmatrix}$, the 2×2 identity.

Therefore

$$S^2 = P_A^2 + P_B^2 - P_A P_B - P_B P_A = P_A + P_B = \mathbb{1}_{2r\times 2r} = SS^{-1},$$

which implies that $S = S^{-1}$. Summarizing,

$$S = S^\dagger = S^{-1}. \tag{2.18}$$

These properties are alike for the matrix $\mathcal{S}$.

A general Bloch Hamiltonian is transformed by the chiral operator according to

$$\mathcal{S}\mathcal{H}(k)\mathcal{S}^{-1} = \mathcal{P}_A\mathcal{H}(k)\mathcal{P}_A + \mathcal{P}_B\mathcal{H}(k)\mathcal{P}_B - \mathcal{P}_A\mathcal{H}(k)\mathcal{P}_B - \mathcal{P}_B\mathcal{H}(k)\mathcal{P}_A, \tag{2.19}$$

where Eqs. (2.17) and (2.18) for the matrices were used. Consider instead a chiral symmetric Bloch Hamiltonian, for which $\mathcal{P}_A\mathcal{H}(k)\mathcal{P}_A = \mathcal{P}_B\mathcal{H}(k)\mathcal{P}_B = 0$. Then

$$\mathcal{S}\mathcal{H}(k)\mathcal{S}^{-1} = -\mathcal{P}_A\mathcal{H}(k)\mathcal{P}_B - \mathcal{P}_B\mathcal{H}(k)\mathcal{P}_A.$$

Rewriting this with Eq. (2.14) it is found that

$$\boxed{\mathcal{S}\mathcal{H}(k)\mathcal{S}^{-1} = -\mathcal{H}(k).} \tag{2.20}$$

A system is chiral symmetric if it obeys Eq. (2.20) with a chiral matrix $\mathcal{S}$ defined by Eq. (2.17) in the chiral basis.

Chiral symmetry is not a conventional symmetry because its existence is dependent on how the subsystems are defined. It is possible to define two subsystems within which there exists bonds. Then that particular chiral symmetry is not present. Conventional symmetries do not possess such an ambiguity. Nevertheless, chiral symmetry is still referred to as a symmetry in most, if not all literature and will be done so throughout this text as well. To find the invariance relation of the single-particle operators compute SHS^{-1} with Eqs. (2.11) and (2.16)

$$SHS^{-1} = \sum_{kk'k''} |k\rangle\, \mathcal{S}\, \langle k|k'\rangle\, \mathcal{H}(k')\, \langle k'|k''\rangle\, \mathcal{S}^{-1}\, \langle k''| = \sum_{kk'k''} |k\rangle\, \mathcal{S}\mathcal{H}(k')\mathcal{S}^{-1}\, \langle k''|\, \delta_{kk'}\delta_{k'k''} =$$

$$= \sum_k |k\rangle\, \mathcal{S}\mathcal{H}(k)\mathcal{S}^{-1}\, \langle k|\,,$$

applying Eq. (2.20),

$$SHS^{-1} = -\sum_k |k\rangle\, \mathcal{H}(k)\, \langle k| = -H.$$

Therefore

$$\{S, H\} = 0. \tag{2.21}$$

The single-particle chiral operator anticommutes with the single-particle Hamiltonian.

Chiral symmetry may have a great effect on the topological properties of a system. This will be discussed in Section 3.3 on the Su-Schrieffer-Heeger model.

2.2 Time Reversal Symmetry T

Time reversal is the operation which causes a system to evolve backwards in time. Whether or not time reversal is an appropriate name is a debated topic [20]. What is universally agreed upon is how it is implemented and what it does. The time reversal operator T reverses the sign for momentum-like quantities

and does nothing to position i.e. $T\hat{p}T^{-1} = -\hat{p}$ and $T\hat{x}T^{-1} = \hat{x}$. Furthermore, it reverses the sign of spin, due to its angular momentum-like behaviour, $T\hat{S}T^{-1} = -\hat{S}$. Time reversal symmetry remains a conventional symmetry for single-particle Hamiltonians in the sense that a system is said to be time reversal invariant if its single-particle Hamiltonian commutes with T,

$$[T, H] = 0. \tag{2.22}$$

Eq. (2.22) is consistent with the results found in appendix A. Properties of the time reversal operator depends on the number of particles in the system and their statistics.

2.2.1 Time Reversal Operator

Wigner's theorem states that any symmetry of a physically relevant Hamiltonian must be either *unitary* or *antiunitary* [21]. The theorem is based on the conservation of expectation values of observables. A transformation is said to be antiunitary if it obeys Eqs. (2.23a) and (2.23b),

$$\langle\psi_\alpha|\psi_\beta\rangle \to (\langle\psi_\alpha|\psi_\beta\rangle)^*, \qquad \text{(complex conjugation of inner product)} \tag{2.23a}$$

$$a\,|\psi_\alpha\rangle + b\,|\psi_\beta\rangle \to a^*\,|\psi'_\alpha\rangle + b^*\,|\psi'_\beta\rangle\,. \qquad \text{(antilinearity)} \tag{2.23b}$$

A simple argument shows the antilinearity of T. The *fundamental commutation relations* are

$$\hat{x}\hat{p} - \hat{p}\hat{x} = i\hbar.$$

Transforming this with the time reversal operator

$$Ti\hbar T^{-1} = T\hat{x}T^{-1}T\hat{p}T^{-1} - T\hat{p}T^{-1}T\hat{x}T^{-1} = -(\hat{x}\hat{p} - \hat{p}\hat{x}) = -i\hbar.$$

This is precisely the antilinearity property Eq. (2.23b). Because an operator can not be antilinear and unitary at the same time, T must be antiunitary. For a more rigorous proof of the antiunitarity property of T, see [20].

Being antiunitary, the time reversal operator can be implemented [22] in the form

$$T = UK, \tag{2.24}$$

where U is a unitary operator and K is the *complex conjugation operation.* Note that $K^2 = 1$, $K^\dagger = K$. Furthermore, K reverses the sign of momentum and does nothing to position, as is required by T. This can be understood because $\hat{p} = -i\hbar\partial_x$ and $\hat{x} = x$. The complex conjugation operator does not have a matrix representation[5]. T acts on a state according to $T\,|\psi_\alpha\rangle = U\,|\psi^*_\alpha\rangle$. Thus Eq. (2.23a) is fulfilled,

$$\langle\psi_\alpha|\psi_\beta\rangle \to \langle\psi_\alpha|T^\dagger T|\psi_\beta\rangle = \langle\psi^*_\alpha|U^\dagger U|\psi^*_\beta\rangle = (\langle\psi_\alpha|\psi_\beta\rangle)^*.$$

It is also antilinear, as in Eq. (2.23b),

$$a\,|\psi_\alpha\rangle + b\,|\psi_\beta\rangle \to UK(a\,|\psi_\alpha\rangle + b\,|\psi_\beta\rangle) = a^*UK\,|\psi_\alpha\rangle + b^*UK\,|\psi_\beta\rangle = a^*\,|\psi'_\alpha\rangle + b^*\,|\psi'_\beta\rangle\,.$$

Applying the time reversal symmetry operation twice must give back the same physical state, up to a non-measurable constant,

$$T^2 = \alpha \cdot \mathbb{1}, \tag{2.25}$$

[5]This is not completely true. The complex conjugation operator can be given a matrix representation [14], however, it is often treated as a non-trivial operator for practical purposes.

where the constant alpha obeys $|\alpha|^2 = 1$. In this way α can be written as a phase factor $\alpha = e^{i\theta}$. Taking the square of Eq. (2.24) and equating it with Eq. (2.25),

$$T^2 = UKUK = UU^*K^2 = UU^* = \alpha \cdot \mathbb{1}.$$

It can be deduced that

$$U^* = \alpha U^\dagger = \alpha (U^*)^T = \alpha (\alpha U^\dagger)^T = \alpha^2 U^*,$$

which requires $\alpha = \pm 1$ and when substituting back into Eq. (2.25),

$$T^2 = \pm 1. \tag{2.26}$$

The value of T^2 is related to the physical properties of the system, as is discussed below. Using Eq. (2.24) the single-particle operator is found by inserting identities

$$T = \sum_{k,k',i,j} |k,i\rangle \langle k,i| T |k',j\rangle \langle k',j| = \sum_{k,k',i,j} |k,i\rangle \langle k,i| U |-k',j\rangle \langle -k',j| K.$$

The sum over k' can be redefined to remove the minus sign

$$T = \sum_{k,k',i,j} |k,i\rangle \langle k,i| U |k',j\rangle \langle k',j| K.$$

It is noted that the only way time reversal impacts momentum is by a flip of sign which is carried out by the complex conjugator and therefore U does nothing to momentum,

$$T = \sum_{k,k',i,j} |k,i\rangle \langle k|k'\rangle \langle i| U |j\rangle \langle k',j| K = \sum_{k,i,j} |k,i\rangle \langle i| U |j\rangle \langle k,j| K \equiv \sum_{k,i,j} |k,i\rangle \mathcal{T}_{ij} \langle k,j| K.$$

From the matrix elements

$$\mathcal{T}_{ij} = \langle i| U |j\rangle \tag{2.27}$$

the matrix $\mathcal{T}$ is constructed and in a given spinor representation $|k\rangle$, the time reversal operator is given by

$$T = \sum_k |k\rangle \mathcal{T} \langle k| K. \tag{2.28}$$

One now computes

$$THT^{-1} = \sum_{k,k',k''} |k\rangle \mathcal{T} \langle k| K |k'\rangle \mathcal{H}(k') \langle k'|K|k''\rangle \mathcal{T}^{-1} \langle k''| =$$

$$= \sum_{k,k',k''} |k\rangle \mathcal{T} \langle k| - k'\rangle \mathcal{H}^*(k') \langle -k'|k''\rangle \mathcal{T}^{-1} \langle k''| = \sum_k |k\rangle \mathcal{T}\mathcal{H}^*(-k)\mathcal{T}^{-1} \langle k| .$$

Because H is invariant Eq. (2.22), $THT^{-1} = H$ holds and therefore

$$\sum_k |k\rangle \mathcal{T}\mathcal{H}^*(-k)\mathcal{T}^{-1} \langle k| = \sum_k |k\rangle \mathcal{H}(k) \langle k| ,$$

which gives the important result

$$\boxed{\mathcal{T}\mathcal{H}^*(-k)\mathcal{T}^{-1} = \mathcal{H}(k).} \tag{2.29}$$

This is the invariance relation for any time reversal symmetric system's Bloch Hamiltonian.

The form of $\mathcal{T}$ is presented here for spin-1/2 and spinless particles. It was stated that spin changes sign under time reversal. This can be represented by a rotation with π about some axis which is chosen to be the y-axis by convention. The *single-particle* time reversal operator Eq. (2.24) takes the form

$$T = e^{-i\pi \hat{S}_y/\hbar} K,$$

where $\hat{S}_y$ is the y-direction spin operator, which for spin-1/2 takes the form $\hat{S}_y = \hbar\hat{\sigma}_y/2$. The full power series expansion can be evaluated because $(-i\hat{\sigma}_y)^2 = -\mathbb{1}$,

$$e^{-i\pi\hat{\sigma}_y/2} = \sum_{n=0}^{\infty} \frac{\left(-i\pi\hat{\sigma}_y/2\right)^n}{n!} = \cos\left(\frac{\pi}{2}\right)\begin{pmatrix}1 & 0\\ 0 & 1\end{pmatrix} + \sin\left(\frac{\pi}{2}\right)\begin{pmatrix}0 & -1\\ 1 & 0\end{pmatrix} = -i\hat{\sigma}_y.$$

Thus, for a spin-1/2 particle, Eq. (2.24) takes the form

$$T = -i\hat{\sigma}_y K. \tag{2.30}$$

The squared time reversal operator becomes

$$T^2 = -i\hat{\sigma}_y i\hat{\sigma}_y^* KK = -\mathbb{1}. \tag{2.31}$$

Therefore the single-particle time reversal operator is minus its own inverse

$$T = -T^{-1}. \tag{2.32}$$

Consider a time reversal symmetric, spinful Hamiltonian, describing a system with $2r$ internal degrees of freedom. The time reversal operator can also be written in terms of bipartite spinors

$$T = \sum_k |k\rangle \mathcal{T} \langle k| K, \tag{2.33}$$

where

$$\mathcal{T} = -i\sigma_y \otimes \mathbb{1}_{r\times r}. \tag{2.34}$$

Here the bipartite spinors are chosen to be sorted in terms of spin, which is different from the chiral basis Eq. (2.6), this is referred to as the *spin basis* of the spinors

$$|k\rangle = \left(|k,1,+\rangle \ldots |k,r,+\rangle, |k,1,-\rangle \ldots |k,r,-\rangle\right). \tag{2.35}$$

In this way, the operator Eq. (2.33), with matrix representation Eq. (2.34), acts on a $2r$-dimensional state vector, $(-i\sigma_y)$ acts on spin degrees of freedom performing a spin flip and $\mathbb{1}_{r\times r}$ acts trivially on the remaining internal degrees of freedom.

Consider now spinless systems. Effective spinless systems, where the spin of all particles are aligned can be realized experimentally by spin polarization techniques, or alternatively by strong spin-orbit coupling [14]. For spinless systems the time reversal operator, $T = UK$ is given by $U = \mathbb{1}$, the complex conjugation changes the sign of momentum and there is no other degree of freedom to be influenced by the time reversal. It follows that T squares to unity and by the discussion of the complex conjugation operator in the previous section it follows that $T = T^\dagger = T^{-1}$.

2.2.2 Kramers' Theorem

Recall that T is a single-particle operator. For a system of n, non-interacting spin-1/2 particles the many-body time reversal operator $\mathscr{T}$ acts upon a state according to

$$\mathscr{T}\left(\left|k,i,\sigma\right\rangle_1 \otimes \left|k,i,\sigma\right\rangle_2 \ldots \otimes \left|k,i,\sigma\right\rangle_n\right) = T\left|k,i,\sigma\right\rangle_1 \otimes T\left|k,i,\sigma\right\rangle_2 \ldots \otimes T\left|k,i,\sigma\right\rangle_n .$$

As a result, $\mathscr{T}^2 = -1$ only if the system has an odd number of fermions, otherwise $\mathscr{T}^2 = 1$. If $\mathscr{T}^2 = -1$, then the spectrum of a time reversal symmetric model attains a property that is summarized in *Kramers' theorem*,

Theorem 2.1 (Kramers' theorem) *In a time reversal symmetric, spinful system where $\mathscr{T}^2 = -1$, all energy levels are (at least) doubly degenerate.*

To prove this theorem it must first be established that $\left|\Psi\right\rangle$ and $\mathscr{T}\left|\Psi\right\rangle$ are different eigenstates of $\mathscr{H}$. Assume the opposite, namely that the states are equivalent, then

$$\mathscr{T}\left|\Psi\right\rangle = e^{i\phi}\left|\Psi\right\rangle .$$

This would imply that

$$\mathscr{T}^2\left|\Psi\right\rangle = \mathscr{T}e^{i\phi}\left|\Psi\right\rangle = e^{-i\phi}\mathscr{T}\left|\Psi\right\rangle = e^{-i\phi+i\phi}\left|\Psi\right\rangle = \left|\Psi\right\rangle .$$

From which it follows that $\mathscr{T}^2 = 1$, contrary to the requirement. Thus $\left|\Psi\right\rangle$ and $\mathscr{T}\left|\Psi\right\rangle$ are different states. With $\mathscr{H}\left|\Psi\right\rangle = E\left|\Psi\right\rangle$ and $[\mathscr{T},\mathscr{H}] = 0$ it can be concluded that

$$\mathscr{H}\mathscr{T}\left|\Psi\right\rangle = \mathscr{T}\mathscr{H}\left|\Psi\right\rangle = E\mathscr{T}\left|\Psi\right\rangle ,$$

such that both $\left|\Psi\right\rangle$ and $\mathscr{T}\left|\Psi\right\rangle$ are different eigenstates of $\mathscr{H}$ with the same energy. Therefore the system is (at least) doubly degenerate. Furthermore it is noted that $\mathscr{T}\left|\Psi(k)\right\rangle$ is an eigenstate with momentum $-k$. Therefore the states $\left|\Psi(k)\right\rangle$ and $\mathscr{T}\left|\Psi(k)\right\rangle$ have the same energy but opposite momenta and the spectrum is symmetric under inversion of the energy axis (flipping the sign of momentum). It follows that every energy level has a symmetric partner in the other half of the Brillouin zone. At the so called *time reversal invariant momenta* $k = \pm\pi, 0$ the energy levels must meet with its symmetric partner and they are glued together at these points. This is because $k = 0$ is mapped to $k = -0 = 0$ by time reversal and likewise $k = \pi$ is mapped to $k = -\pi$ which is identified as the same point in the Brillouin zone. In this way a given energy level and its symmetric partner has the same energy and momentum at these points and therefore they meet.

2.3 Particle-Hole Symmetry C

A third symmetry known to influence topological properties is *particle-hole symmetry* or *charge conjugation symmetry.* A particle occupying a state of energy E is equivalent to a hole occupying a state with energy $-E$. This property will be reflected in the spectrum of particle-hole invariant models. The single-particle Hamiltonian is therefore symmetric under the particle-hole transformation, C, if it fulfills

$$\{C, H\} = 0. \tag{2.36}$$

Eq. (2.36) is consistent with the results found in appendix A.

2.3.1 Particle-Hole Operator

The particle-hole operator is, just like the time reversal operator, antiunitary. This can be understood because it can be interpreted as a charge conjugator. Because of this the operation should change the sign of terms like $ie\mathbf{A}$, which appears in a minimal coupling Hamiltonian [23]. The particle-hole operator thus fulfills antilinearity Eq. (2.23b), and by Wigner's theorem the particle-hole operator is antiunitary and can be written in the form Eq. (2.24), namely $C = UK$. By the same arguments as for time reversal symmetry, this implies

$$C^2 = \pm 1.$$

As discussed in [14], whenever a system exhibits time reversal and particle-hole symmetry, chiral symmetry is automatically present. Even more generally, whenever two out of the three symmetries are present, all three symmetries are present. This will be discussed later on in Chapter 8. *The three symmetries are related* [14] *by*

$$S = TC. \tag{2.37}$$

Having already discussed chiral symmetry and time reversal symmetry, it becomes effective to study particle hole symmetry in the form

$$C = T^{-1}S. \tag{2.38}$$

Caution must be taken because T^{-1} is different for spinful and spinless systems. To find the matrix representation of C, apply Eqs. (2.16) and (2.33),

$$C = T^{-1}S = \sum_{k,k'} K\left|k\right\rangle \mathcal{T}^{-1}\left\langle k|k'\right\rangle \mathcal{S}\left\langle k'\right| = \sum_{k} K\left|k\right\rangle \mathcal{T}^{-1}\mathcal{S}\left\langle k\right| = \sum_{k} \left|-k\right\rangle \mathcal{T}^{-1}\mathcal{S}\left\langle -k\right| K.$$

Redefine the sum over k and find

$$C = \sum_{k} \left|k\right\rangle \mathcal{C}\left\langle k\right| K \tag{2.39}$$

with

$$\mathcal{C} = \mathcal{T}^{-1}\mathcal{S}. \tag{2.40}$$

One now computes

$$\begin{aligned} CHC^{-1} &= \sum_{k,k',k''} \left|k\right\rangle \mathcal{C}\left\langle k\right| K\left|k'\right\rangle \mathcal{H}(k')\left\langle k'|K|k''\right\rangle \mathcal{C}^{-1}\left\langle k''\right| = \\ &= \sum_{k,k',k''} \left|k\right\rangle \mathcal{C}\left\langle k\right| - k'\right\rangle \mathcal{H}^{*}(k')\left\langle -k'|k''\right\rangle \mathcal{C}^{-1}\left\langle k''\right| = \sum_{k} \left|k\right\rangle \mathcal{C}\mathcal{H}^{*}(-k)\mathcal{C}^{-1}\left\langle k\right|. \end{aligned} \tag{2.41}$$

Then by Eq. (2.36) this implies

$$CHC^{-1} = \sum_{k} \left|k\right\rangle \mathcal{C}\mathcal{H}^{*}(-k)\mathcal{C}^{-1}\left\langle k\right| = -H = -\sum_{k} \left|k\right\rangle \mathcal{H}(k)\left\langle k\right|.$$

The invariance relation for the Bloch Hamiltonian under particle-hole symmetry becomes

$$\boxed{\mathcal{C}\mathcal{H}^{*}(-k)\mathcal{C}^{-1} = -\mathcal{H}(k).} \tag{2.42}$$

It can be shown explicitly that particle-hole is a symmetry when chiral and time reversal are symmetries of the Hamiltonian. The starting point is Eq. (2.41) with $\mathcal{C}$ given by Eq. (2.40),

$$CHC^{-1} = \sum_{k} \left|k\right\rangle \mathcal{T}^{-1}\mathcal{S}\mathcal{H}^{*}(-k)\mathcal{S}^{-1}\mathcal{T}\left\langle k\right|.$$

Using Eq. (2.20),

$$CHC^{-1} = -\sum_k |k\rangle \mathcal{T}^{-1}\mathcal{H}^*(-k)\mathcal{T} \langle k| .$$

Further by applying Eq. (2.29) it is found that

$$CHC^{-1} = -\sum_k |k\rangle \mathcal{H}(k) \langle k| = -H, \tag{2.43}$$

in agreement with Eq. (2.36).

What is the $\mathcal{C}$ matrix for spin-1/2 and spinless particles? To construct the matrix $\mathcal{C}$ in a spinful system with arbitrary many internal degrees of freedom, S and T must be written in the same basis. Remember that chiral symmetry was discussed using the chiral basis Eq. (2.6), where the spin index is was taken to be alternating at every entry, and time reversal symmetry was discussed in the spin basis Eq. (2.35). To summarize,

$$|k\rangle = \big(|k, i_1, +\rangle , |k, i_1, -\rangle \dots |k, i_r, +\rangle , |k, r_1, -\rangle \big), \qquad \text{(Chiral basis)} \tag{2.44a}$$

$$|k\rangle = \big(|k, i_1, +\rangle \dots |k, i_r, +\rangle , |k, i_1, -\rangle \dots |k, r_1, -\rangle \big). \qquad \text{(Spin basis)} \tag{2.44b}$$

Choosing to work in the chiral basis means that $\mathcal{S}$ becomes Eq. (2.17), namely $\mathcal{S} = \sigma_z \otimes \mathbb{1}_{r\times r}$. Time reversal symmetry $\mathcal{T}$ becomes

$$\mathcal{T} = \mathbb{1}_{r\times r} \otimes (-i\sigma_y).$$

The matrix $\mathcal{C}$ is different depending on how many internal degrees of freedom the system has. This is because when multiplying

$$\mathcal{T}^{-1} = -\mathcal{T} = \mathbb{1}_{r\times r} \otimes (i\sigma_y) = \begin{cases} i\sigma_y, & r = 1 \\ \mathbb{1}_{2\times 2} \otimes \mathbb{1}_{\frac{r}{2}\times\frac{r}{2}} \otimes (i\sigma_y), & r \geq 2 \end{cases} \tag{2.45}$$

and

$$\mathcal{S} = \sigma_z \otimes \mathbb{1}_{r\times r} = \begin{cases} \sigma_z, & r = 1 \\ \sigma_z \otimes \mathbb{1}_{\frac{r}{2}\times\frac{r}{2}} \otimes \mathbb{1}_{2\times 2}, & r \geq 2 \end{cases} \tag{2.46}$$

the $\mathcal{C}$ matrix given by Eq. (2.40) becomes

$$\mathcal{C} = \mathcal{T}^{-1}\mathcal{S} = \begin{cases} -\sigma_x, & r = 1 \\ \sigma_z \otimes \mathbb{1}_{\frac{r}{2}\times\frac{r}{2}} \otimes (i\sigma_y), & r \geq 2 \end{cases} \tag{2.47}$$

in the chiral basis.

For a spinless system the time reversal matrix is $\mathcal{T} = \mathbb{1}$ as discussed in the previous section. The particle-hole matrix reduces to Eq. (2.46),

$$\mathcal{C} = \sigma_z \otimes \mathbb{1}_{r\times r},$$

in the chiral basis.

Now that the three symmetries important for topological properties have been introduced, it is time to look closer at specific models. Later, in Chapter 8, Hamiltonians will be systematically characterized depending on the presence or absence of these symmetries.

3 Models of Interest

This section serves as an introduction to the type of models that could be of interest in condensed matter research or models which are simply instructive. The models considered are non-interacting and include only hopping and on-site potentials. Before considering a model with topologically non-trivial properties, namely the *Su-Schrieffer-Heeger* (SSH) *model*, a brief overview of more general tight binding models is given. Many naturally non-occurring models can be realized in the lab using ultracold quantum gases confined on an optical lattice [24]. In that sense, no toy model is irrelevant. The effect of the discrete symmetries, introduced in Section 2.1, on the band structure (spectrum) of these models is discussed.

3.1 Spinful Non-Interacting Tight Binding Two-Band Model

Tight-binding models [25] describe electrons on a discrete lattice that models the array of atoms in a crystal. The electrons are allowed to hop between different sites; this corresponds to kinetic energy of a continuum model modulated by the crystalline potential generated by the atomic nuclei. There is also an energy associated to each position on the lattice, an on-site potential. The tight-binding approximation corresponds to the limit of small overlap between atomic orbitals of neighbouring atoms on a lattice [14]. Here no superconducting pairing or electron-electron interaction is considered.

The most general, one-dimensional, spinful, tight binding two-band model with these restrictions is

$$\begin{aligned}\mathscr{H} = \sum_{m=1}^{N} \sum_{\sigma=+,-} \big(& \alpha c^\dagger_{m,\sigma} c_{m+1,\sigma} \quad + \beta\sigma c^\dagger_{m,\sigma} c_{m+1,\sigma} \\ & + \tilde{\alpha} c^\dagger_{m,\sigma} c_{m+1,-\sigma} + \tilde{\beta}\sigma c^\dagger_{m,\sigma} c_{m+1,-\sigma} \\ & + \mu' c^\dagger_{m,\sigma} c_{m,\sigma} \quad + \nu'\sigma c^\dagger_{m,\sigma} c_{m,\sigma} \\ & + \tilde{\mu}' c^\dagger_{m,\sigma} c_{m,-\sigma} \quad + \tilde{\nu}'\sigma c^\dagger_{m,\sigma} c_{m,-\sigma} \big) + h.c. \,, \quad (N+1=1),\end{aligned} \tag{3.1}$$

where $c^\dagger_{m,\sigma}$ $(c_{m,\sigma})$ creates (annihilates) fermions on lattice site m with spin σ and $h.c.$ denotes the Hermitian conjugate and periodic boundary conditions are employed by $N+1=1$. The model (Figure 3.1) and Eq. (3.1) describes spinful particles on a translation invariant chain of N lattice sites, being allowed to hop to neighbouring lattice sites $(c^\dagger_m c_{m+1})$ as well as to have an on-site potential $(c^\dagger_m c_m)$. The complex coefficients may be either *spin dependent* or *spin independent*. The hopping and on-site potentials are either *spin conserving* or *spin flipping*, the latter is indicated by a tilde on the coefficients.

To find the Bloch Hamiltonian, one must Fourier transform to momentum space. Due to the periodicity of the real space atomic lattice, momentum k is discretized. The discrete Fourier transformation of the

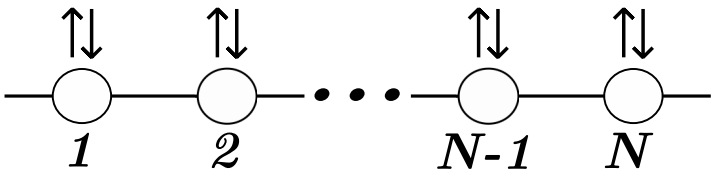

Figure 3.1: Illustration of the spinful, translation invariant, one-dimensional chain with N lattice sites. Straight lines represent hopping, circles represent the different sites and the arrows illustrate the internal spin degree of freedom.

creation and annihilation operators become[6]

$$c_m^\dagger = \frac{1}{\sqrt{N}} \sum_{k \in BZ} e^{-imk} c_k^\dagger, \tag{3.2a}$$

$$c_m = \frac{1}{\sqrt{N}} \sum_{k \in BZ} e^{imk} c_k. \tag{3.2b}$$

In the *first Brillouin zone* (BZ), the dimensionless momentum takes on the values

$$k = \pm \frac{2\pi n}{N},\ n = 1, 2 \ldots N/2. \tag{3.3}$$

Transforming Eq. (3.1) with Eqs. (3.2a) and (3.2b) gives,

$$\begin{aligned} \mathscr{H} = \frac{1}{N} \sum_{k \in BZ} \sum_{k' \in BZ} \sum_{m=1}^{N} \sum_{\sigma=+,-} \\ \Big(& \alpha e^{ik'} e^{im(k'-k)} c_{k,\sigma}^\dagger c_{k',\sigma} \quad + \beta\sigma e^{ik'} e^{im(k'-k)} c_{k,\sigma}^\dagger c_{k',\sigma} \\ & + \tilde{\alpha} e^{ik'} e^{im(k'-k)} c_{k,\sigma}^\dagger c_{k',-\sigma} + \tilde{\beta}\sigma e^{ik'} e^{im(k'-k)} c_{k,\sigma}^\dagger c_{k',-\sigma} \\ & + \mu' e^{im(k'-k)} c_{k,\sigma}^\dagger c_{k',\sigma} \quad + \nu'\sigma e^{im(k'-k)} c_{k,\sigma}^\dagger c_{k',\sigma} \\ & + \tilde{\mu}' e^{im(k'-k)} c_{k,\sigma}^\dagger c_{k',-\sigma} \quad + \tilde{\nu}'\sigma e^{im(k'-k)} c_{k,\sigma}^\dagger c_{k',-\sigma} \Big) + h.c.\ . \end{aligned} \tag{3.4}$$

This is vastly simplified by noting that

$$\{c_k^\dagger, c_{k'}\} = \frac{1}{N} \sum_{mm'} \{c_m^\dagger, c_{m'}\} e^{imk} e^{-im'k'}.$$

Applying Eq. (2.2c) on the right-hand side,

$$\{c_k^\dagger, c_{k'}\} = \frac{1}{N} \sum_{mm'} \delta_{mm'} e^{imk} e^{-im'k'} = \frac{1}{N} \sum_{m} e^{im(k-k')}.$$

Applying Eq. (2.2c) on the left-hand side,

$$\frac{1}{N} \sum_{m} e^{im(k-k')} = \delta_{kk'}. \tag{3.5}$$

Using Eq. (3.5) to rewrite Eq. (3.4) and letting the delta function remove the sum over k',

$$\begin{aligned} \mathscr{H} = \sum_{k,\sigma} \big(& \alpha e^{ik} c_{k,\sigma}^\dagger c_{k,\sigma} \quad + \beta\sigma e^{ik} c_{k,\sigma}^\dagger c_{k,\sigma} \\ & + \tilde{\alpha} e^{ik} c_{k,\sigma}^\dagger c_{k,-\sigma} + \tilde{\beta}\sigma e^{ik} c_{k,\sigma}^\dagger c_{k,-\sigma} \\ & + \mu' c_{k,\sigma}^\dagger c_{k,\sigma} \quad + \nu'\sigma c_{k,\sigma}^\dagger c_{k,\sigma} \\ & + \tilde{\mu}' c_{k,\sigma}^\dagger c_{k,-\sigma} \quad + \tilde{\nu}'\sigma c_{k,\sigma}^\dagger c_{k,-\sigma} \big) + h.c.\ , \end{aligned} \tag{3.6}$$

[6] It follows that $c_k = \frac{1}{\sqrt{N}} \sum_{m=1}^{N} e^{-imk} c_m$. $c_k^\dagger$ is simply given by the Hermitian conjugate.

where $\sum_{k\in 1BZ}\sum_{\sigma=+,-}$ was written as $\sum_{k,\sigma}$. Working out the $h.c.$ terms,

$$\begin{aligned}\mathscr{H} = \sum_{k,\sigma}\Big[&\big(\alpha e^{ik} + \alpha^* e^{-ik} + \beta\sigma e^{ik} + \beta^*\sigma e^{-ik} + \mu' + (\mu')^* + \nu'\sigma + (\nu')^*\sigma\big)c^\dagger_{k,\sigma}c_{k,\sigma} \\ &+\big(\tilde{\alpha}e^{ik} + \tilde{\alpha}^* e^{-ik} - \tilde{\beta}\sigma e^{ik} + \tilde{\beta}^*\sigma e^{-ik} + \tilde{\mu}' + (\tilde{\mu}')^* - \tilde{\nu}'\sigma + (\tilde{\nu}')^*\sigma\big)c^\dagger_{k,-\sigma}c_{k,\sigma}\Big].\end{aligned} \tag{3.7}$$

The Hamiltonian can be written in the form

$$\mathscr{H} = \sum_{k,\sigma,\sigma'} c^\dagger_{k,\sigma}\mathcal{H}_{\sigma\sigma'}(k)c_{k,\sigma'}, \tag{3.8}$$

when comparing with Eq. (3.7), $\mathcal{H}_{\sigma\sigma'}(k)$ is found to be

$$\begin{aligned}H_{\sigma\sigma'}(k) =&\big(\alpha e^{ik} + \alpha^* e^{-ik} + \beta\sigma e^{ik} + \beta^*\sigma e^{-ik} + \mu' + (\mu')^* + \nu'\sigma + (\nu')^*\sigma\big)\delta_{\sigma,\sigma'} \\ &+\big(\tilde{\alpha}e^{ik} + \tilde{\alpha}^* e^{-ik} - \tilde{\beta}\sigma e^{ik} + \tilde{\beta}^*\sigma e^{-ik} + \tilde{\mu}' + (\tilde{\mu}')^* - \tilde{\nu}'\sigma + (\tilde{\nu}')^*\sigma\big)\delta_{\sigma,-\sigma'}.\end{aligned}$$

Defining the spinor

$$c^\dagger_k \equiv \big(c^\dagger_{k,+},\ c^\dagger_{k,-}\big),$$

the Hamiltonian becomes

$$\mathscr{H} = \sum_k c^\dagger_k\mathcal{H}(k)c_k. \tag{3.9}$$

The Bloch Hamiltonian thus takes the form

$$\mathcal{H}(k) = \begin{pmatrix}\mathcal{H}_{++}(k) & \mathcal{H}_{+-}(k)\\ \mathcal{H}_{-+}(k) & \mathcal{H}_{--}(k)\end{pmatrix}. \tag{3.10}$$

To further simplify this it is preferable to write the Hamiltonian with purely real constants. To this end, define the following parameters

$$\begin{aligned} a &= 2Re\alpha, \quad b = -2Im\alpha,\\ c &= 2Re\beta, \quad d = -2Im\beta,\\ e &= 2Re\tilde{\alpha}, \quad f = -2Im\tilde{\alpha},\\ g &= 2Re\tilde{\beta}, \quad h = 2Im\tilde{\beta},\end{aligned} \tag{3.11}$$

and

$$\begin{aligned}\mu &= 2Re\mu', \quad \nu = 2Re\nu',\\ \tilde{\mu} &= 2Re\tilde{\mu}', \quad \tilde{\nu} = 2Im\tilde{\nu}'.\end{aligned}$$

These definitions are motivated by how the constants couple in the Hamiltonian. For example,

$$\begin{aligned}\alpha e^{ik} + \alpha^* e^{-ik} &= (\mathrm{Re}\alpha + i\mathrm{Im}\alpha)(\cos k + i\sin k) + (\mathrm{Re}\alpha - i\mathrm{Im}\alpha)(\cos k - i\sin k) = \\ &= 2\mathrm{Re}\alpha\cos k - 2\mathrm{Im}\alpha\sin k = a\cos k + b\sin k.\end{aligned}$$

Note that Hermicity already puts constraints on the on-site parameters $\mu, \tilde{\mu}, \nu$ and $\tilde{\nu}$ for the most general model. They do not enter in to the Hamiltonian with both a real and imaginary parts. By defining the functions

$$f_\sigma(k) = a\cos k + b\sin k + \mu + \sigma(c\cos k + d\sin k + \nu), \tag{3.12a}$$

$$g_\sigma(k) = e\cos k + f\sin k + \tilde{\mu} + i\sigma(g\sin k + h\cos k + \tilde{\nu}), \tag{3.12b}$$

the Bloch Hamiltonian Eq. (3.10) is given by

$$\mathcal{H}(k) = \begin{pmatrix} f_+(k) & g_+(k) \\ g_-(k) & f_-(k) \end{pmatrix}. \tag{3.13}$$

The Bloch Hamiltonian fully characterizes the single-particle spectrum of the system. It is straightforward to diagonalize Eq. (3.13) and find that the eigenenergies are given by

$$E_\pm = \frac{1}{2}\left(f_+ + f_- \pm \sqrt{(f_+ - f_-)^2 + 4g_+g_-} \right). \tag{3.14}$$

This is the energy spectrum of the model Eq. (3.1) when it is not subjected to any symmetry restrictions.

3.1.1 Symmetry Restrictions

In this section, it is shown how the terms of the Hamiltonian Eq. (3.1) are affected by the three symmetries S, T and C and what these restrictions imply for the energy spectrum.

Starting out with demanding the Hamiltonian to be chiral symmetric. This implies that the Hamiltonian obeys Eq. (2.20), namely, $\mathcal{S}\mathcal{H}(k)\mathcal{S}^{-1} = -\mathcal{H}(k)$. Let the chiral partition be made in terms of spin up and spin down subsystems. Writing S according to $S = P_A - P_B$ in the chiral basis Eq. (2.6), implies that $\mathcal{S} = \sigma_z$. To find the restrictions on $\mathcal{H}(k)$ compute

$$\mathcal{S}\mathcal{H}(k)\mathcal{S}^{-1} = \begin{pmatrix} 1 & 0 \\ 0 & -1 \end{pmatrix} \begin{pmatrix} f_+(k) & g_+(k) \\ g_-(k) & f_-(k) \end{pmatrix} \begin{pmatrix} 1 & 0 \\ 0 & -1 \end{pmatrix} = \begin{pmatrix} f_+(k) & -g_+(k) \\ -g_-(k) & f_-(k) \end{pmatrix}.$$

By Eq. (2.20) this is $-\mathcal{H}(k)$,

$$\begin{pmatrix} f_+(k) & -g_+(k) \\ -g_-(k) & f_-(k) \end{pmatrix} = \begin{pmatrix} -f_+(k) & -g_+(k) \\ -g_-(k) & -f_-(k) \end{pmatrix},$$

it follows that $f_+(k) = f_-(k) = 0$ and that the Hamiltonian is off-diagonal

$$\mathcal{H}(k) = \begin{pmatrix} 0 & g_+(k) \\ g_-(k) & 0 \end{pmatrix}. \tag{3.15}$$

This was expected because $f_\sigma(k)$ contains all spin conserving terms and the non-internally bonded subsystem was defined by spin. Thus, there must not exist spin conserving hopping or on-site potential.

What happens to the spectrum under chiral symmetry? For a given single-particle eigenstate $|\psi\rangle$ of the single-particle Hamiltonian,

$$H|\psi\rangle = E|\psi\rangle,$$

there exists a chiral symmetric eigenstate $S|\psi\rangle$ with opposite eigenenergy.

$$H(S|\psi\rangle) = -SH|\psi\rangle = -E(S|\psi\rangle),$$

where Eq. (2.21) was used in the first step. This fact is also seen in by inserting $f_\sigma(k) = 0$ into Eq. (3.14),

$$E_\pm(k) = \pm\sqrt{g_+(k)g_-(k)}. \tag{3.16}$$

The eigenenergies of the system are symmetric around $E = 0$.

By setting all real parameters in Eq. (3.12b) to zero and one by one setting them to one, it is verified that the spectrum is symmetric around zero energy, see Figure 3.2. That is, *in a chiral symmetric model there exists a chiral symmetric partner state with energy $-E(k)$ to every state with energy $E(k)$.*

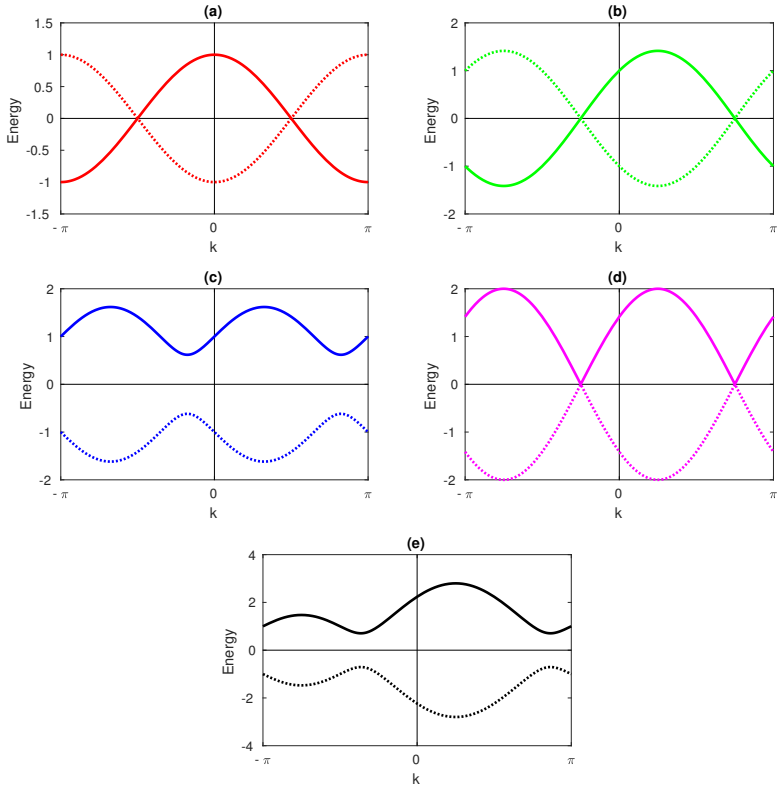

Figure 3.2: Spectra of the chiral invariant model described by Eqs. (3.16) and (3.12b). Regular lines are $E_+(k)$ and dashed lines are $E_-(k)$. Red: $e = 1$, Green: $e = f = 1$, Blue: $e = f = g = 1$, Magenta: $e = f = g = h = 1$, Black: $e = f = g = h = \tilde{\nu} = 1$, others zero and $\tilde{\mu}$ is always zero.

Secondly, consider now instead that the general Hamiltonian Eq. (3.1) is time reversal invariant. In this case, the Bloch Hamiltonian obeys Eq. (2.29), namely, $\mathcal{T}\mathcal{H}^*(-k)\mathcal{T}^{-1} = \mathcal{H}(k)$. Applying Eq. (2.29) with $\mathcal{H}(k)$ given by Eq. (3.13) and $\mathcal{T} = -i\sigma_y$ as seen in Eq. (2.34), the following constraints for the matrix elements of the Bloch Hamiltonian are found

$$f_-^*(-k) = f_+(k), \quad -g_+^*(-k) = g_-(k).$$

The Eqs. (3.12a) and (3.12b) take the form

$$f_\sigma(k) = a\cos k + \mu + \sigma d \sin k, \tag{3.17a}$$
$$g_\sigma(k) = f\sin k + i\sigma g \sin k. \tag{3.17b}$$

The time reversal symmetric model is given by

$$\mathcal{H}(k) = \begin{pmatrix} f_+(k) & g_+(k) \\ g_-(k) & f_-(k) \end{pmatrix},$$

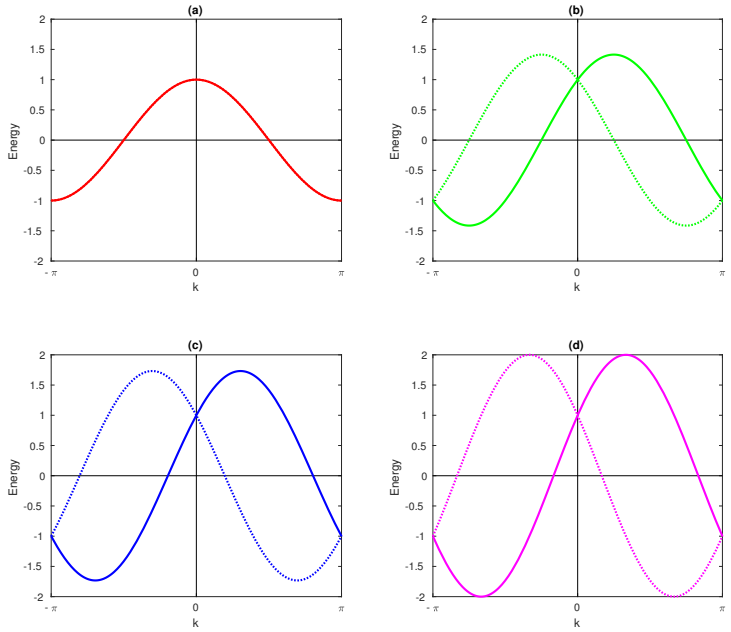

Figure 3.3: Spectra of the time reversal symmetric model given by Eq. (3.14) with $f_\sigma(k)$ and $g_\sigma(k)$ described by Eqs. (3.17a) and (3.17b) respectively. Regular lines are $E_+(k)$ and dashed lines are $E_-(k)$. In subfigure (a) the spectrum is doubly degenerate. Red: $a = 1$, Green: $a = d = 1$, Blue: $a = d = f = 1$, Magenta: $a = d = f = g = 1$, others zero and μ is always zero.

using Eqs. (3.17a) and (3.17b). The spectrum of this model given by Eq. (3.14), when sequentially setting parameters to one can be plotted in the same manner as for the chiral symmetric model. The result is summarized in Figure 3.3. In Figure 3.3 (a) the spin dependence is not resolved because the only non-zero parameter a corresponds to spin-independent hopping. Only after turning on a spin-dependent term can the spin degeneracy be lifted except for at so called time reversal invariant momenta introduced in Section 2.2.2, namely at $k = \pm\pi, 0$.

The spectrum is symmetric under inversion of momentum. That is, *in a time reversal invariant model there exists a partner state to a state of momentum k, spin σ and energy E with momentum $-k$, spin $-\sigma$ and the same energy E.*

Lastly, consider imposing particle-hole invariance for the general Hamiltonian Eq. (3.1), such that the Bloch Hamiltonian obeys Eq. (2.42) $\mathcal{C}\mathcal{H}^*(-k)\mathcal{C}^{-1} = -\mathcal{H}(k)$, with $\mathcal{C} = -\sigma_x$ as seen in Eq. (2.47). The constraints for the matrix elements of the Bloch Hamiltonian become

$$f_-^*(-k) = -f_+(k), \quad g_+^*(-k) = -g_-(k).$$

The Eqs. (3.12a) and (3.12b) are reduced to

$$f_\sigma(k) = b\sin k + \sigma(c\cos k + \nu) \tag{3.18a}$$
$$g_\sigma(k) = f\sin k + i\sigma g\sin k. \tag{3.18b}$$

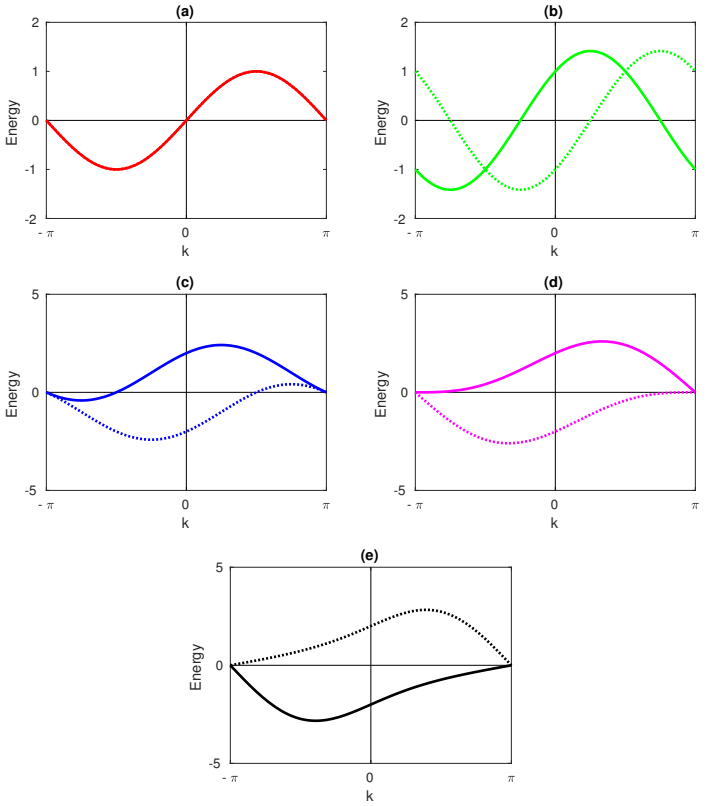

Figure 3.4: Spectra of the particle-hole symmetric model given by Eq. (3.14) with $f_\sigma(k)$ and $g_\sigma(k)$ described by Eqs. (3.18a) and (3.18b) respectively. Regular lines are $E_+(k)$ and dashed lines are $E_-(k)$. In subfigure (a) the spectrum is doubly degenerate. Red: $b = 1$, Green: $b = c = 1$, Blue: $b = c = \nu = 1$, Magenta: $b = c = \nu = f = 1$, Black: $b = c = \nu = f = g = 1$, others zero.

The eigenvalues Eq. (3.14) with $f_\sigma(k)$ and $g_\sigma(k)$ given by Eqs. (3.18a) and (3.18b) gives the eigenspectrum illustrated in Figure 3.4.

The spectrum is symmetric under inversion of energy through the origin. That is, *in a particle-hole invariant model there exists a partner state to a state of momentum k, spin σ and energy E with momentum $-k$, spin $-\sigma$ and energy $-E$.*

Figure 3.5 summarizes the properties of the energy eigenvalues for spectra that are invariant under one of the symmetries.

Taking the overlap of what is allowed by a chiral symmetric, time reversal symmetric and particle-hole symmetric system, the only terms that remain are

$$\mathcal{H}(k) = \begin{pmatrix} 0 & f\sin k + ig\sin k \\ f\sin k - ig\sin k & 0 \end{pmatrix}.$$

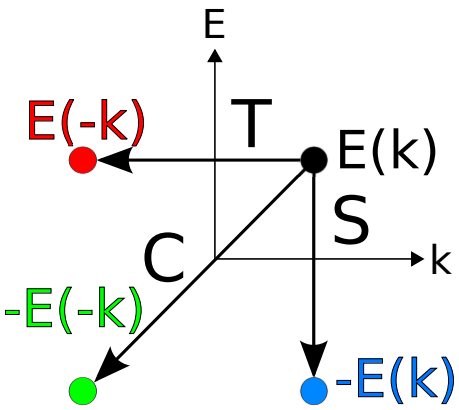

Figure 3.5: Given an eigenenergy, $E(k)$, a chiral symmetric model has a partner state (blue) with energy $-E(k)$, a time reversal invariant model has a partner state (red) of energy $E(-k)$ and a particle-hole invariant model has a partner state (green) of energy $-E(-k)$.

Consulting Eq. (3.11) it is found that the only remaining terms in a general, S, T and C symmetric, non-interacting, two-band Hamiltonian, are *imaginary, spin independent, spin flipping hopping* and *real, spin dependent, spin flipping hopping*. The eigenenergies of this model are given by

$$E_{\pm}(k) = \pm\sqrt{f^2 + g^2}|\sin(k)| \tag{3.19}$$

with the spectrum shown in Figure 3.6 with $f = g = 1$.

3.2 Spinful Non-Interacting Tight Binding Multi-Band Model

Most of the mathematics and conclusions are equivalent when the two-band model is generalized to a multi-band model. This section will however, derive a powerful result. The Hamiltonian will include the same general terms as in the previous section, but it will also be allowed to be of arbitrary size. Solving this model for the general Bloch Hamiltonian is the main result of this section. With this result at hand, if some

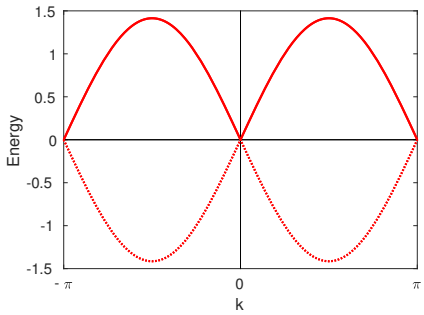

Figure 3.6: Spectrum of the chiral-, time reversal- and particle-hole symmetric model given by Eq. (3.19) with $f = g = 1$. The regular line is $E_+(k)$ and the dashed line is $E_-(k)$.

model under consideration is a special case of this general model, it suffices to insert appropriate values for the parameters in the general Hamiltonian to solve that model.

To construct a model with an arbitrary number of bands, each unit cell must have an arbitrary number of internal degrees of freedom. In the model described by Figure 3.7, each unit cell has r sites, each with spin up and down. The total number of internal degrees of freedom is $2r$. Such a situation occurs, for example, when the hopping amplitudes and on-site potentials appearing in Eq. (3.1) are position dependent functions and periodic with wave length $\lambda = ra$ (a being the lattice spacing). In this case, the lattice is translation invariant by a unit cell (as it is defined in Figure 3.7) displacement. Each unit cell with $2r$ internal sites is repeated N times on a one dimensional chain.

To make the notation more compact, spin dependent and spin independent constants enter into the same quantity,

$$\begin{aligned} \gamma_{i\sigma} &= \alpha_i + \sigma\beta_i, \quad \rho_{i\sigma} = \mu'_i + \sigma\nu'_i, \\ \tilde{\gamma}_{i\sigma} &= \tilde{\alpha}_i + \sigma\tilde{\beta}_i, \quad \tilde{\rho}_{i\sigma} = \tilde{\mu}'_i + \sigma\tilde{\nu}'_i, \end{aligned} \tag{3.20}$$

where i labels the internal sites of the unit cell and $\sigma = \{+, -\}$. As before, all constants are complex and the Hamiltonian becomes

$$\begin{aligned} \mathscr{H} = \sum_{m=1}^{N} \Bigg[& \sum_{i=1}^{r-1} \sum_{\sigma} \left(\gamma_{i,\sigma} c^{\dagger}_{m,i,\sigma} c_{m,i+1,\sigma} \quad + \tilde{\gamma}_{i,\sigma} c^{\dagger}_{m,i,\sigma} c_{m,i+1,-\sigma} \right) \\ & + \sum_{\sigma} \left(\gamma_{r,\sigma} c^{\dagger}_{m,r,\sigma} c_{m+1,1,\sigma} + \tilde{\gamma}_{r,\sigma} c^{\dagger}_{m,r,\sigma} c_{m+1,1,-\sigma} \right) \\ & + \sum_{i=1}^{r} \sum_{\sigma} \left(\rho_{i,\sigma} c^{\dagger}_{m,i,\sigma} c_{m,i,\sigma} + \tilde{\rho}_{i,\sigma} c^{\dagger}_{m,i,\sigma} c_{m,i,-\sigma} \right) \Bigg] + h.c. \ , \end{aligned} \tag{3.21}$$

with $N + 1 = 1$. In the special case $r = 1$, this Hamiltonian reduces to the two band model Eq. (3.1) by insertion of Eq. (3.20). With the same reasoning used to find Eq. (3.6), Eq. (3.21) is Fourier transformed into k-space. The Hamiltonian takes the form

$$\begin{aligned} \mathscr{H} = \sum_{k} \Bigg[& \sum_{i=1}^{r-1} \sum_{\sigma} \left(\gamma_{i,\sigma} c^{\dagger}_{k,i,\sigma} c_{k,i+1,\sigma} + \tilde{\gamma}_{i,\sigma} c^{\dagger}_{k,i,\sigma} c_{k,i+1,-\sigma} + \rho_{i,\sigma} c^{\dagger}_{k,i,\sigma} c_{k,i,\sigma} + \tilde{\rho}_{i,\sigma} c^{\dagger}_{k,i,\sigma} c_{k,i,-\sigma} \right) \\ & + \sum_{\sigma} \left(\gamma_{r,\sigma} e^{ik} c^{\dagger}_{k,r,\sigma} c_{k,1,\sigma} + \tilde{\gamma}_{r,\sigma} e^{ik} c^{\dagger}_{k,r,\sigma} c_{k,1,-\sigma} + \rho_{r,\sigma} c^{\dagger}_{k,r,\sigma} c_{k,r,\sigma} + \tilde{\rho}_{r,\sigma} c^{\dagger}_{k,r,-\sigma} c_{k,r,-\sigma} \right) \Bigg] + h.c. \ . \end{aligned} \tag{3.22}$$

From this, it is straightforward to produce the Bloch Hamiltonian defined by

$$\mathscr{H} = \sum_{k} c^{\dagger}_{k} \mathcal{H}(k) c_{k}.$$

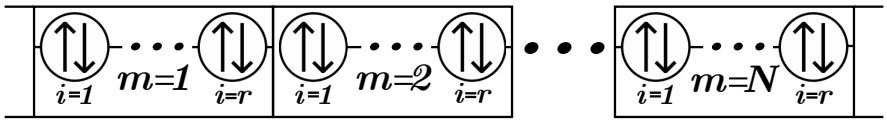

Figure 3.7: Illustration of the multi-band model. The N unit cells are labeled by m, each hosts r sites each with two possible spin orientations.

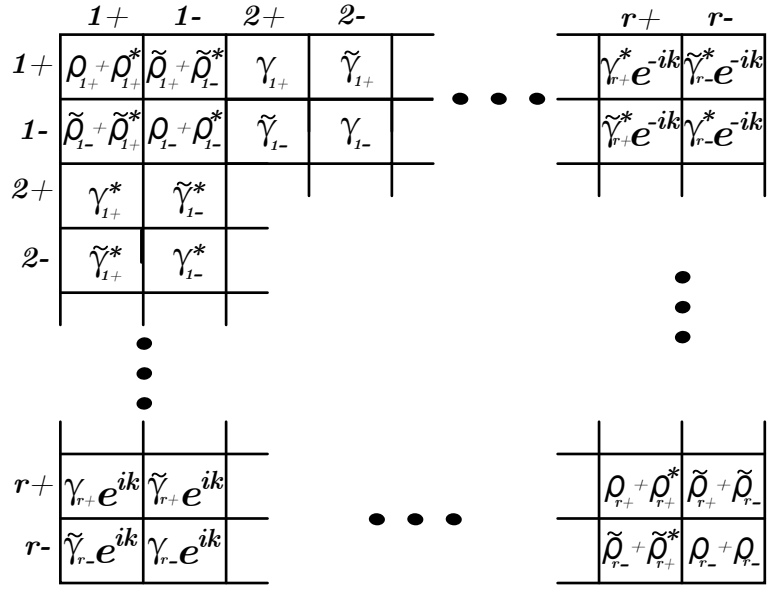

Figure 3.8: The form of the Bloch Hamiltonian for the general n-band model. The upper left part repeats $r-1$ times along the diagonal while changing the internal site index.

With the bipartite spinor $c_k^\dagger$ given by

$$c_k^\dagger = \left(c_{k,1,+}^\dagger,\ c_{k,1,-}^\dagger,\ c_{k,2,+}^\dagger,\ c_{k,2,-}^\dagger \cdots\ c_{k,r,+}^\dagger,\ c_{k,r,-}^\dagger\right)$$

the structure of the Bloch Hamiltonian is given by Figure 3.8.

This Bloch Hamiltonian is directly applicable to any model with form of the original Hamiltonian Eq. (3.21). One must only make sure to use the same Fourier transformation convention and that the bipartite spinors are defined in the same way, when comparing the result to some specific model.

3.3 The Su-Schrieffer-Heeger (SSH) Model

The simplest model known to exhibit topological properties is the so called *Su-Schrieffer-Heeger* (SSH) *model*. The model describes spinless electrons, hopping on a one-dimensional, open chain. The chain consists of N unit cells, each of which hosts two sites, one on sublattice A and the other on sublattice B. The structure of the lattice is given by Figure 3.9. The second quantized Hamiltonian of the SSH model is

$$\mathscr{H} = v\sum_{m=1}^{N} c_{m,B}^\dagger c_{m,A} + w\sum_{m=1}^{N-1} c_{m+1,A}^\dagger c_{m,B} + h.c.\ . \tag{3.23}$$

The hopping amplitudes are alternating and in fact, this situation occurs naturally due to what is known as *Pierls instability*, which says that the system will arrange itself such that the amplitudes are staggered because it is energetically favourable [19]. Furthermore, the amplitudes are taken to be real and positive for simplicity.

As per usual, the goal is to find the Bloch Hamiltonian and thereby the energy spectrum. Notice that the SSH model can be divided into two subsystems, A and B (according to Figure 3.9), within which there

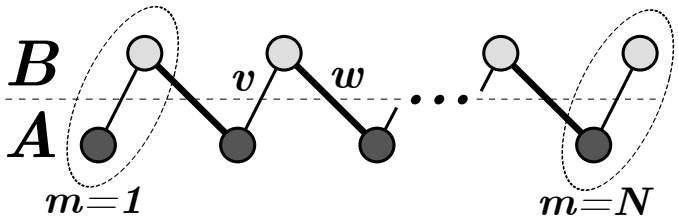

Figure 3.9: Schematic drawing of the SSH chain. It consists of N unit cells, each with two sites. The dark (light) sites make up the sublattice A (B). The intercell (intracell) hopping amplitude is w (v).

exists no bonds. This is exactly the condition for chiral symmetry, which was discussed in Section 2.1. Thus, the Bloch Hamiltonian is expected to be off-diagonal.

Fourier transformation is only possible when real space is periodic and near the edges of an open chain the periodicity vanishes. To that end, define the translation invariant Hamiltonian

$$\mathscr{H}_{bulk} = v \sum_{m=1}^{N} c^{\dagger}_{m,B} c_{m,A} + w \sum_{m=1}^{N-1} c^{\dagger}_{m+1,A} c_{m,B} + h.c.\ , \quad (N+1=1). \tag{3.24}$$

The condition $N+1=1$, closes the chain. The SSH chain can be separated into a bulk part and a boundary part. The boundary consists of the regions in close proximity to two edges of the chain, the bulk makes up the inner section of the chain and without any edges to terminate the chain the bulk is translation invariant. Hence $\mathscr{H}_{bulk}$ is called the *bulk Hamiltonian*. In the thermodynamic limit the properties of the model are given mostly by the bulk, thus for now, only the bulk Eq. (3.24) is investigated.

To find the Bloch Hamiltonian one applies the Fourier transforms Eqs. (3.2a) and (3.2b) and defines a basis

$$c^{\dagger}_{k} = (c^{\dagger}_{k,A},\ c^{\dagger}_{k,B}).$$

The bulk SSH Hamiltonian Eq. (3.24) can be written

$$\mathscr{H}_{bulk} = \sum_{k} c^{\dagger}_{k} \mathcal{H}(k) c_{k}.$$

In this basis, $\mathcal{H}(k)$ becomes

$$\mathcal{H}(k) = \begin{pmatrix} 0 & v + we^{-ik} \\ v + we^{ik} & 0 \end{pmatrix} \tag{3.25}$$

Because the matrix is off-diagonal it can be squared to find the energies, $\mathcal{H}(k)^2 = E(k)^2 \mathbb{1}$ and it is found that the energies are given by

$$E_{\pm}(k) = \pm|v + we^{-ik}| = \pm\sqrt{v^2 + w^2 + 2vw\cos k}. \tag{3.26}$$

The SSH model has two internal degrees of freedom and therefore it has two bands. There exists a gap Δ between these bands and it is defined as the difference between the energies of these two bands when they are the closest to each other,

$$\Delta = min(E_{+}(k)) - max(E_{-}(k)) = E_{+}(\pi) - E_{-}(\pi) = 2|v - w|. \tag{3.27}$$

Due to the existence of a gap, the system describes an *insulator*. If $v = w$, then the gap closes at $k = \pm\pi$ and the system is said to be a *conductor*. These are two distinct states of matter. What is interesting is that there are even more distinct states of matter hidden in the SSH model.

3.3.1 Topological Features of the SSH Model

The goal is to find a topological phase of matter which is distinct from a trivial insulator or conductor. Recall that a *unique phase of matter corresponds to a system with a unique set of physical properties.* In the following the physical properties that will be clearly distinct between the topological and trivial phase is the band structure. The goal is thus to find a region in the parameter space where the SSH model's eigenspectrum behaves differently.

Consider the SSH Hamiltonian Eq. (3.23) in the real space basis,

$$c^\dagger = \big(c^\dagger_{1,A},\ c^\dagger_{1,B},\ c^\dagger_{2,A}\ c^\dagger_{2,B} \dots\ c^\dagger_{N,A},\ c^\dagger_{N,B}\big).$$

Note that now, the full SSH model, with edges, is being considered. The Hamiltonian becomes

$$\mathscr{H} = c^\dagger \mathcal{H} c.$$

As an example, let $N = 3$. The real space Hamiltonian matrix $\mathcal{H}$, is given by

$$\mathcal{H} = \begin{pmatrix} 0 & v & 0 & 0 & 0 & 0 \\ v & 0 & w & 0 & 0 & 0 \\ 0 & w & 0 & v & 0 & 0 \\ 0 & 0 & v & 0 & w & 0 \\ 0 & 0 & 0 & w & 0 & v \\ 0 & 0 & 0 & 0 & v & 0 \end{pmatrix}. \tag{3.28}$$

Two insulators are said to be *topologically equivalent* if their Hamiltonians can be adiabatically deformed into one another. More details on *adiabatic deformations* will be given in Section 5.1. For now, *an adiabatic deformation is a continuous change of the parameters in the Hamiltonian, such that, the symmetries of the Hamiltonian are unchanged and the band gap never closes.* In mathematics one wants to find the different equivalence classes of topological spaces where the equivalence relation is a continuous deformations of the space. Here the continuous deformation is an adiabatic deformation, and it too defines an equivalence relation. If a Hamiltonian can be adiabatically deformed into another Hamiltonian, then these Hamiltonians belong to the same equivalence class and in fact, they belong to the same phase. The different phases that arise have fundamentally different properties. For the SSH model there exists two regions in parameter space which can not be connected by adiabatic deformations, because the energy gap will close. One of these two states will be fundamentally different and host gapless boundary modes, a defining property of topological insulators. The goal is to investigate this phase transition.

By looking at the band gap Eq. (3.27), it is clear that an adiabatic deformation can not let v become equal to w. If that were to happen, the band gap closes and that would correspond to a phase transition. Thus, the regions $v < w$ and $v > w$ must describe two topologically, non-equivalent insulating states. In fact, because these different states have such different eigenspectra (to be shown in short), they describe different phases of matter. Figure 3.10 (a) is the solution for the energy spectrum of Eq. (3.28) with $w = 1$ and where $v \in [0, 3]$. The radical change in the spectrum occurs around $v = 0.5$, this is a finite system size effect. In the thermodynamic limit where $N \to \infty$ the change occurs at $v = w$. The appearance of zero energy states in Figure 3.10 (a) indicates a topologically non-trivial state. The fact that they do no change under deformation is due to what is known as *topological protection.* Topological protection happens only in a topological phase, as opposed to a trivial phase, to be discussed in Chapter 9.

Clearly, the regions $v < w$ and $v > w$ describe topologically distinct phases (see Figure 3.10 (b)), and the $v < w$ has *topologically protected* zero energy states. The two equivalence classes which correspond to the two phases are given by all Hamiltonians in the gray and white area respectively. What characterizes these two different phases? The concept of *topological invariants* provides the answer.

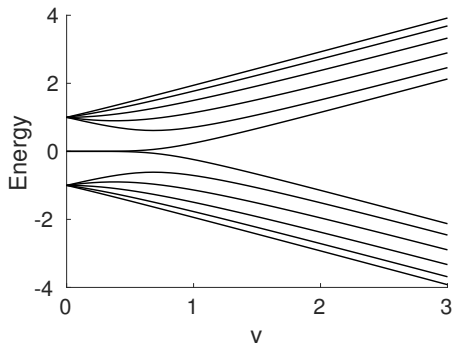

(a) The spectrum of the SSH model in real space for $N = 3$, $w = 1$ and where $v \in [0, 3]$. The appearance of topologically protected, zero energy stated indicates a phase transition.

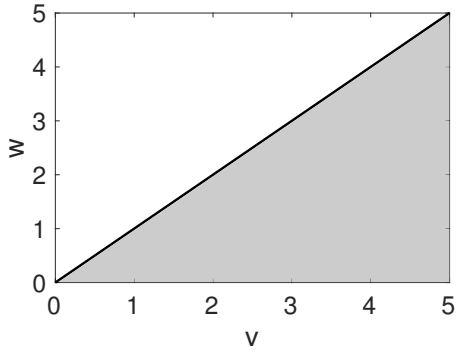

(b) The two distinct phases, topological phase (white) and topologically trivial phase (gray), of the SSH model. They are separated by the line $v = w$ which no adiabatic deformation can cross because the gap closes.

Figure 3.10

Definition 3.1 (Topological invariant) *An integer that characterizes an insulating Hamiltonian and does not change under adiabatic deformation of the parameters in the Hamiltonian.*

Topological invariants are only well defined in the thermodynamic limit [19]. There exists such an invariant for the SSH model and it does indeed take on different integer values for the regions $v < w$ and $v > w$.

3.3.2 Topological Invariant of the SSH Model

The goal is to find the topological invariant of the SSH model. To this end, the Bloch Hamiltonian Eq. (3.25) is rewritten in terms of Pauli matrices,

$$\mathcal{H}(k) = d_0(k)\sigma_0 + \mathbf{d}(k) \cdot \boldsymbol{\sigma}, \tag{3.29}$$

where $\sigma_0 = \mathbb{1}$ and $\boldsymbol{\sigma} = (\sigma_x, \sigma_y, \sigma_z)$. The coefficients are found to be

$$d_x = v + w\cos k, \quad d_y = w\sin k \ \text{ and } \ d_z = d_0 = 0. \tag{3.30}$$

In fact, any two-band, chiral symmetric Hamiltonian written in the chiral basis must have $d_z = d_0 = 0$, because of its off-diagonal form.

The vector $\mathbf{d}(k)$ traces out a path with its endpoint as k is taken through the first Brillouin zone, i.e. $k = [-\pi, \pi]$. Due to the periodicity in k-space, this is necessarily a closed loop. Changing the parameters v and w displaces and deforms the loop, see Figure 3.11. In particular v displaces the loop in d_x-direction and w determines the radius of the loop. If the loop were to at some point cross the origin, all the parameters in the Hamiltonian vanish $\big(d_x = d_y = 0 \Rightarrow E_\pm = 0\big)$ and therefore gap closes and the system is in a conducting state. Thus, *under any adiabatic deformation, a loop that winds around the origin can not cross the origin* because the gap is not allowed to close. Likewise, any loop that does not enclose the origin can not be made to do so.

It is seen in Figure 3.11 that while $v < w$, the loop encloses the origin (topological) and while $v > w$, the loop does not enclose the origin (trivial). The topological invariant of the SSH model is *the number of windings of* $\mathbf{d}$*(k) about the origin.* Clearly, this must be an integer and it has already been established that it can not change under an adiabatic deformation. The requirements for a topological invariants are fulfilled. 3.11.

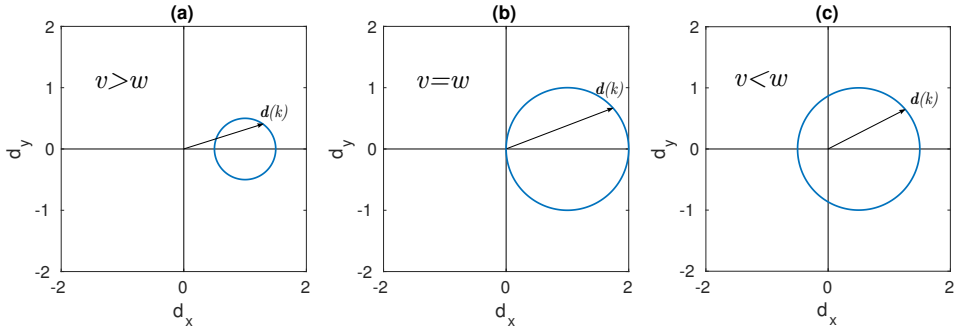

Figure 3.11: Winding of $\mathbf{d}$(k) as k sweeps through the first Brillouin zone. (a) $v = 1$ and $w = 0.5$ the winding number is zero indicating a trivial phase. (b) $v = w = 1$ the loop intersects the origin indicating a gap closing and phase transition point. (c) $v = 0.5$ and $w = 1$ the winding number is one indicating a topological phase.

It should be noted that for a more general model, the number of windings can be greater than one. This topological invariant is the so called *winding number* n, to be discussed in greater detail in Chapter 4. The phase diagram Figure 3.10 (b) has been completely characterized, see Figure 3.12.

3.3.3 The Bulk-Boundary Correspondence in the SSH Model

The zero energy levels in Figure 3.10 (a) are in Section 9.1 identified as *gapless edge states* and the corresponding wave functions are shown to be highly located near the edges. The edge states occur at the phase transition point $v = w$ in the thermodynamic limit and therefore there is always an equivalence between the number of gapless edge states (at one side of the chain) and the winding number, hence the former is also a topological invariant. In fact, it is possible to derive a mathematical equivalence between the number of edge states at one side of the chain and the topological invariant of the SSH model [26]. This is a clear example of what is known as the *bulk-boundary correspondence*, to be discussed in Chapter 9. The bulk-

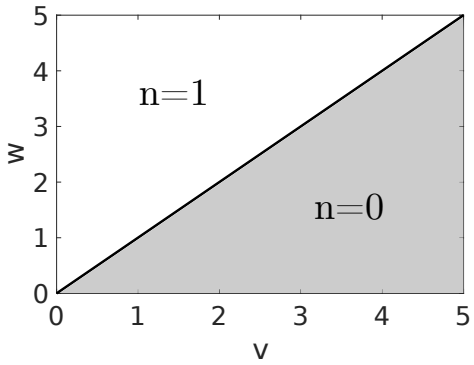

Figure 3.12: Phase diagram of the SSH model characterized by winding number n.

boundary correspondence states that the number of edge modes is characterized by a topological invariant of the bulk. What is interesting is that a property defined only in the bulk of the model (winding number) makes predictions for the boundary (number of edge states). The bulk-boundary correspondence is realized experimentally in for example the quantum Hall effect [27], to be discussed in Chapter 7.

The bulk-boundary correspondence is a recurring phenomenon in topological matter that has received increased attention as of late. For a more in-depth discussion and further examples refer to [28, 29].

4 Winding Number

The *winding number* is a purely mathematical property defined for any smooth and closed curve. It was discussed briefly in Section 3.3.2. The winding number plays its part in physics as a topological invariant. In this section, the winding number is generalized and alternative definitions are presented.

The winding number of a smooth closed curve is the number of turns (or windings) about some point, that the tangent vector to the curve makes as one passes around the curve [30]. For the SSH model, the curve was defined by the tangent of $\mathbf{d}(k)$ (defined in Eq. (3.30)) in the xy-plane. The winding number about the origin was calculated as all momenta in the first Brillouin zone were swept over. This method of computing the winding number is limited to two-band models. Of course, the winding number is much more general and can in fact be defined for any off-diagonal multi-band Hamiltonian.

Firstly, winding number is defined in a more general setting and it will be shown that the new definition is equivalent to how it was defined for the SSH model. Afterwards an alternative expression in terms of poles and zeros will be given.

4.1 Winding Number in One Dimension

A general off-diagonal Hamiltonian of size $2r \times 2r$ can be put in the form

$$\mathcal{H} = \begin{pmatrix} 0 & \mathcal{H}_{AB}(k) \\ \mathcal{H}_{AB}^{\dagger}(k) & 0 \end{pmatrix}. \tag{4.1}$$

The winding number n is defined as the *number of revolutions of det* $\big[\mathcal{H}_{AB}\big]$ *about the origin of the complex plane as* k *varies in* $[-\pi, \pi]$ [31]. The determinant is generally a complex number which can be written

$$\det\big[\mathcal{H}_{AB}(k)\big] = m_1(k) + im_2(k) = R(k)e^{i\phi(k)}. \tag{4.2}$$

The number of revolutions of $\det\big[\mathcal{H}_{AB}\big]$ about the origin of the complex plane is

$$\boxed{n = -\frac{1}{2\pi}\int_{-\pi}^{\pi} \frac{d\phi(k)}{dk} dk,} \tag{4.3}$$

which is obviously nothing other than

$$n = -\frac{1}{2\pi}\big[\phi(\pi) - \phi(-\pi)\big] = -\frac{1}{2\pi}\Delta\phi. \tag{4.4}$$

If $\det\big[\mathcal{H}_{AB}(k)\big]$ takes l turns, then $\Delta\phi = l2\pi$ and Eq. (4.4) gives $n = l$.

Is this definition of winding number equivalent to how the winding number was calculated for the SSH model in Section 3.3.2? Comparing Eqs. (3.25) and (4.1) one concludes that, for the SSH model[7]

$$\det\big[\mathcal{H}_{AB}\big] = v + we^{-ik} = v + w\cos k + iw\sin k.$$

It is seen that

$$\mathrm{Re}(\det\big[\mathcal{H}_{AB}\big]) = d_x, \quad \mathrm{Im}(\det\big[\mathcal{H}_{AB}\big]) = d_y.$$

Therefore, the winding number of the complex number $\det\big[\mathcal{H}_{AB}\big]$ about the origin of the complex plane is equal to the winding of the vector $\mathbf{d}(k)$ defined in Eq. (3.30) about the origin of the $d_x d_y$-plane.

[7] It is noted that under a change of sign in the Fourier transform convention the function $\det\big[\mathcal{H}_{AB}\big] = v + we^{-ik} \to \det\big[\mathcal{H}_{AB}\big] = v + we^{ik}$ and in effect $n \to -n$.

4.1.1 Winding Number in Terms of Poles and Zeros

In certain cases, more is known about the region enclosed by the curve than about the curve itself. The winding number can be expressed in terms of *poles* and *zeros* inside the curve. Call $\det\big[\mathcal{H}_{AB}\big] \equiv f(k)$ and note from Eq. (4.2) that

$$\ln f(k) = \ln R(k) + i\phi(k),$$

such that

$$\phi(k) = \frac{1}{i}\big[\ln f(k) - \ln R(k)\big].$$

Rewriting Eq. (4.3) with this expression yields

$$n = \frac{1}{2\pi i}\bigg(-\int_{-\pi}^{\pi} \frac{d}{dk}\ln f(k)dk + \int_{-\pi}^{\pi} \frac{d}{dk}\ln R(k)dk\bigg).$$

The second integral becomes $\ln R(\pi) - \ln R(-\pi)$, which vanishes because $R(k)$, unlike $f(k)$, is a single valued function and π and $-\pi$ are equivalent points. Using the logarithmic derivative puts the winding number into the form

$$n = -\frac{1}{2\pi i}\int_{-\pi}^{\pi} \big[\frac{d}{dk}f(k)\big]\frac{1}{f(k)}dk. \tag{4.5}$$

The derivative of $f(k)$ can be rewritten by defining $z(k) = e^{-ik}$,

$$\frac{d}{dk}f(k) = \bigg(\frac{dz(k)}{dk}\bigg)\bigg(\frac{d}{dz(k)}f\big(z(k)\big)\bigg) = -ie^{-ik}\frac{d}{dz(k)}f\big(z(k)\big).$$

Now Eq. (4.5) takes the form

$$n = -\frac{1}{2\pi i}\int_{-\pi}^{\pi}\bigg[\frac{d}{dz(k)}f\big(z(k)\big)\bigg]\frac{1}{f\big(z(k)\big)}\big(-ie^{-ik}\big)dk.$$

Define

$$g\big(z(k)\big) \equiv \bigg[\frac{d}{dz(k)}f\big(z(k)\big)\bigg]\frac{1}{f\big(z(k)\big)}.$$

Such that

$$n = -\frac{1}{2\pi i}\int_{-\pi}^{\pi} g\big(z(k)\big)z'(k)dk. \tag{4.6}$$

A standard result from contour integration theory [32] is

$$\int_C g(\tau)d\tau = \int_a^b g\big(\tau(t)\big)\tau'(t)dt, \tag{4.7}$$

where $\tau(t)$ parameterizes the curve C when $a < t < b$. The function $\tau(t)$ is complex valued and the parameter t is real. Applying theorem Eq. (4.7) to Eq. (4.6) where $\tau(t)$ corresponds to $z(k) = e^{-ik}$,

$$n = -\frac{1}{2\pi i}\oint g(z)dz = -\frac{1}{2\pi i}\oint \frac{f'(z)}{f(z)}dz.$$

The curve is oriented clockwise because it is parameterized by e^{-ik} and $k \in [-\pi, \pi]$. The direction of the curve can be reversed by changing the sign

$$n = \frac{1}{2\pi i}\oint \frac{f'(z)}{f(z)}dz. \tag{4.8}$$

The closed curve is the counter-clockwise path around the unit circle in the complex plane. By *the argument principle of complex analysis* [33], Eq. (4.8) becomes

$$\boxed{n = N_f - P_f,} \tag{4.9}$$

where N_f and P_f denote the number of zeros and poles of $f(z)$ enclosed by the curve, respectively. Each zero and pole is weighted by their *multiplicity*[8] and *order*, respectively. It is assumed that there are no zeros and poles on the curve.

Can Eq. (4.9) be applied to the SSH model? The function $f(k)$ of the SSH model is $f(k) = v + we^{-ik}$, such that $f(z) = v + wz$. The function $f(z)$ has no poles, but it has a zero of multiplicity one:

$$f(-v/w) = f(z_0) = 0.$$

The zero $z_0 = -v/w$ is always negative (because the parameters were taken to be positive) and only inside the unit circle if $v < w$. Thus, using Eq. (4.9),

$$n = N_f - P_f = \begin{cases} 1 - 0 = 1, & v < w \\ 0 - 0 = 0, & v > w \end{cases} .$$

The topological invariant has a non-trivial value in the region $v < w$ and a trivial value if $v > w$ in accordance with what was found in Section 3.3.2. If $v = w$ then the spectrum is known to be conducting and the description of topological invariants is not well-defined. For this case the zero of $f(z)$ occurs at $z_0 = -1$ which is on the unit circle, contrary to the above assumption.

4.2 Winding Number in Three Dimensions

Previously, the winding number was defined for one-dimensional momentum. Next, one would like to calculate winding numbers for higher dimensions. However, no topological phases in two dimensions are characterized by winding numbers, because they are described by Chern numbers or $\mathbb{Z}_2$-invariants, this will be shown in Chapter 8. Thus, the only remaining dimension that remains to be discussed is $d = 3$. The discussion given here is very limited. For a more in-depth coverage see [34].

To construct a three-dimensional winding number, define the Q-matrix

$$Q(\mathbf{k}) \equiv \mathbb{1} - 2P(\mathbf{k}),$$

where $P(\mathbf{k}) \equiv \sum_{\alpha}^{filled} |\psi_\alpha(\mathbf{k})\rangle \langle\psi_\alpha(\mathbf{k})|$ is the projection operator over filled Bloch states.

As for in one dimension, the winding number in three dimensions is defined for Hamiltonians which can be brought into an off-diagonal form. In such a case, the Q-matrix is also off-diagonal [34],

$$Q = \begin{pmatrix} 0 & q(\mathbf{k}) \\ q^\dagger(\mathbf{k}) & 0 \end{pmatrix}.$$

The three-dimensional winding number [34] is given by

$$n = \int \frac{d^3k}{24\pi^2} \epsilon^{\mu\nu\rho} Tr[(q^{-1}\partial_{k_\mu} q)(q^{-1}\partial_{k_\nu} q)(q^{-1}\partial_{k_\rho} q)] \tag{4.10}$$

and it counts the number of non-trivial windings of the map $\mathbf{k} \to$ space of $q(\mathbf{k})$ [14]. The integral is taken over all momenta in the first Brillouin zone, $\epsilon^{\mu\nu\rho}$ is the antisymmetric tensor and μ, ν and $\rho = x, y, z$.

[8] A zero of the form $a_k(z - z_0)^k$ is of multiplicity k. A pole of the form $a_p \frac{1}{(z-z_0)^p}$ is of order p.

The winding number Eq. (4.10) is often tricky to compute numerically and even more so analytically. In principle, one can construct simple models and calculate Eq. (4.10) analytically, see [17], but more often numerical solutions are required. In [17] the three dimensional winding number is calculated for continuum Dirac Hamiltonian. The result is curiously enough a half integer. This can occur for continuum model and in particular, for the Dirac Hamiltonian it reflects the fact that the continuum model does not correctly capture the high energy limit of the wave functions [14].

5 Berryology

The concept of geometric phases, or *Berry Phases*, is important in the study of topological properties of materials because it enters into the description of a very important topological invariant known as *Chern number*. To understand how Berry phases arise physically, some knowledge of the *adiabatic theorem of quantum mechanics*, or simply the *adiabatic theorem*, is essential. This will be discussed in Section 5.1. When it has been established what an *adiabatic deformation* implies, the Berry phase is introduced in both the discrete and continuous case in Section 5.2. The following chapter will make use of the Berry phase to understand Chern numbers.

5.1 Adiabatic Theorem

A general Hamiltonian depends on two types of variables, *degrees of freedom* and *parameters*. The degrees of freedom evolve dynamically with time and are for example position and spin. The parameters are usually set by experimental conditions and are for example the various hopping amplitudes and interaction strengths of the Hamiltonian. It should be noted that for a given model one is free to consider any degree of freedom, say momentum as a parameter. It is just a matter of choice to say that in this particular problem, momentum can be controlled externally.

Under a change of the parameters of a Hamiltonian describing some quantum system, the eigenstates may change. However, consider a very *slow* deformation of the parameters in the Hamiltonian. A slow deformation in this context, is known as an *adiabatic deformation*. What characterizes such a deformation is that it happens on a time scale that is much larger than the typical time scale of the system that it deforms. The external time T_e is the time during which the deformation is carried out. Let the system's internal time dependence be of order T_i. Then an adiabatic deformation is one for which $T_e \gg T_i$. Furthermore, an adiabatic deformation must never close the energy gap of an insulator and may not affect the symmetries of the system.

One all important theorem can now be introduced,

Theorem 5.1 (Adiabatic theorem) *A particle initially in the nth eigenstate of H, will remain in the nth eigenstate of a new Hamiltonian H' if the deformation from H to H' is adiabatic.*

A practical example helps to make this understandable. The Hamiltonian describing a particle in a box depends on the box size, a. Suppose the box is slowly enlarged, that is, a parameter in H is deformed. A particle originally in the ground state of the first Hamiltonian will still be in the ground state of H'.

5.1.1 Proof of the Adiabatic theorem

The proof given here follows the proof given in [35] which is restricted to non-degenerate systems.

As time moves for an eigenstate ψ_n that is time independent, the eigenstate pick up a phase due to the time evolution operator

$$\Psi_n(t) = \psi_n e^{-iE_n t/\hbar}. \tag{5.1}$$

If the Hamiltonian changes with time the eigenstate $\psi_n(t)$ fulfills

$$H(t)\psi_n(t) = E_n(t)\psi_n(t) \tag{5.2}$$

and they constitute a complete and orthogonal set of functions at any instant in time. As time moves for a system that is time dependent, the eigenstates pick up a phase due to the time evolution operator according to

$$\Psi_n(t) = e^{-\frac{i}{\hbar}\int_0^t E_n(t')dt'}\psi_n(t) \equiv e^{i\theta_n(t)}\psi_n(t), \tag{5.3}$$

where $\theta_n(t) = -\frac{1}{\hbar}\int_0^t E_n(t')dt'$ is known as the *dynamical phase*. The time dependent Schrödinger equation for the full wave function $\Psi(t)$ is

$$i\hbar\partial_t\Psi(t) = H(t)\Psi(t) \tag{5.4}$$

and at any time $\Psi(t)$ can be written as a linear combination of the complete set of states Eq. (5.2),

$$\Psi(t) = \sum_n c_n(t)e^{i\theta_n(t)}\psi_n(t). \tag{5.5}$$

To prove the adiabatic theorem Eq. (5.8), it must be shown that everything other than $\psi_n(t)$ in Eq. (5.5) is just a phase. Inserting Eq. (5.5) into Eq. (5.4),

$$i\hbar\sum_n \left(\dot{c}_n\psi_n + c_n\dot{\psi}_n + ic_n\psi_n\dot{\theta}_n\right)e^{i\theta_n} = \sum_n c_nH\psi_ne^{i\theta_n} = \sum_n c_nE_n\psi_ne^{i\theta_n}.$$

The third term on the left hand side cancels with the right hand side because, $\dot{\theta}_n = -\frac{1}{\hbar}E_n(t)$. Moving forward, now in Dirac notation, multiply what remains by $\langle\psi_m|$,

$$\sum_n \dot{c}_n\delta_{mn}e^{i\theta_n} = -\sum_n c_n\langle\psi_m|\dot{\psi}_n\rangle e^{i\theta_n}.$$

Moving terms

$$\dot{c}_m = -\sum_n c_n\langle\psi_m|\dot{\psi}_n\rangle e^{i(\theta_n-\theta_m)}. \tag{5.6}$$

To find $\langle\psi_m|\dot{\psi}_n\rangle$, take the time derivative of Eq. (5.2) and multiply by $\langle\psi_m|$,

$$\langle\psi_m|\dot{H}|\psi_n\rangle + \langle\psi_m|H|\dot{\psi}_n\rangle = \dot{E}_n\delta_{mn} + E_n\langle\psi_m|\dot{\psi}_n\rangle.$$

Letting H act on the bra it is found that

$$\langle\psi_m|\dot{H}|\psi_n\rangle = (E_n - E_m)\langle\psi_m|\dot{\psi}_n\rangle + \dot{E}_n\delta_{mn}.$$

When $n \neq m$ and assuming $|\psi_n\rangle$ and $|\psi_m\rangle$ are non-degenerate,

$$\langle\psi_m|\dot{\psi}_n\rangle = \frac{\langle\psi_m|\dot{H}|\psi_n\rangle}{(E_n - E_m)}.$$

Plugging this back into Eq. (5.6),

$$\dot{c}_m(t) = -c_m(t)\langle\psi_m(t)|\dot{\psi}_m(t)\rangle - \sum_{n\neq m} c_n(t)\frac{\langle\psi_m(t)|\dot{H}|\psi_n(t)\rangle}{(E_n(t) - E_m(t))}e^{i(\theta_n-\theta_m)}.$$

The adiabatic theorem relies on the *adiabatic approximation* which assumes that $\dot{H}$ is negligible when the Hamiltonian is deformed very slowly (adiabatically), such that the second term vanishes. For a discussion on when this approximation is justified see [36]. What remains is a differential equation for $c_m(t)$,

$$\dot{c}_m(t) = -c_m(t)\langle\psi_m(t)|\partial_t\psi_m(t)\rangle.$$

It is solved by

$$c_m(t) = e^{-\int_0^t\langle\psi_m(t')|\partial_{t'}\psi_m(t')\rangle dt'}. \tag{5.7}$$

Inserting Eq. (5.7) into Eq. (5.5) the adiabatic theorem is complete,

$$\boxed{\Psi_n(t) = \psi_n(t) e^{i\theta_n(t)} e^{-\int_0^t \langle \psi_n(t') | \partial_{t'} \psi_n(t') \rangle dt'}.} \tag{5.8}$$

If the eigenstates are non-degenerate the wave function remains in the same eigenstate under an adiabatic deformation, up to a phase. The theorem holds as long as the deformation happens much slower than the time scale defined by the energy gap. The new phase that emerges in addition to the dynamical phase is the subject of the next section.

5.2 Berry Phase

Consider a system which is deformed adiabatically, that is, one or more of the parameters in the Hamiltonian are changed slowly. Suppose the system was initially in the nth eigenstate of H, $|\psi_n(0)\rangle$, and after some time t, the system is in the nth eigenstate of H', $|\psi'_n(t)\rangle$. If the path taken by the Hamiltonian, in parameter space, is not closed. Then

$$|\psi_n(0)\rangle \not\sim |\psi'_n(t)\rangle \,,$$

because the states are eigenstates of different Hamiltonians. If however, H is changed in a way such that it comes back to itself at the time t, that is, the Hamiltonian is changed according to a closed path in parameter space, then $|\psi_n(0)\rangle \sim |\psi'_n(t)\rangle$ and in fact

$$|\psi_n(0)\rangle \to e^{i\theta_n(t)} e^{i\gamma(t)} |\psi_n(t)\rangle \,,$$

by virtue of the adiabatic theorem Eq. (5.8). The adiabatic theorem ensures that, if the deformation was adiabatic and the states are non-degenerate, then the final state is the same as the initial state, up to a phase. Naturally, a dynamical phase is picked up which depends on the time it took to carry out the deformation. The adiabatic theorem does not forbid the eigenstate to pick up yet another phase, γ known as a *geometrical phase*, or the *Berry phase*. From Eq. (5.8) the Berry phase factor is

$$e^{i\gamma(t)} = e^{-\int_0^t \langle \psi_n(t') | \partial_{t'} \psi_n(t') \rangle dt'}. \tag{5.9}$$

The Berry phase is

$$\gamma(t) = -\int_0^t \langle \psi_n(t') | \partial_{t'} \psi_n(t') \rangle \, dt'. \tag{5.10}$$

Typically, $|\psi_n(t)\rangle$ depends on time through some parameters $R_1, R_2 \ldots R_N$. One of these parameters could be for example, a hopping amplitude or a magnetic field strength. This allows one to rewrite

$$\frac{\partial}{\partial t} |\psi_n(t)\rangle = \frac{\partial}{\partial R_1} |\psi_n(t)\rangle \frac{\partial R_1}{\partial t} + \frac{\partial}{\partial R_2} |\psi_n(t)\rangle \frac{\partial R_2}{\partial t} + \ldots = \nabla_{\mathbf{R}} |\psi_n(t)\rangle \cdot \frac{\partial \mathbf{R}}{\partial t}. \tag{5.11}$$

Where $|\psi_n(R_1(t), R_2(t) \ldots R_N(t))\rangle$ is written $|\psi_n(\mathbf{R})\rangle$. Plugging Eq. (5.11) into Eq. (5.10),

$$\gamma(t) = i \int_{\mathbf{R}_i}^{\mathbf{R}_f} \langle \psi_n(\mathbf{R}) | \nabla_{\mathbf{R}} | \psi_n(\mathbf{R}) \rangle \cdot \frac{\partial \mathbf{R}}{\partial t'} dt' = i \int_{\mathbf{R}_i}^{\mathbf{R}_f} \langle \psi_n(\mathbf{R}) | \nabla_{\mathbf{R}} | \psi_n(\mathbf{R}) \rangle \cdot d\mathbf{R}.$$

When considering a closed loop in parameter space one finds

$$\boxed{\gamma(t) = \oint i \langle \psi_n(\mathbf{R}) | \nabla_{\mathbf{R}} | \psi_n(\mathbf{R}) \rangle \cdot d\mathbf{R}.} \tag{5.12}$$

Thus, the path in parameter space forms a closed loop and the integral is also closed. This equation was derived by Michael Berry in 1984 [37].

Note that throughout this section it was assumed that the states were non-degenerate. There is a generalization of the Berry phase to the degenerate case in which the geometric phase is realized as a matrix that rotates within the degenerate eigenstates. This is often referred to as the non-Abelian Berry phase. For more details see [14].

5.2.1 Berry Phase in Terms of Relative Phases

To gain a better understanding of the Berry phase it is useful to take a step back and consider a more pictorial description in a discrete Hilbert space. It is possible to define the Berry phase as a sum of relative phases. It will be shown that in the continuous limit, it is possible to regain the form Eq. (5.12).

The relative phase of two quantum states $|\psi_1\rangle, |\psi_2\rangle$ can be written

$$\gamma_{12} = -\arg\langle\psi_1|\psi_2\rangle = -\arg\big[|\langle\psi_1|\psi_2\rangle| e^{-i\gamma_{12}}\big]. \tag{5.13}$$

The overlap is a complex number and the argument of that number is the angle of that number's polar form. The relative phases of interest are those between neighbouring states in different, adiabatically connected Hamiltonians. Let $|\psi_n(\mathbf{R}_1)\rangle$ be an eigenstate of $H(\mathbf{R}_1)$, and $|\psi_n(\mathbf{R}_2)\rangle$ be an eigenstate of $H(\mathbf{R}_2)$ that has been adiabatically evolved from $H(\mathbf{R}_1)$ under the time $t_2 - t_1$. The time dependence of the states is characterized by the time dependence of the parameters $R_1(t), R_2(t) \dots R_N(t)$. The relative phase between these states is

$$\gamma_{\mathbf{R_1},\mathbf{R_2}} = -\arg\langle\psi_n(\mathbf{R}_1)|\psi_n(\mathbf{R}_2)\rangle\,.$$

Consider a gauge transformation

$$|\psi_n(\mathbf{R})\rangle \to e^{i\alpha_n(\mathbf{R})}|\psi_n(\mathbf{R})\rangle\,.$$

The relative phase is obviously not invariant under this transformation,

$$\gamma_{\mathbf{R_1},\mathbf{R_2}} \to e^{i[\alpha_n(\mathbf{R}_2)-\alpha_n(\mathbf{R}_1)]}\gamma_{\mathbf{R_1},\mathbf{R_2}}.$$

Generally, a sum of relative phases,

$$-\arg\big[\,\langle\psi_n(\mathbf{R}_1)|\psi_n(\mathbf{R}_2)\rangle\,\langle\psi_n(\mathbf{R}_2)|\psi_n(\mathbf{R}_3)\rangle\dots\langle\psi_n(\mathbf{R}_{N-1})|\psi_n(\mathbf{R}_N)\rangle\,\big], \tag{5.14}$$

also changes under this transformation because there is no corresponding ket for the first bra and likewise for the last ket. The argument of overlaps Eq. (5.14) is indeed a sum of relative phases because it can be written

$$-\arg\big[\prod_{i=1}^{N-1}\langle\psi_n(\mathbf{R_i})|\psi_n(\mathbf{R_{i+1}})\rangle\,\big] = \sum_{i=1}^{N-1}\gamma_{i,i+1} + 2\pi n, \quad n\in\mathbb{Z}.$$

The factor $2\pi n$ comes about because the argument of a phase outside the range $[0, 2\pi]$ is shifted by this factor to remain inside the range. However, if the Hamiltonian is deformed in such a way as to come back to the original form at the end, that is, form a closed loop in parameter space, then the sum of relative phases,

$$-\arg\big[\,\langle\psi_n(\mathbf{R}_1)|\psi_n(\mathbf{R}_2)\rangle\,\langle\psi_n(\mathbf{R}_2)|\psi_n(\mathbf{R}_3)\rangle\dots\langle\psi_n(\mathbf{R}_{N-1})|\psi_n(\mathbf{R}_N)\rangle\,\langle\psi_n(\mathbf{R}_N)|\psi_n(\mathbf{R}_1)\rangle\,\big],$$

is gauge invariant. In fact, this is an alternative definition of the Berry phase.

$$\gamma = -\arg\big[\,\langle\psi_n(\mathbf{R}_1)|\psi_n(\mathbf{R}_2)\rangle\,\langle\psi_n(\mathbf{R}_2)|\psi_n(\mathbf{R}_3)\rangle\dots\langle\psi_n(\mathbf{R}_N)|\psi_n(\mathbf{R}_1)\rangle\,\big]. \tag{5.15}$$

Thus, *the Berry phase is simply the sum of all the relative phases between neighbouring states as the Hamiltonian is adiabatically deformed in parameter space,* see Figure 5.1.

To see that this is equivalent to Eq. (5.12), let the eigenstates of H be separated by continuous parameters. The relative phase between two neighbouring states becomes

$$\delta\gamma = -\arg\langle\psi_n(\mathbf{R})|\psi_n(\mathbf{R}+d\mathbf{R})\rangle\,.$$

Therefore:

$$e^{-i\delta\gamma} = \frac{\langle\psi_n(\mathbf{R})|\psi_n(\mathbf{R}+d\mathbf{R})\rangle}{|\langle\psi_n(\mathbf{R})|\psi_n(\mathbf{R}+d\mathbf{R})\rangle|}. \tag{5.16}$$

The ket can be expanded to first order in $d\mathbf{R}$,

$$|\psi_n(\mathbf{R}+d\mathbf{R})\rangle = |\psi_n(\mathbf{R})\rangle + \nabla_{\mathbf{R}}|\psi_n(\mathbf{R})\rangle\cdot d\mathbf{R},$$

and the relative phase can be assumed to be small for neighbouring states. Expanding the left hand side of Eq. (5.16) in $\delta\gamma$ and the right hand side in $d\mathbf{R}$ gives

$$1 - i\delta\gamma = \frac{\langle\psi_n(\mathbf{R})|\psi_n(\mathbf{R})\rangle + \langle\psi_n(\mathbf{R})|\nabla_{\mathbf{R}}|\psi_n(\mathbf{R})\rangle\cdot d\mathbf{R}}{|\langle\psi_n(\mathbf{R})|\psi_n(\mathbf{R})\rangle + \langle\psi_n(\mathbf{R})|\nabla_{\mathbf{R}}|\psi_n(\mathbf{R})\rangle\cdot d\mathbf{R}|}.$$

To simplify the denominator, note that $\langle\psi_n(\mathbf{R})|\nabla_{\mathbf{R}}\psi_n(\mathbf{R})\rangle$ with $|\nabla_{\mathbf{R}}\psi_n(\mathbf{R})\rangle \equiv \nabla_{\mathbf{R}}|\psi(\mathbf{R})\rangle$ must be imaginary,

$$\begin{aligned}0 = \nabla_{\mathbf{R}}\langle\psi_n(\mathbf{R})|\psi_n(\mathbf{R})\rangle = \langle\nabla_{\mathbf{R}}\psi_n(\mathbf{R})|\psi_n(\mathbf{R})\rangle + \langle\psi_n(\mathbf{R})|\nabla_{\mathbf{R}}\psi_n(\mathbf{R})\rangle = \\ = \langle\psi_n(\mathbf{R})|\nabla_{\mathbf{R}}\psi_n(\mathbf{R})\rangle + \langle\psi_n(\mathbf{R})|\nabla_{\mathbf{R}}\psi_n(\mathbf{R})\rangle^*\,.\end{aligned}$$

The absolute value in the denominator becomes one, to first order in $d\mathbf{R}$ because, $|a+ib| = \sqrt{a^2-b^2}$ and therefore

$$|\langle\psi_n(\mathbf{R})|\psi_n(\mathbf{R})\rangle + \langle\psi_n(\mathbf{R})|\nabla_{\mathbf{R}}|\psi_n(\mathbf{R})\rangle\cdot d\mathbf{R}| = |\langle\psi_n(\mathbf{R})|\psi_n(\mathbf{R})\rangle - i\mathrm{Im}\langle\psi_n(\mathbf{R})|\nabla_{\mathbf{R}}|\psi_n(\mathbf{R})\rangle\cdot d\mathbf{R}| =$$

$$= \sqrt{\langle\psi_n(\mathbf{R})|\psi_n(\mathbf{R})\rangle^2 - \mathrm{Im}\langle\psi_n(\mathbf{R})|\nabla_{\mathbf{R}}\psi_n(\mathbf{R})\rangle^2\cdot d\mathbf{R}^2} = \langle\psi_n(\mathbf{R})|\psi_n(\mathbf{R})\rangle^2 + \mathcal{O}(d\mathbf{R}^2) = 1.$$

The relative phase becomes

$$\delta\gamma = i\langle\psi_n(\mathbf{R})|\nabla_{\mathbf{R}}|\psi_n(\mathbf{R})\rangle\cdot d\mathbf{R}.$$

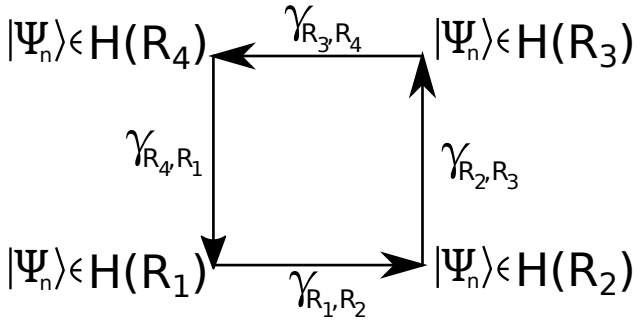

Figure 5.1: The relative phases that contribute to the Berry phase under the deformation of H along a closed path in a discrete parameter space.

By definition, the Berry phase is the sum of relative phases, see Eq. (5.15). In the continuum limit this becomes an integral,

$$\gamma(t) = \oint i \langle \psi_n(\mathbf{R}) | \nabla_{\mathbf{R}} | \psi_n(\mathbf{R}) \rangle \cdot d\mathbf{R} \tag{5.17}$$

which is carried out along a closed loop since the initial and final points in parameter space are the same. This is exactly equation Eq. (5.12).

5.2.2 Berry Connection and Berry Curvature

It is customary to write the Berry phase in terms of the *Berry connection*

$$\boxed{\mathbf{A}(\mathbf{R}) \equiv i \langle \psi_n(\mathbf{R}) | \nabla_{\mathbf{R}} | \psi_n(\mathbf{R}) \rangle .} \tag{5.18}$$

With this definition Eq. (5.17) becomes

$$\gamma(t) = \oint \mathbf{A}(\mathbf{R}) \cdot d\mathbf{R}. \tag{5.19}$$

It was argued that the Berry phase in the discrete limit was gauge invariant, as long as the path in parameter space was closed, Eq. (5.15). This property must of course be fulfilled in the continuum limit and the proof is simple when the Berry connection has been introduced. Under the gauge transformation,

$$|\psi_n(\mathbf{R})\rangle \to e^{i\alpha_n(\mathbf{R})} |\psi_n(\mathbf{R})\rangle ,$$

the Berry connection Eq. (5.18) is transformed according to

$$\mathbf{A}(\mathbf{R}) \to i \Bigg(\langle \psi_n(\mathbf{R}) | e^{-i\alpha_n(\mathbf{R})} \times$$
$$\times \Big[i(\nabla_{\mathbf{R}} \alpha_n(\mathbf{R})) e^{i\alpha_n(\mathbf{R})} |\psi_n(\mathbf{R})\rangle + e^{i\alpha_n(\mathbf{R})} |\nabla_{\mathbf{R}} \psi_n(\mathbf{R})\rangle \Big] \Bigg).$$

The exponentials cancel, what is left is

$$\mathbf{A}(\mathbf{R}) \to \mathbf{A}(\mathbf{R}) - \nabla_{\mathbf{R}} \alpha_n(\mathbf{R}). \tag{5.20}$$

This implies that the Berry phase Eq. (5.19) is transformed as

$$\gamma(t) \to \oint (\mathbf{A}(\mathbf{R}) - \nabla_{\mathbf{R}} \alpha_n(\mathbf{R})) \cdot d\mathbf{R}.$$

The contribution from local phase $\alpha_n(\mathbf{R})$ vanished because the curve is closed ($\mathbf{R}_i = \mathbf{R}_f$), i.e.,

$$\alpha_n(\mathbf{R}_i) - \alpha_n(\mathbf{R}_f) = 0.$$

As such, the Berry phase is gauge invariant[9] (for closed loops in parameter space)

$$\gamma(t) \to \gamma(t). \tag{5.21}$$

It is possible to define the Berry phase in terms of an integral of a gauge invariant quantity. For simplicity, consider a Hamiltonian depending on three continuous parameters. It is the simpler case because then the

[9] This is however not the full story of the gauge invariance of the Berry phase, see Section 5.2.3.

familiar Stoke's theorem from vector calculus can be applied instead of the d-dimensional generalization from differential geometry. The closed path in parameter space is ∂S and it encloses a surface S and the manifold of states is assumed to be smooth. In this case, Stoke's theorem can be applied to Eq. (5.19), turning the line integral into a surface integral,

$$\gamma(t) = \oint_{\partial S} \mathbf{A}(\mathbf{R}) \cdot d\mathbf{R} = \int_S (\nabla_{\mathbf{R}} \times \mathbf{A}(\mathbf{R})) \cdot d\mathbf{S} \equiv \int_S \mathbf{\Omega}(\mathbf{R}) \cdot d\mathbf{S}, \tag{5.22}$$

where $\mathbf{\Omega}(\mathbf{R})$ is called the *Berry curvature*. It can be written as,

$$\boxed{\mathbf{\Omega}(\mathbf{R}) = \nabla_{\mathbf{R}} \times \mathbf{A}(\mathbf{R}) = i\nabla_{\mathbf{R}} \times \langle \psi_n(\mathbf{R}) | \nabla_{\mathbf{R}} \psi_n(\mathbf{R}) \rangle \,.} \tag{5.23}$$

Using the identity $\nabla \times f\mathbf{F} = f(\nabla \times \mathbf{F}) + (\nabla f) \times \mathbf{F}$, and the fact that the curl of a gradient is zero,

$$\mathbf{\Omega}(\mathbf{R}) = i \left\langle \nabla_{\mathbf{R}} \psi_n(\mathbf{R}) \right| \times \left| \nabla_{\mathbf{R}} \psi_n(\mathbf{R}) \right\rangle . \tag{5.24}$$

The Berry curvature is gauge invariant because from Eq. (5.20) it holds that

$$\mathbf{\Omega}(\mathbf{R}) = \nabla_{\mathbf{R}} \times \mathbf{A}(\mathbf{R}) \to \nabla_{\mathbf{R}} \times (\mathbf{A}(\mathbf{R}) - \nabla_{\mathbf{R}} \alpha_n(\mathbf{R})).$$

By the vanishing of the curl of a gradient it follows that

$$\mathbf{\Omega}(\mathbf{R}) \to \mathbf{\Omega}(\mathbf{R}) \tag{5.25}$$

under a gauge transformation. Eqs. (5.22) and (5.24) are valid only for three dimensional parameter space. In the case of a more general Hamiltonian, that depends on d parameters a Berry curvature *tensor*[10] is defined as

$$\Omega_{\mu\nu}(\mathbf{R}) = \frac{\partial}{\partial R^\mu} A_\nu(\mathbf{R}) - \frac{\partial}{\partial R^\nu} A_\mu(\mathbf{R}) = -2\mathrm{Im} \left\langle \partial_\mu \psi_n(\mathbf{R}) | \partial_\nu \psi_n(\mathbf{R}) \right\rangle . \tag{5.26}$$

Using the d dimensional Stoke's theorem

$$\gamma(t) = \frac{1}{2} \int_S dR^\mu \wedge dR^\nu \Omega_{\mu\nu}(\mathbf{R}) \equiv \int_S \mathcal{F}. \tag{5.27}$$

Here $\mathcal{F}$ is referred to as the Berry curvature two-form. For a detailed treatment on this see [14]. For an introduction to *differential forms* and an explanation of the *wedge product* that appears in Eq. (5.27) see appendix B. The Berry curvature vector Eq. (5.24) and the Berry curvature tensor Eq. (5.26) are related by

$$\Omega_{\mu\nu}(\mathbf{R}) = \epsilon_{\mu\nu\rho} \Omega^\rho(\mathbf{R}). \tag{5.28}$$

Berry referred to his findings about the geometrical phase as "mysterious". It was Simon [38] who demystified the notion of geometrical phases by interpreting them as a *holonomy*. If a *connection* is defined for the manifold, then the holonomy of that connection measures how much the geometrical data changes under parallel transport of a closed loop. A *parallel transportation* is a way to move geometrical information (a vector for example) along a manifold. The Berry phase is the quantum mechanical analog of these kinds of classical holonomies [14]. A connection is needed to define parallel transport and are usually defined in the context of *principal fiber bundles*. A simpler way of discussing connections is in terms of *covariant derivatives* [39]. For a proper review on Berry phase and parallel transport see [38].

[10] The Berry curvature is a tensor under coordinate transformations which means that it transforms like, $\Omega_{\mu\nu} = \frac{\partial x^\lambda}{\partial x^\mu} \frac{\partial x^\rho}{\partial x^\nu} \Omega_{\lambda\rho}$.

5.2.3 Gauge Invariance Modulo 2π

So far, the adiabatic deformation has been closed in the sense that $\mathbf{R}$ comes back to the initial point with the same numerical value. In this way

$$\mathbf{R}_i = \mathbf{R}_f \Rightarrow \alpha_n(\mathbf{R}_i) - \alpha_n(\mathbf{R}_f) = 0.$$

But, if a parameter is periodic in the same sense as the xy-plane angle ϕ in spherical coordinates, where $\phi = 0$ and $\phi = 2\pi$ are identified physically as the same point, then the gauge invariance of the Berry phase is not ensured. In these considerations position is taken as a parameter that can be varied. The angle ϕ is limited to the interval $[0, 2\pi]$ and physically $\phi = 0$ and $\phi = 2\pi$ represent the same point in real space, but the local parameter $\alpha_n(\mathbf{R})$ need not be aware of this fact. Such that, if the path in parameter space starts at the state corresponding to $\phi = 0$ and ends at the state corresponding to $\phi = 2\pi$, then the local parameter $\alpha_n(\mathbf{R})$ can differ between these states, but because they are physically the same, it can only differ by 2π times an integer. That is

$$\mathbf{R}_i \text{ is physically equal to } \mathbf{R}_f \Rightarrow \alpha_n(\mathbf{R}_i) - \alpha_n(\mathbf{R}_f) = 2\pi m, \quad m \in \mathbb{Z}.$$

The same is true for the discrete case where the first bra and the last ket correspond to the physically equivalent but different states.

Theorem 5.2 (Gauge invariance of the Berry phase) *In general, the Berry phase is gauge invariant up to $2\pi n$. It is invariant as a phase.*

The formula Eq. (5.21) is generalized to

$$\boxed{\gamma(t) \to \gamma(t) + 2\pi n} \tag{5.29}$$

for parameters that are periodic in the sense mentioned above. The same considerations apply when momentum which is periodic in the Brillouin zone is considered as a parameter. It will be shown that this fact is strongly related to quantization of *Chern number*.

5.3 Calculation of the Berry phase of a Two-Band Model

Consider the following Hamiltonian matrix which describes a spinful particle in a magnetic field

$$\mathcal{H}(\mathbf{B}) = -\mathbf{B} \cdot \boldsymbol{\sigma} + B. \tag{5.30}$$

The magnetic field $\mathbf{B}$ with $B = |\mathbf{B}|$ is considered a parameter that can be varied. The shift B was put in for convenience such that the two eigenstates become

$$\mathcal{H}(\mathbf{B}) \left|+\right\rangle = 2B \left|+\right\rangle, \quad \mathcal{H}(\mathbf{B}) \left|-\right\rangle = 0.$$

In spherical coordinates the magnetic field becomes

$$\mathbf{B} = \left(B \sin\theta \cos\phi, B \sin\theta \sin\phi, B \cos\theta\right).$$

It should be noted that nothing is assumed about the vector $\mathbf{B}$, hence, this is a general two-band model. The name was simply chosen to make the analogy with magnetic monopoles clearer, but from here on $\mathbf{B}$ will be considered a generic vector parameter of $\mathcal{H}(\mathbf{B})$. The Hamiltonian Eq. (5.30) rewritten in spherical coordinates takes the form

$$\mathcal{H}(\mathbf{B}) = -B \begin{pmatrix} \cos\theta - 1 & e^{-i\phi} \sin\theta \\ e^{i\phi} \sin\theta & -\cos\theta - 1 \end{pmatrix}.$$

The eigenstates are given by,

$$|-\rangle = \begin{pmatrix} e^{-i\phi}\cos(\frac{\theta}{2}) \\ \sin(\frac{\theta}{2}) \end{pmatrix}, \quad |+\rangle = \begin{pmatrix} e^{-i\phi}\sin(\frac{\theta}{2}) \\ -\cos(\frac{\theta}{2}) \end{pmatrix}.$$

Note that when the polar angle $\theta = 0$ or π, the azimutal angle $\phi = \arctan(\frac{y}{x})$ is undefined because $x = y = 0$ at those two points on the sphere. If at any time, $\theta = 0$ or π and ϕ is present, then the states are not well defined. As a result, one has to remove ϕ by some gauge transformation. In fact, there is no way of finding a gauge in which the eigenstates are well defined all over the sphere [19]. The state $|+\rangle$ is undefined when $\theta = \pi$. When $\theta = 0$ there is no problem because ϕ is not present.

The evolution of the state $|+\rangle$ is now calculated as the parameter $\mathbf{B}$ (or effectively B, θ, ϕ) is varied. For now, the parameters will be varied in such a way as to avoid the south pole ($\theta = \pi$). For the Berry connection Eq. (5.18) the quantity to compute is,

$$\langle +|\nabla +\rangle .$$

The gradient in spherical coordinates is

$$\nabla |+\rangle = \hat{\mathbf{r}}\frac{\partial}{\partial r}|+\rangle + \hat{\boldsymbol{\theta}}\frac{1}{r}\frac{\partial}{\partial \theta}|+\rangle + \hat{\boldsymbol{\phi}}\frac{1}{r\sin\theta}\frac{\partial}{\partial \phi}|+\rangle =$$

$$= \hat{\boldsymbol{\theta}}\frac{1}{2r}\begin{pmatrix} e^{-i\phi}\cos(\frac{\theta}{2}) \\ \sin(\frac{\theta}{2}) \end{pmatrix} + \hat{\boldsymbol{\phi}}\frac{1}{r\sin\theta}\begin{pmatrix} (-i)e^{-i\phi}\sin(\frac{\theta}{2}) \\ 0 \end{pmatrix}.$$

Here $r = B$ is really the radius of $\mathbf{B}$ in spherical coordinates. From this it is found that

$$\langle +|\nabla +\rangle = \hat{\boldsymbol{\phi}}\frac{i}{r\sin\theta}\sin^2(\frac{\theta}{2}).$$

One now evaluates the Berry curvature Eq. (5.23),

$$\nabla \times \langle +|\nabla +\rangle .$$

The curl in spherical coordinates is

$$\nabla \times \mathbf{f} = \frac{\hat{\boldsymbol{r}}}{r\sin\theta}\left(\frac{\partial(f_\phi \sin\theta)}{\partial\theta} - \frac{\partial f_\theta}{\partial\phi}\right) + \frac{\hat{\boldsymbol{\theta}}}{r}\left(\frac{1}{\sin\theta}\frac{\partial f_r}{\partial\phi} - \frac{\partial(f_\phi r)}{\partial r}\right) + \frac{\hat{\boldsymbol{\phi}}}{r}\left(\frac{\partial(f_\theta r)}{\partial r} - \frac{\partial f_r}{\partial\theta}\right).$$

From this is it found that

$$\nabla \times \langle +|\nabla +\rangle = \frac{i}{2}\frac{\hat{\boldsymbol{r}}}{r^2}.$$

Such that,

$$\boldsymbol{\Omega} = -\frac{\hat{\boldsymbol{r}}}{2r^2} = -\frac{\hat{\boldsymbol{B}}}{2B^2}.$$

Using equation Eq. (5.28), namely $\Omega_{\mu\nu}(\mathbf{R}) = \epsilon_{\mu\nu\rho}\Omega_\rho(\mathbf{R})$, this can be written in index notation

$$\Omega_{ij} = -\epsilon_{ijk}\frac{B_k}{2|B|^3}.$$

The Berry phase is given by Eq. (5.22),

$$\gamma(t) = \int_S \boldsymbol{\Omega}(\mathbf{R})\cdot d\mathbf{S},$$

with the surface element

$$d\mathbf{S} = B^2 d\Omega \hat{\boldsymbol{r}}.$$

The non-bold, non-indexed omega denotes the solid angle. The Berry phase becomes

$$\gamma = -\frac{1}{2}\int_S d\Omega = -\frac{\Omega}{2}.$$

Thus, the Berry phase for a two-band model is just minus half of the solid angle swept out by the magnetic field as it is varied in such a way as to come back to itself.

If one evaluates the integral over a closed surface, interesting results emerge. This will be done in Chapter 6 on Chern numbers.

5.4 The Aharonov–Bohm Effect

Classically, the (magnetic) vector potential[11] $\mathbf{A}$ is unphysical. The physics is contained within the electric and magnetic fields. This is not entirely true quantum mechanically and this is the subject of the *Aharonov-Bohm effect*. It is a phenomenon in which a charged particle is affected by the vector potential in a region where the electric and magnetic fields vanish. It will be shown that it is essentially the Berry phase which allows the vector potential to induce observable effects. Even though the Aharonov-Bohm effect is not directly relevant to topological band theory it provides a pedagogical explanation for how the Berry phase can have observable effects.

Consider the following experiment, a particle is free to move outside of a solenoid with a magnetic field pointing upwards in the $\hat{\mathbf{z}}$-direction. The magnetic field vanish everywhere outside the solenoid. The particle is confined inside a box, the condition is enforced by adding a potential which is infinite outside the box. The box is taken to be small enough such that the vector potential is approximately constant inside. Let one of the box's edge coordinate be $\mathbf{R}$. The eigenstate is given by [37]

$$\langle \mathbf{r}|\psi_n(\mathbf{R})\rangle = e^{\frac{ie}{\hbar}\int_{\mathbf{R}}^{\mathbf{r}} \mathbf{A}(\mathbf{r}')\cdot d\mathbf{r}'}\phi_n(\mathbf{r}-\mathbf{R}). \tag{5.31}$$

where $\phi_n(\mathbf{r}-\mathbf{R})$ is the nth wave function for a particle in a box problem [40] and $e<0$ is the charge of an electron. It is this eigenstate which will be deformed as the parameter $\mathbf{R}$ is varied. This is the eigenstate for any value of $\mathbf{R}$, the snapshot eigenstate. The goal is to calculate the Berry phase from when the box is swept around the solenoid while being maintained in the plane. The Berry connection Eq. (5.18) becomes

$$\mathbf{A}_c(\mathbf{R}) = i\left\langle \psi_n(\mathbf{R})|\nabla_{\mathbf{R}}\psi_n(\mathbf{R})\right\rangle.$$

To avoid confusion, the index c has been given to the Berry connection. Insert a position identity

$$\mathbf{A}_c(\mathbf{R}) = i\int d\mathbf{r} e^{-\frac{ie}{\hbar}\int_{\mathbf{R}}^{\mathbf{r}} \mathbf{A}(\mathbf{r}')\cdot d\mathbf{r}'}\phi_n^*(\mathbf{r}-\mathbf{R})\nabla_{\mathbf{R}}\left(e^{\frac{ie}{\hbar}\int_{\mathbf{R}}^{\mathbf{r}} \mathbf{A}(\mathbf{r}')\cdot d\mathbf{r}'}\phi_n(\mathbf{r}-\mathbf{R})\right).$$

Note that $\nabla_{\mathbf{R}}\int_{\mathbf{R}}^{\mathbf{r}}\mathbf{A}(\mathbf{r}')d\mathbf{r}' = -\nabla_{\mathbf{R}}\int_{\mathbf{r}}^{\mathbf{R}}\mathbf{A}(\mathbf{r}')d\mathbf{r}' = -\mathbf{A}(\mathbf{R})$ by the fundamental theorem of calculus. The result becomes

$$\mathbf{A}_c(\mathbf{R}) = i\int d\mathbf{r}\phi_n^*(\mathbf{r}-\mathbf{R})\left(-\frac{ie}{\hbar}\mathbf{A}(\mathbf{R})\phi_n(\mathbf{r}-\mathbf{R}) + \nabla_{\mathbf{R}}\phi_n(\mathbf{r}-\mathbf{R})\right). \tag{5.32}$$

The second term of Eq. (5.32) vanishes for a particle in a box problem [40]. This gives

$$\mathbf{A}_c(\mathbf{R}) = \frac{e}{\hbar}\mathbf{A}(\mathbf{R})$$

[11] Not to be confused with the Berry connection, even though there are similarities.

by orthonormality of $\phi_n(\mathbf{r}-\mathbf{R})$. It is curious how the Berry connection, which is similar to the gauge potential of electromagnetism in this case equals the gauge potential. The Berry phase Eq. (5.19) becomes

$$\gamma(t) = \oint \mathbf{A}_c(\mathbf{R}) \cdot d\mathbf{R} = \frac{e}{\hbar} \oint \mathbf{A}(\mathbf{R}) \cdot d\mathbf{R}. \tag{5.33}$$

The box takes one full turn in the plane such that the integral is a closed loop. By Stoke's theorem the vector potential in a circle around the solenoid equals the integral over magnetic field of the enclosed surface, this is

$$\gamma(t) = \int_S \mathbf{B}(\mathbf{R}) \cdot d\mathbf{S}.$$

The magnetic field is of constant strength B inside the solenoid and the area with non-vanishing magnetic field is the area of the solenoid itself. Thus, the integral becomes

$$\gamma(t) = \frac{e}{\hbar} BA \equiv -\frac{e}{\hbar}\Phi,$$

where A is the area of the solenoid and Φ is known as the *magnetic flux*. The eigenstate picks up a geometrical phase which depends on the strength of the magnetic flux due to the presence of a vector potential. Thus the Aharonov-Bohm effect can be interpreted in terms of geometrical phase factors, experiments confirming the effect have been carried out [41].

6 Chern Number

The Chern number is a topological invariant and it is defined as the surface integral of the Berry curvature over a *closed surface*. This surface may be the entire manifold of parameter space or a subset of that, as long as it is closed, see Figure 6.1.

In a three-dimensional parameter space the Chern number is integrated over a two dimensional surface and is similar to the Berry phase of three dimensional parameter space Eq. (5.22). The definition[12] of a Chern number in three-dimensional parameter space [13] is

$$\boxed{C = \frac{1}{2\pi} \oint_S \mathbf{\Omega}(\mathbf{R}) \cdot d\mathbf{S}.} \tag{6.1}$$

In index notation for an arbitrary dimensional parameter space this becomes

$$C = \frac{1}{4\pi} \oint_S dR^\mu \wedge dR^\nu \Omega_{\mu\nu}(\mathbf{R}) = \frac{1}{2\pi} \oint_S \mathcal{F}, \tag{6.2}$$

where Eq. (5.27) was integrated over a closed surface. From here on out, *momentum is considered a parameter of the Hamiltonian.* This allows for the Chern number to be integrated over the closed surface that is the Brillouin zone. The Chern number becomes

$$C = \frac{1}{2\pi} \oint_{1BZ} \Omega_{xy} d^2k, \tag{6.3}$$

with a Berry curvature defined by

$$\Omega_{xy} = \frac{\partial A_x}{\partial k_y} - \frac{\partial A_x}{\partial k_x}, \tag{6.4}$$

and the Berry connection in the first Brillouin zone as

$$A_i(\mathbf{k}) = i \left\langle \psi_{\mathbf{k}} | \partial_{k_i} | \psi_{\mathbf{k}} \right\rangle . \tag{6.5}$$

Any further parameters are not integrated over and may be deformed in the usual sense. The Chern number integrated over a Brillouin zone is often called a Zak phase [42], after the person who first considered it.

Consider again the general two-band model

$$\mathcal{H}(\mathbf{R}) = \mathbf{h}(\mathbf{R}) \cdot \boldsymbol{\sigma}, \quad \mathbf{h}(\mathbf{R}) = (h_x, h_y, h_z), \tag{6.6}$$

that depends on three parameters $\mathbf{R}$. The vector $\mathbf{h}(\mathbf{R})$ is a new parameterization of $\mathbf{R}$ in terms of three independent parameters h_x, h_y and h_z. The Berry curvature is

$$\mathbf{\Omega} = \frac{\mathbf{h}}{2h^3} \tag{6.7}$$

in accordance with Section 5.3. With $\Omega_{\mu\nu}$ given by $\Omega_{\mu\nu} = \epsilon_{\mu\nu\rho}\Omega^\rho$, the Chern number Eq. (6.2) becomes

$$C = \frac{1}{4\pi} \oint_S \epsilon_{\mu\nu\rho} \Omega^\rho dh^\mu \wedge dh^\nu = \frac{1}{8\pi} \oint_S \epsilon_{\mu\nu\rho} \frac{h^\rho}{h^3} dh^\mu \wedge dh^\nu.$$

[12] There are more general Chern numbers in mathematics. But in physics, the study of adiabatic phases leads to this particular quantity which is identified as a Chern number.

[13] This is known as the *first Chern number.* The *second Chern number* is defined analogously but in four dimensions.

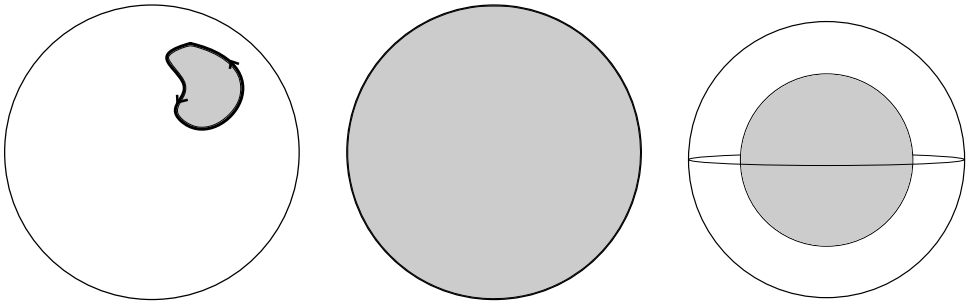

(a) The open surface being integrated over in the calculation of a Berry phase.

(b) A closed surface being integrated over in the calculation of a Chern number could be the entire parameter space.

(c) A closed surface being integrated over in the calculation of a Chern number can be any closed surface.

Figure 6.1: The difference in region of integration between the Berry phase (a) and Chern number (b)-(c), for a parameter space characterized by a sphere.

It is assumed that two of the parameters are the x and y momenta and therefore the closed surface in parameter space that is to be integrated over is taken to be the Brillouin zone torus. In this way, the closed surface S is the image of the Brillouin zone in $\mathbf{h}$-space. This can be rewritten to be integrated over momentum

$$C = \frac{1}{8\pi} \oint_S \epsilon_{\mu\nu\rho} \frac{h^\rho}{h^3} \frac{\partial h^\mu}{\partial k^\alpha} \frac{\partial h^\nu}{\partial k^\beta} dk^\alpha \wedge dk^\beta.$$

Using that

$$\epsilon_{\mu\nu\rho} \frac{h^\rho}{h^3} \frac{\partial h^\mu}{\partial k^\alpha} \frac{\partial h^\nu}{\partial k^\beta} = \frac{1}{h^3} \left[h_x \left(\frac{\partial h^y}{\partial k^\alpha} \frac{\partial h^z}{\partial k^\beta} - \frac{\partial h^z}{\partial k^\alpha} \frac{\partial h^y}{\partial k^\beta} \right) - h_y \left(\frac{\partial h^x}{\partial k^\alpha} \frac{\partial h^z}{\partial k^\beta} - \frac{\partial h^z}{\partial k^\alpha} \frac{\partial h^x}{\partial k^\beta} \right) \right.$$
$$\left. + h_z \left(\frac{\partial h^x}{\partial k^\alpha} \frac{\partial h^y}{\partial k^\beta} - \frac{\partial h^y}{\partial k^\alpha} \frac{\partial h^x}{\partial k^\beta} \right) \right] = \frac{\mathbf{h}}{h^3} \cdot \left(\frac{\partial \mathbf{h}}{\partial k^\alpha} \times \frac{\partial \mathbf{h}}{\partial k^\beta} \right)$$

the Chern number in vector form is

$$C = \frac{1}{8\pi} \int_{BZ} \mathbf{h} \cdot \left(\frac{\partial \mathbf{h}}{\partial k^\alpha} \times \frac{\partial \mathbf{h}}{\partial k^\beta} \right) dk^\alpha \wedge dk^\beta.$$

For momentum in the xy-plane then

$$C = \frac{1}{8\pi} \int_{BZ} \mathbf{h} \cdot \left(\frac{\partial \mathbf{h}}{\partial k^x} \times \frac{\partial \mathbf{h}}{\partial k^y} \right) dk^x \wedge dk^y. \tag{6.8}$$

This is a general result for any two-band model.

6.1 Quantization of the Chern Number

At first, it might seem that C should be zero. A closed surface does not have a boundary and therefore, by Stoke's theorem, the integral over a closed surface vanishes. There exists a similar statement, the *Gauss-Bonnet theorem* [15], which says that the closed integral of the Gaussian curvature is an integer. Here, two arguments will be made that show that Chern number can be non-zero.

6.1.1 No Continuous Global Gauge

The Berry curvature $\mathbf{\Omega}$ has singularities on the unit sphere at points which depend on the chosen gauge. Because no gauge can get rid of all singularities everywhere on the sphere [19], one is forced to use different gauges for different parts of the surface. Because the Berry phase is gauge invariant modulo 2π, this can lead to to a non-zero Chern number.

Following the reasoning of [22] consider the Berry phase from Figure 6.1 (a). The surface enclosed by the loop is ambiguous. The usual choice is the smaller, shaded region, S_+, but the complement of that region, S_-, is of course also enclosed. Chern number is the integral over the entire region, which can be separated into an integral over the shaded and the unshaded part.

$$C = \frac{1}{2\pi} \oint_S \mathbf{\Omega}(\mathbf{R}) \cdot d\mathbf{S} = \frac{1}{2\pi} \left(\int_{S_+} \mathbf{\Omega}(\mathbf{R}) \cdot d\mathbf{S} + \int_{S_-} \mathbf{\Omega}(\mathbf{R}) \cdot d\mathbf{S} \right). \tag{6.9}$$

Now suppose that the Berry curvature is singular once only on the sphere and that the singularity lies in the region S_-. The Berry curvature is gauge invariant (Eq. (5.25)) and so one is free to calculate the integral over S_- in a gauge which makes the Berry curvature well-defined everywhere, so that Eq. (6.9) becomes

$$C = \frac{1}{2\pi} \left(\int_{S_+} \mathbf{\Omega}(\mathbf{R}) \cdot d\mathbf{S} + \int_{S_-} \mathbf{\Omega}'(\mathbf{R}) \cdot d\mathbf{S} \right). \tag{6.10}$$

The boundary ∂S of the two surfaces is the same, but it has opposite orientation. Applying Stoke's theorem as in Eq. (5.22)

$$\oint_{S_\pm} \mathbf{\Omega}(\mathbf{R}) \cdot d\mathbf{S} = \pm \oint_{\partial S} \mathbf{A}(\mathbf{R}) \cdot d\mathbf{S}.$$

The Chern number Eq. (6.10) becomes

$$C = \frac{1}{2\pi} \oint_{\partial S} \mathbf{A}(\mathbf{R}) \cdot d\mathbf{S} - \frac{1}{2\pi} \oint_{\partial S} \mathbf{A}'(\mathbf{R}) \cdot d\mathbf{S}.$$

This is by Eq. (5.19) the difference of two Berry phases $C = \frac{1}{2\pi}(\gamma - \gamma')$ over the same path but the Berry connections $\mathbf{A}(\mathbf{R})$ differ by a gauge transformation. Therefore, by gauge invariance modulo 2π of Berry phases it is found that

$$C = \frac{1}{2\pi}(\gamma - \gamma') = \frac{1}{2\pi}(\gamma - \gamma + 2\pi n) = n. \tag{6.11}$$

Therefore the Chern number is an integer.

$$C = n \in \mathbb{Z}.$$

Being an integer, the Chern number can not be changed by any continuous deformation and therefore C is a topological invariant. If the Berry connection was well-defined everywhere on the sphere then the Chern number would indeed vanish by Stoke's theorem. Due to the singularities that arise, this is not the case.

6.1.2 Chern Number and Monopoles

Another way to understand that the Chern number is non-zero comes from intuition about charges and the accompanying flux. In Section 5.3 the eigenstate $|+\rangle$ of the Hamiltonian $\mathcal{H}(\mathbf{B}) = -\mathbf{B} \cdot \boldsymbol{\sigma} + B$ was deformed as $\mathbf{B}$ was changed. The Berry curvature was found to be

$$\mathbf{\Omega}(\mathbf{R}) = -\frac{\hat{\mathbf{B}}}{2B^2} = -\frac{\mathbf{B}}{2B^3}, \tag{6.12}$$

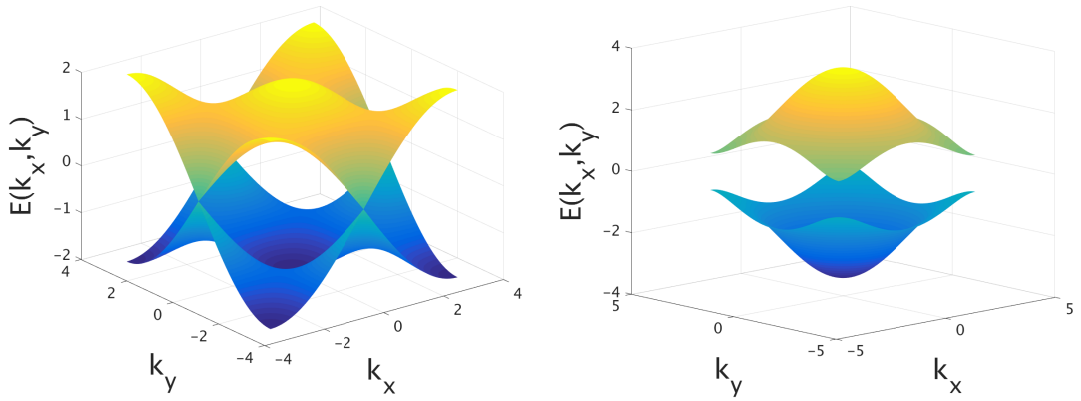

(a) Energy spectrum of the QWZ model with $u = 0$.

(b) Energy spectrum of the QWZ model with $u = 1.4$.

Figure 6.2: The energy spectrum of the QWZ model has gap closing for certain values of the parameter u. One such example is shown in (a). Panel (b) shows that the model is gapped for a generic value of μ.

where the Berry phase was to be computed with

$$\gamma(t) = \int_S \mathbf{\Omega}(\mathbf{R}) \cdot d\mathbf{R}.$$

Consider closing the surface of integration, that is, let S be a closed surface. In doing so, the calculation takes the form of a Chern number Eq. (6.1) times 2π.

The curious thing about Eq. (6.12) is that it has the form of an *effective magnetic monopole*. It is the field given by Coulomb's law for a hypothetical point charge with magnetic charge $-1/2$. Gauss's law from electromagnetism relates the flux Φ_E of the electric field $\mathbf{E}$ out of a closed surface to the enclosed charge

$$\Phi_E = \oint_S \epsilon_0 \mathbf{E} \cdot d\mathbf{S} = mq,$$

where m is the number of identical particles of charge q enclosed. Any charge located outside the surface must have its field lines enter and leave the surface and therefore does not contribute to the flux. Only enclosed charges contribute to the net flux. In an analogous way, the closed surface integral enclosing effective magnetic monopoles, $\mathbf{\Omega}(\mathbf{R})$ in this case, of charge $q_{mag} = -1/2$ gives[14]

$$\Phi_M = \oint_S \mathbf{\Omega}(\mathbf{R}) \cdot d\mathbf{S} = 4\pi m q_{mag}. \tag{6.13}$$

This measures the flux out of the surface S generated by the field $\mathbf{\Omega}$. Finally, using Eqs. (6.1) and (6.13) with $q_{mag} = -1/2$ it is found that

$$C = m = \text{The number of enclosed monopoles.} \tag{6.14}$$

[14]The factor 4π appears because of the difference in prefactors of E and B. The electric field from a point charge is given by

$$\boldsymbol{E} = \left(\frac{mq}{4\pi\epsilon_0}\right)\frac{\boldsymbol{r}}{r^3}.$$

Comparing this to the field containing the monopole Eq. (6.12) it is seen that there is no factor 4π.

Combining what was learned about monopoles and about the singularities in the previous section it can be concluded that, *whenever there is a monopole enclosed by the surface, then there exists singularities in the Berry curvature (implying that there is no global gauge) and hence a non-zero Chern number arises.*

6.2 The Qi-Wu-Zhang (QWZ) Model

A model with a non-zero value of the Chern number over the Brillouin zone is commonly referred to as a *Chern insulator*. To do an example, let the Hamiltonian of Eq. (6.6) be described by

$$\mathbf{h}(\mathbf{k}) = (\sin k_x, \sin k_y, u + \cos k_x + \cos k_y). \tag{6.15}$$

This is the Qi-Wu-Zhang (QWZ) model which corresponds to a tight-binding model with a nearest neighbor approximation on a square lattice [14]. The spectrum of this two-band model is computed by diagonalization and is given by

$$E_\pm = \pm|\mathbf{h}(k_x, k_y)| = \pm\sqrt{\sin^2 k_x + \sin^2 k_y + (u + \cos k_x + \cos k_y)^2}. \tag{6.16}$$

The energy spectrum for two values of the parameter u is given in Figure 6.2. It is straightforward to find that the energy gap closes at

$$\begin{cases} u = -2: & k_x = k_y = 0, \\ u = \ \ 0: & k_x = 0, k_y = \pi \text{ and } k_x = \pi, k_y = 0, \\ u = +2: & k_x = k_y = \pi, \end{cases} \quad .$$

At the various gap closings the system shows what is known as *Dirac points*. There the dispersion relation is characterized by linear dependence on momentum.

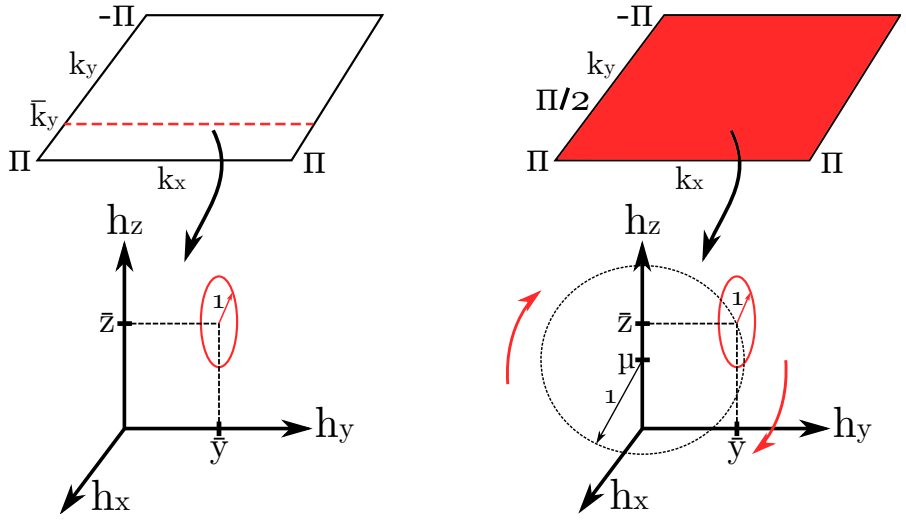

(a) For fixed y-momentum $\bar{k}_y$ the surface Σ is a unit circle in the xz-plane with the centre $(\bar{y}, \bar{z})$ given by Eq. (6.17).

(b) When $k_y \in [-\pi, \pi]$ the centre coordinate of the circle of panel (a) follows another unit circle with a centre given by Eq. (6.18).

Figure 6.3: Illustration of the surface of the image of the Brillouin zone in parameter space.

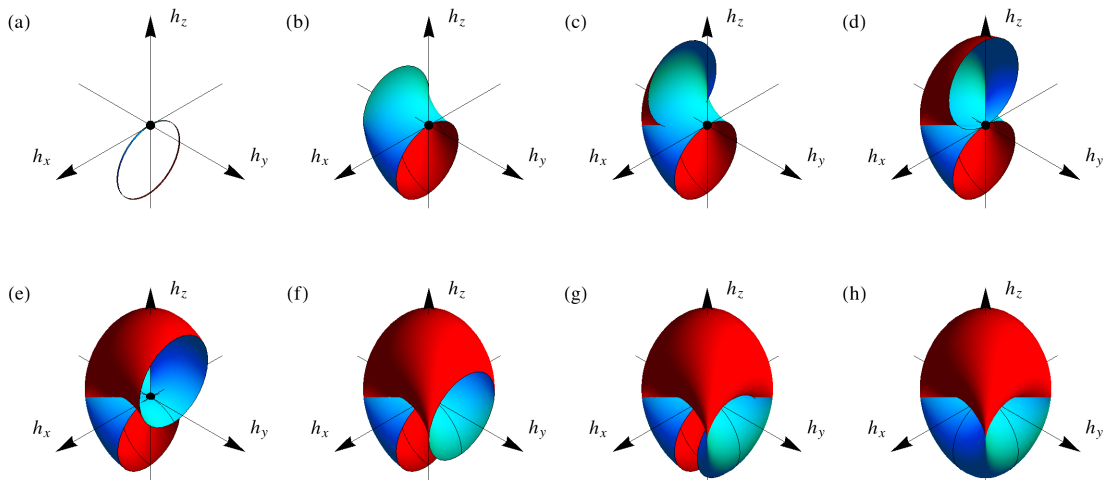

Figure 6.4: Gradual sweep of the surface of the image of the Brillouin zone in parameter space. In panel (a) $k_y = 0$ and $k_x \in [-\pi, \pi]$, the subsequent panels shows the evolution of the surface when k_y is allowed to take on further values in the Brillouin zone. The inside of the surface (red) contributes to a positive flux out of the torus, while the upper half of the torus has switched insides and outsides thus the outside (blue) contributes negatively to the flux. Figure credit: J. Asbóth *et al.* A Short Course on Topological Insulators: Band-structure topology and edge states in one and two dimensions.

In most scenarios there are multiple equivalent ways of determining the topological invariant of a model. Different situations call for different approaches. In the present case, a Chern number is to be calculated. There are several ways to do this. 1.) A brute force calculation of Eq. (6.8) with the **h**-space parameters given by Eq. (6.15). This turns out to be, even for this rather simple model, analytically very challenging. 2.) The Chern number can be interpreted as number of times the surface $\mathbf{h}(\mathbf{k})$ (when the momenta sweep through the Brillouin zone) wraps around the unit sphere [14]. Note the similarities to a winding number. 3.) The monopole interpretation given in section 6.1.2 can applied, thus requiring the identification of degeneracies in the image of the Brillouin zone in parameter space.

The third option turns out to be simple enough in this case. When k_x, k_y sweep through the Brillouin zone, $\mathbf{h}(k)$ traces out a closed torus in the parameter space. Let this surface be denoted by Σ. If, at any Brillouin zone point, the surface intersects the origin of parameter space, then the gap closes (see Eq. (6.16)) and there is a possibility of a topological phase transition. It is known that the origin can be interpreted as the source of a monopole from Eq. (6.7).

What does the surface Σ look like? For the moment let k_y be fixed $k_y = \bar{k}_y$ and let $k_x \in [-\pi, \pi]$. The parameters Eq. (6.15) become

$$h_x = \sin k_x, \quad h_y = \sin \bar{k}_y \equiv \bar{y}, \quad h_z = (u + \cos \bar{k}_y) + \cos k_x \equiv \bar{z} + \cos k_x. \tag{6.17}$$

From this it is found that

$$h_x^2 + (h_z - \bar{z})^2 = \sin^2 k_x + \cos^2 k_x = 1,$$

which is the equation for a circle of radius one centered at $(0, \bar{z})$ in the $h_x h_z$-plane. The circle intersects the h_y-axis at $h_y = \bar{y}$ as illustrated in Figure 6.3 (a). Now let $k_y \in [-\pi, \pi]$ such that the circle traces out a

torus. The centre of the circle in the yz-planes is given by

$$(y, z) = (u + \cos k_y, \sin k_y). \tag{6.18}$$

From

$$y^2 + (z - u)^2 = \sin^2 k_y + \cos^2 k_y = 1$$

it is seen that the center of the original circle which lied in the $h_x h_z$-plane follows a circle of radius one in the $h_y h_z$-plane, see Figure 6.3 (b).

The full torus Σ looks rather complicated. This is because it intersects itself as it changes directions in the y-direction and at the same time the surface also wraps inside out. It is best shown as a gradual sweep of the surface, see Figure 6.4. The inside (red) surface is seen to become the outside between (b) and (c). Likewise, the outside (blue) becomes the inside. Due to the inside-out wrapping of the surface, any flux through the surface becomes negative in those regions.

Having integrated out the momenta the only parameter left to deform is u, which causes the entire torus to be shifted along the z-axis when varied. As a result, whenever $u \in (-2, 0)$ the origin is enclosed in the upper half of the torus, where Σ is wrapped inside out. When $u \in (0, 2)$ the origin is enclosed in the lower half of the torus, where the surface is normally wrapped. Otherwise the origin is not enclosed by the surface.

By equation Eq. (6.14), $C = m =$ The number of enclosed magnetic monopoles, it is found that the Chern number of the QWZ model is

$$C = \begin{cases} 0, & u < -2, \\ -1, & -2 < u < 0, \\ +1, & 0 < u < 2, \\ 0, & 2 < u, \end{cases} .$$

For more illustrations of the torus see [19].

7 Quantum Hall Effect

The Hall effect experiment consists of electrons which are restricted to move in a two dimensional plane. The setup is given by Figure 7.1. Current is allowed to flow out of the sample only in x-direction and a magnetic field is turned on in the z-direction. This will induce a voltage (*Hall voltage*) between the edges of the sample in the y-direction. The transverse (ρ_{xy}) and longitudinal (ρ_{xx}) resistivities will be shown to be linear and constant in the magnetic field strength, respectively, see Figure 7.2 (a). Much more interesting is the resistivities that emerge when the sample is cooled down to very low temperatures and the magnetic field is very strong. The *quantum Hall effect* is the phenomenon which make the resistivities look like Figure 7.2 (b). The line with plateaux is the transverse resistivity and it takes on stable *integer* values (in units of e^2/h) on those plateaux in certain regions of the magnetic field strength. In those regions the longitudinal resistivity is zero, it peaks only when the transverse resistivity changes.

The reason for this phenomenon is topological and will be shown in this Chapter to be related to Chern numbers. Firstly, the classical Hall effect is introduced for background knowledge.

7.1 Classical Hall Effect

The aim is to find the transverse and longitudinal resistivity of the setup given by Figure 7.1. The transverse resistivity is referred to as the *Hall resistivity*. The *conductivity tensor* σ is given by *Ohm's law*,

$$J_\alpha = \sigma_{\alpha\beta} E_\beta. \tag{7.1}$$

The sample itself is taken to be rotationally invariant so the conductivity tensor obeys $S\sigma S^{-1} = \sigma$ with

$$S = \begin{pmatrix} \cos\phi & \sin\phi \\ -\sin\phi & \cos\phi \end{pmatrix}$$

for some angle ϕ. As a consequence σ is given by

$$\sigma = \begin{pmatrix} \sigma_{xx} & \sigma_{xy} \\ -\sigma_{xy} & \sigma_{xx} \end{pmatrix}.$$

The resistivity is simply

$$\rho = \sigma^{-1} = \frac{1}{\sigma_{xx}^2 + \sigma_{xy}^2} \begin{pmatrix} \sigma_{xx} & -\sigma_{xy} \\ \sigma_{xy} & \sigma_{xx} \end{pmatrix} = \begin{pmatrix} \rho_{xx} & \rho_{xy} \\ \rho_{yx} & \rho_{yy} \end{pmatrix}. \tag{7.2}$$

Note that $\rho_{\alpha\beta}$ is not always just $1/\sigma_{\alpha\beta}$. Ultimately, ρ and σ are the quantities of interest.

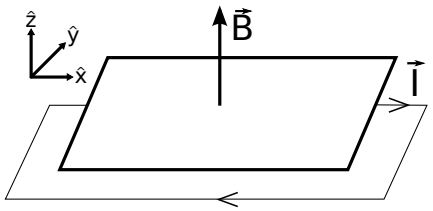

Figure 7.1: Schematic setup of the Hall experiment.

To make current flow, an electric field is turned on such that the electrons flow in the positive x-direction. Due to the presence of a magnetic field, the electrons bend off towards the edge in $-y$-direction. Eventually, a potential difference builds up between that edge and the opposite edge. This induces another electric field which cancels the pull of the magnetic field on the electrons such that they flow in a straight line in x-direction. The voltage induced between the two edges is called the Hall voltage.

The electrons are now moving in both an electric and a magnetic field. Classically, this can be described by the *Drude model*. In the Drude model [43], electrons are essentially considered balls which may "bounce" into each other. A friction term is added to the equation of motion which is given by

$$m\frac{d\mathbf{v}}{dt} = -e\mathbf{E} - e\mathbf{v} \times \mathbf{B} - \frac{m}{\tau}\mathbf{v}. \tag{7.3}$$

The coefficient τ scales as the inverse strength of friction. Of interest are solutions which fulfill $d\mathbf{v}/dt = 0$ (equilibrium). The equation becomes

$$0 = e\mathbf{E} + e\mathbf{v} \times \mathbf{B} + \frac{m}{\tau}\mathbf{v}.$$

The current density is $\mathbf{J} = -ne\mathbf{v}$, using this and moving terms around

$$\mathbf{J} + \frac{\tau e}{m}\mathbf{J} \times \mathbf{B} = \frac{\tau e}{m}\mathbf{E}.$$

The electrons may only move in the plane and the magnetic field is in z-direction. Because of this, the cross product has no $z-$component. Demoting the three component vectors to two component vectors gives

$$\mathbf{J} + \frac{\tau eB}{m}\begin{pmatrix} J_y \\ -J_x \end{pmatrix} = \frac{\tau ne^2}{m}\mathbf{E}.$$

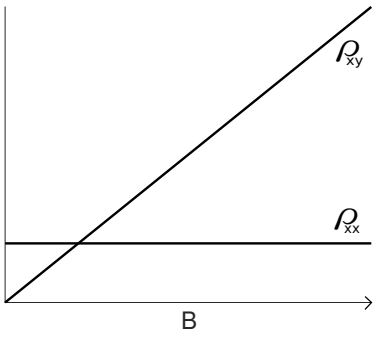

(a) The resistivities of the Hall experiment predicted from the classical Hall effect.

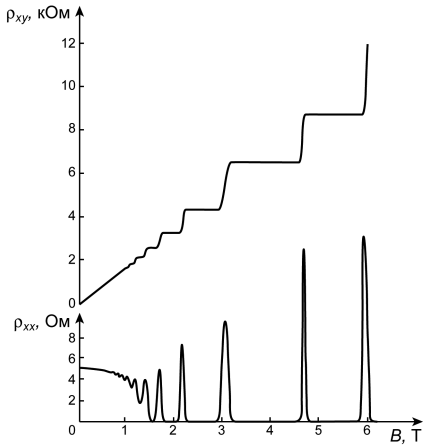

(b) The resistivities measured in a Hall experiment at low temperatures with strong magnetic fields. Figure credit: *Antikon at Russian Wikipedia [GFDL (http://www.gnu.org/copyleft/fdl.html)*

Figure 7.2: Comparison of the Hall experiment outcomes in two different regimes of the parameters. Left (a), describes the classical Hall effect. Right (b) describes the quantum Hall effect.

In matrix form

$$\frac{m}{\tau n e^2}\begin{pmatrix} 1 & \frac{\tau eB}{m} \\ -\frac{\tau eB}{m} & 1 \end{pmatrix}\mathbf{J} = \mathbf{E}.$$

Comparing to Eq. (7.1) this is already the inverse of the conductivity tensor. One can simply read of the Hall and longitudinal resistivity

$$\rho_{xy} = \frac{B}{ne}, \quad \rho_{xx} = \frac{m}{\tau n e^2}.$$

These are the linear and constant resistivities that are measured in the classical Hall effect (Figure 7.2 (a)). However, as the temperature lowers the classical description will be inadequate, which is when quantum mechanics must be applied.

7.2 Kubo Formula Approach to the Hall Conductivity

The goal is to explain the resistivities of the Hall experiment that emerge when temperatures are low and magnetic fields are strong (Figure 7.2 (b)). The focus will be on explaining the plateaux of the Hall resistivity. The derivation will be very general and the starting point is the *Kubo formula* for the Hall conductivity, a result from *linear response theory* [44]. Roughly, linear response theory is concerned with how observables change in the presence of perturbations. The Hamiltonian is given by [43],

$$H = H_0 + \Delta H.$$

The perturbation ΔH describes the applied electric field. The solution of the unperturbed system is known,

$$H_0 \left|n\right\rangle = E_n \left|n\right\rangle.$$

The current due to ΔH depends on the electric field and Ohm's law thus provides the conductivity. The *Kubo formula* for the *Hall conductivity* [43] is

$$\sigma_{xy} = i\hbar \sum_{n\neq 0} \frac{\langle 0|I_y|n\rangle \langle n|I_x|0\rangle - \langle 0|I_x|n\rangle \langle n|I_y|0\rangle}{(E_n - E_0)^2}, \tag{7.4}$$

where I_i is the current in i-direction. Electrons are restricted to move on a two dimensional lattice. Furthermore they are effectively spinless due to the Zeeman splitting of spin up and spin down energy levels brought on by the magnetic field. For strong magnetic fields there is a large splitting and in the low energy limit the upper level can be neglected [43]. Consider non-interacting particles with Bloch wave functions

$$\psi_{\mathbf{k}}(\mathbf{x}) = e^{i\mathbf{k}\cdot\mathbf{x}} u_{\mathbf{k}}(\mathbf{x}).$$

The wave functions are plane waves modulated by a Bloch factor $u_{\mathbf{k}}(\mathbf{x})$ which has the periodicity of the lattice. The distance between lattice points is a and b in x and y respectively. Within the first Brillouin zone

$$-\frac{\pi}{a} < k_x \leq \frac{\pi}{a}, \quad -\frac{\pi}{b} < k_y \leq \frac{\pi}{b}.$$

Momentum in the first Brillouin zone lies on a torus, $\mathbf{k} \in \mathbf{T}^2$. Furthermore, each state in the first Brillouin zone is labeled by a band index

$$\psi^{\alpha}_{\mathbf{k}}(\mathbf{x}) = \langle \mathbf{x}|\mathbf{u}^{\alpha}_{\mathbf{k}}\rangle.$$

The ground state $|0\rangle$ in Eq. (7.4) is made up of all the filled bands (α) and the sum over $\sum_{n\neq 0}$ is made up of the unfilled bands (β). It is assumed that all bands are either completely filled or empty. The Hall conductivity becomes

$$\sigma_{xy} = i\hbar \sum_{\alpha}^{\text{filled}} \sum_{\beta}^{\text{unfilled}} \int_{\mathbf{T}^2} \frac{d\mathbf{k}}{(2\pi)^2} \frac{\langle \mathbf{u}^{\alpha}_{\mathbf{k}}|I_y|\mathbf{u}^{\beta}_{\mathbf{k}}\rangle \langle \mathbf{u}^{\beta}_{\mathbf{k}}|I_x|\mathbf{u}^{\alpha}_{\mathbf{k}}\rangle - \langle \mathbf{u}^{\alpha}_{\mathbf{k}}|I_x|\mathbf{u}^{\beta}_{\mathbf{k}}\rangle \langle \mathbf{u}^{\beta}_{\mathbf{k}}|I_y|\mathbf{u}^{\alpha}_{\mathbf{k}}\rangle}{(E^{\beta}_{\mathbf{k}} - E^{\alpha}_{\mathbf{k}})^2}. \tag{7.5}$$

What is the current I_i? Classically $\mathbf{I} = e\dot{\mathbf{x}}$, but consider the Schrödinger equation of Bloch states

$$H_0 \left|\psi_k\right\rangle = E_{\mathbf{k}} \left|\psi_k\right\rangle \Rightarrow e^{-i\mathbf{k}\cdot\mathbf{x}} H_0 e^{i\mathbf{k}\cdot\mathbf{x}} \left|\mathbf{u}_{\mathbf{k}}\right\rangle = E_{\mathbf{k}} \left|\mathbf{u}_{\mathbf{k}}\right\rangle .$$

Define $\tilde{H}_0 \equiv e^{-i\mathbf{k}\cdot\mathbf{x}} H e^{i\mathbf{k}\cdot\mathbf{x}}$ and let the current be defined by

$$\mathbf{I} = \frac{e}{\hbar}\frac{\partial \tilde{H}_0}{\partial \mathbf{k}}. \tag{7.6}$$

This definition is consistent because the unperturbed Hamiltonian is $H = \frac{1}{2m}(\mathbf{p} + e\mathbf{A})^2$ with $\mathbf{A}$ as the vector potential, hence

$$\tilde{H} = \frac{1}{2m} e^{-i\mathbf{k}\cdot\mathbf{x}}(p^2 + e^2A^2 + 2e\mathbf{p}\cdot\mathbf{A})e^{i\mathbf{k}\cdot\mathbf{x}} = \frac{1}{2m}(\hbar^2\mathbf{k}^2 + e^2\mathbf{A}^2 + 2e\hbar\mathbf{k}\cdot\mathbf{A}).$$

The current Eq. (7.6) becomes

$$\mathbf{I} = \frac{e}{\hbar}\frac{\partial \tilde{H}_0}{\partial \mathbf{k}} = \frac{e}{2m\hbar}(2\hbar^2\mathbf{k} + 2e\hbar\mathbf{A}) = \frac{e}{m}(\hbar\mathbf{k} + e\mathbf{A}) = e\dot{\mathbf{x}}.$$

The last equality follows from the fact that the Lagrangian for an electron in an electromagnetic field in the *Landau gauge* ($\mathbf{A} = xB\hat{\mathbf{y}},\ \ \phi = -Ex$) can be written $L = \frac{1}{2}m + \dot{\mathbf{x}}^2 - e\dot{\mathbf{x}}\dot{\mathbf{A}} + eEx$, with the speed of light $c = 1$. From the definition of canonical momentum $\mathbf{p} = \frac{\partial L}{\partial \dot{\mathbf{x}}} \Rightarrow m\dot{\mathbf{x}} = \mathbf{p} + e\mathbf{A}$.

Inserting Eq. (7.6) into Eq. (7.5),

$$\sigma_{xy} = \frac{ie^2}{\hbar}\sum_{\alpha,\beta}\int_{\mathbf{T}^2}\frac{d\mathbf{k}}{(2\pi)^2}\frac{\langle \mathbf{u}_{\mathbf{k}}^{\alpha}|\partial_{k_y}\tilde{H}|\mathbf{u}_{\mathbf{k}}^{\beta}\rangle \langle \mathbf{u}_{\mathbf{k}}^{\beta}|\partial_{k_x}\tilde{H}|\mathbf{u}_{\mathbf{k}}^{\alpha}\rangle - \langle \mathbf{u}_{\mathbf{k}}^{\alpha}|\partial_{k_x}\tilde{H}|\mathbf{u}_{\mathbf{k}}^{\beta}\rangle \langle \mathbf{u}_{\mathbf{k}}^{\beta}|\partial_{k_y}\tilde{H}|\mathbf{u}_{\mathbf{k}}^{\alpha}\rangle}{(E_{\mathbf{k}}^{\beta} - E_{\mathbf{k}}^{\alpha})^2}. \tag{7.7}$$

To reduce the size of this equation, start by looking at one braket

$$\begin{aligned}\langle \mathbf{u}_{\mathbf{k}}^{\alpha}|\partial_{k_i}\tilde{H}|\mathbf{u}_{\mathbf{k}}^{\beta}\rangle &= \langle \mathbf{u}_{\mathbf{k}}^{\alpha}|\partial_{k_i}\big(\tilde{H}|\mathbf{u}_{\mathbf{k}}^{\beta}\rangle\big) - \langle \mathbf{u}_{\mathbf{k}}^{\alpha}|\tilde{H}|\partial_{k_i}\mathbf{u}_{\mathbf{k}}^{\beta}\rangle = \\ &= \langle \mathbf{u}_{\mathbf{k}}^{\alpha}|\mathbf{u}_{\mathbf{k}}^{\beta}\rangle\, \partial_{k_i}E_{\mathbf{k}}^{\beta} + \langle \mathbf{u}_{\mathbf{k}}^{\alpha}|\partial_{k_i}\mathbf{u}_{\mathbf{k}}^{\beta}\rangle\, E_{\mathbf{k}}^{\beta} - \langle \mathbf{u}_{\mathbf{k}}^{\alpha}|\partial_{k_i}\mathbf{u}_{\mathbf{k}}^{\beta}\rangle\, E_{\mathbf{k}}^{\alpha}.\end{aligned}$$

The last term's $\tilde{H}$ was made to act upon the bra. The overlap $\langle \mathbf{u}_{\mathbf{k}}^{\alpha}|\mathbf{u}_{\mathbf{k}}^{\beta}\rangle$ is zero because α and β are disjoint.

$$\langle \mathbf{u}_{\mathbf{k}}^{\alpha}|\partial_{k_i}\tilde{H}|\mathbf{u}_{\mathbf{k}}^{\beta}\rangle = \langle \mathbf{u}_{\mathbf{k}}^{\alpha}|\partial_{k_i}\mathbf{u}_{\mathbf{k}}^{\beta}\rangle\,(E_{\mathbf{k}}^{\beta} - E_{\mathbf{k}}^{\alpha}) = -\langle \partial_{k_i}\mathbf{u}_{\mathbf{k}}^{\alpha}|\mathbf{u}_{\mathbf{k}}^{\beta}\rangle\,(E_{\mathbf{k}}^{\beta} - E_{\mathbf{k}}^{\alpha}). \tag{7.8}$$

The last equality follows from a product rule. Strategically using either of the two results in Eq. (7.8) and putting it into Eq. (7.7) the Hall conductivity becomes

$$\sigma_{xy} = \frac{ie^2}{\hbar}\sum_{\alpha,\beta}\int_{\mathbf{T}^2}\frac{d\mathbf{k}}{(2\pi)^2}\Big(\,\langle \partial_x\mathbf{u}_{\mathbf{k}}^{\alpha}|\mathbf{u}_{\mathbf{k}}^{\beta}\rangle \langle \mathbf{u}_{\mathbf{k}}^{\beta}|\partial_y\mathbf{u}_{\mathbf{k}}^{\alpha}\rangle - \langle \partial_y\mathbf{u}_{\mathbf{k}}^{\alpha}|\mathbf{u}_{\mathbf{k}}^{\beta}\rangle \langle \mathbf{u}_{\mathbf{k}}^{\beta}|\partial_x\mathbf{u}_{\mathbf{k}}^{\alpha}\rangle\,\Big).$$

Strategically meant using the expression in such a way as to produce resolutions of identity in β. The expression can be rewritten using $\sum_\beta \left|\mathbf{u}_{\mathbf{k}}^{\beta}\right\rangle \left\langle \mathbf{u}_{\mathbf{k}}^{\beta}\right| = \mathbb{1} - \sum_\alpha \left|\mathbf{u}_{\mathbf{k}}^{\alpha}\right\rangle \left\langle \mathbf{u}_{\mathbf{k}}^{\alpha}\right|$. Using this

$$\begin{aligned}\sigma_{xy} \sim &\sum_{\alpha}\big(\,\langle \partial_x\mathbf{u}_{\mathbf{k}}^{\alpha}|\partial_y\mathbf{u}_{\mathbf{k}}^{\alpha}\rangle - \langle \partial_y\mathbf{u}_{\mathbf{k}}^{\alpha}|\partial_x\mathbf{u}_{\mathbf{k}}^{\alpha}\rangle\,\big) + \\ &+\sum_{\alpha,\alpha'}\big(\,\langle \partial_x\mathbf{u}_{\mathbf{k}}^{\alpha}|\mathbf{u}_{\mathbf{k}}^{\alpha'}\rangle \langle \mathbf{u}_{\mathbf{k}}^{\alpha'}|\partial_y\mathbf{u}_{\mathbf{k}}^{\alpha}\rangle - \langle \partial_y\mathbf{u}_{\mathbf{k}}^{\alpha}|\mathbf{u}_{\mathbf{k}}^{\alpha'}\rangle \langle \mathbf{u}_{\mathbf{k}}^{\alpha'}|\partial_x\mathbf{u}_{\mathbf{k}}^{\alpha}\rangle\,\big).\end{aligned} \tag{7.9}$$

However, the second term vanishes because the first part of it can be rewritten like

$$\langle \partial_x \mathbf{u}_\mathbf{k}^\alpha | \mathbf{u}_\mathbf{k}^{\alpha'} \rangle \langle \mathbf{u}_\mathbf{k}^{\alpha'} | \partial_y \mathbf{u}_\mathbf{k}^\alpha \rangle = \big(\partial_x \langle \mathbf{u}_\mathbf{k}^\alpha | \mathbf{u}_\mathbf{k}^{\alpha'} \rangle - \langle \mathbf{u}_\mathbf{k}^\alpha | \partial_x \mathbf{u}_\mathbf{k}^{\alpha'} \rangle \big) \big(\partial_y \langle \mathbf{u}_\mathbf{k}^{\alpha'} | \mathbf{u}_\mathbf{k}^\alpha \rangle - \langle \mathbf{u}_\mathbf{k}^{\alpha'} | \partial_y \mathbf{u}_\mathbf{k}^\alpha \rangle \big) =$$
$$= \langle \partial_y \mathbf{u}_\mathbf{k}^{\alpha'} | \mathbf{u}_\mathbf{k}^\alpha \rangle \langle \mathbf{u}_\mathbf{k}^\alpha | \partial_x \mathbf{u}_\mathbf{k}^{\alpha'} \rangle .$$

Plugging this back into Eq. (7.9) and renaming the sum it is seen to vanish

$$\sum_{\alpha,\alpha'} \big(\langle \partial_y \mathbf{u}_\mathbf{k}^\alpha | \mathbf{u}_\mathbf{k}^{\alpha'} \rangle \langle \mathbf{u}_\mathbf{k}^{\alpha'} | \partial_x \mathbf{u}_\mathbf{k}^\alpha \rangle - \langle \partial_y \mathbf{u}_\mathbf{k}^\alpha | \mathbf{u}_\mathbf{k}^{\alpha'} \rangle \langle \mathbf{u}_\mathbf{k}^{\alpha'} | \partial_x \mathbf{u}_\mathbf{k}^\alpha \rangle \big) = 0.$$

Finally, the Kubo formula has been reduced to

$$\sigma_{xy} = \frac{ie^2}{\hbar} \sum_\alpha \int_{\mathbf{T}^2} \frac{d\mathbf{k}}{(2\pi)^2} \big(\langle \partial_x \mathbf{u}_\mathbf{k}^\alpha | \partial_y \mathbf{u}_\mathbf{k}^\alpha \rangle - \langle \partial_y \mathbf{u}_\mathbf{k}^\alpha | \partial_x \mathbf{u}_\mathbf{k}^\alpha \rangle \big). \tag{7.10}$$

Recall the definition of Berry curvature Eq. (6.4),

$$\Omega_{xy} = \frac{\partial A_x}{\partial k_y} - \frac{\partial A_y}{\partial k_x}.$$

The Berry connection is given by $A_i(\mathbf{k}) = i \langle \psi_\mathbf{k} | \partial_{k_i} | \psi_\mathbf{k} \rangle$. It is possible to rewrite Ω_{xy} slightly

$$\Omega_{xy} = i\partial_{k_y}(i \langle \psi_\mathbf{k} | \partial_{k_x} | \psi_\mathbf{k} \rangle) - i\partial_{k_x}(i \langle \psi_\mathbf{k} | \partial_{k_y} | \psi_\mathbf{k} \rangle) = i(\langle \partial_y \psi_\mathbf{k} | \partial_x \psi_\mathbf{k} \rangle - \langle \partial_x \psi_\mathbf{k} | \partial_y \psi_\mathbf{k} \rangle). \tag{7.11}$$

Comparing Eqs. (7.10) and (7.11) something remarkable is found. The Hall conductivity is related to the Berry curvature,

$$\sigma_{xy} = -\frac{e^2}{\hbar} \sum_\alpha \int_{\mathbf{T}^2} \frac{d\mathbf{k}}{(2\pi)^2} \Omega_{xy}. \tag{7.12}$$

The integral is taken over momentum on a closed surface so this is indeed a Chern number Eq. (6.9),

$$\boxed{\sigma_{xy} = -\frac{e^2}{2\pi\hbar} \sum_\alpha C_\alpha.} \tag{7.13}$$

This is the famous *TKNN formula* (Thouless, Kohomoto, Nightingale and den Nijs), which is identified as a sum of Chern numbers for different bands. The invariant C_α is often called the TKNN invariant in the context of the quantum Hall effect.

By the same consideration it is possible to calculate the longitudinal conductivity in analogy with Eq. (7.12),

$$\sigma_{xx} = -\frac{e^2}{\hbar} \sum_\alpha \int_{\mathbf{T}^2} \frac{d\mathbf{k}}{(2\pi)^2} \Omega_{xx}.$$

This vanishes because $\Omega_{xx} = \frac{\partial A_x}{\partial k_x} - \frac{\partial A_x}{\partial k_x} = 0$, such that $\sigma_{xx} = 0$. From Eq. (7.2) it follows that

$$\sigma_{xx} = \frac{\rho_{xx}}{\rho_{xx}^2 + \rho_{xy}^2}, \quad \sigma_{xy} = \frac{-\rho_{xy}}{\rho_{xx}^2 + \rho_{xy}^2}.$$

In particular, because $\sigma_{xx} = 0$ it follows that $\rho_{xx} = 0$ and

$$\rho_{xy} = -\frac{1}{\sigma_{xy}}.$$

This resistivity is the one that is observed on the plateaux in the quantum Hall effect resistivity (Figure 7.2 (b)). Two plateaux can not be adiabatically connected without changing a topological invariant $C = \sum_\alpha C_\alpha$. It is known that topological invariants can not change unless the band gap closes. The band gap closes for the Hall experiment when the Chern number changes [17], thus connecting the plateaux.

7.2.1 Stability of the Plateaux

The above calculations for the Hall resistivity do not show why the quantized value remains over a region of the magnetic field strength, as indicated by Figure 7.2 (b). Ironically, this robustness is explained by the presence of disorder in a sample. The disorder breaks translation invariance and even though the latter was assumed in the above derivation it can be argued that this is the correct value of the resistivity on the plateaux [45].

Consider electrons moving freely in two dimensions in the presence of a magnetic field, the Lagrangian is

$$L = \frac{1}{2}m\dot{\mathbf{x}}^2 - e\dot{\mathbf{x}} \cdot \mathbf{A}, \tag{7.14}$$

where $\mathbf{A}$ is the vector potential and with the speed of light $c = 1$. The periodic potential of the lattice may be ignored in the quantum Hall experiment because the wave packets of electrons in a magnetic field are much larger than the period of the lattice [45]. According to the setup (Figure 7.1) the magnetic field is constant in the z-direction, so the vector potential obeys

$$\nabla \times \mathbf{A} = B\hat{z}. \tag{7.15}$$

The *canonical momentum* $\mathbf{p}$ is defined by

$$\mathbf{p} = \frac{\partial L}{\partial \dot{\mathbf{x}}} = m\dot{\mathbf{x}} - e\mathbf{A}$$

and the *mechanical momentum* is

$$\boldsymbol{\pi} = m\dot{\mathbf{x}} = \mathbf{p} + e\mathbf{A}. \tag{7.16}$$

The Hamiltonian is constructed out of Eq. (7.14) according to $H = \dot{\mathbf{x}} \cdot \mathbf{p} - L$ and becomes

$$H = \frac{1}{2m}(\mathbf{p} + e\mathbf{A})^2 = \frac{\boldsymbol{\pi}^2}{2m}. \tag{7.17}$$

The Hamiltonian is rewritten in a new basis by introducing raising and lowering operators in analogy with the harmonic oscillator,

$$a = \frac{1}{\sqrt{2e\hbar B}}(\pi_x - i\pi_y), \quad a^\dagger = \frac{1}{\sqrt{2e\hbar B}}(\pi_x + i\pi_y). \tag{7.18}$$

In the basis Eq. (7.18) the Hamiltonian Eq. (7.17) simplifies to

$$H = \hbar\omega_B(aa^\dagger + \frac{1}{2}), \tag{7.19}$$

where $\omega_B = eB/m$ is the *cyclotron frequency*. Here the position $\mathbf{x}$ and momentum $\mathbf{p}$ are quantum mechanical operators obeying

$$[x_i, p_j] = i\hbar\delta_{ij}, \quad [x_i, x_j] = [p_i, p_j] = 0. \tag{7.20}$$

To find the commutation relations of the operators Eq. (7.18) it is convenient to first find the commutation relation of the mechanical momentum Eq. (7.16). To this end, compute $[\pi_i, \pi_j]$ by letting it act on a test function $f(x, y)$,

$$[\pi_i, \pi_j]f(x,y) = [p_i + eA_i, p_j + eA_j]f(x,y) = \Big([p_i, p_j] + e[p_i, A_j] + e[A_i, p_j] + e^2[A_i, A_j]\Big)f(x,y).$$

The first commutator vanishes by Eq. (7.20) and the last commutator trivially vanishes. Next the $\mathbf{p}$ operator is written in position space as $\mathbf{p} = -i\hbar\partial_x$

$$[\pi_i, \pi_j]f(x,y) = -ie\hbar\Big[\partial_{x_i}\big(A_j f(x,y)\big) - A_j\partial_{x_i}(f(x,y)) + A_i\partial_{x_j}(f(x,y)) - \partial_{x_j}\big(A_i f(x,y)\big)\Big] =$$

$$= -ie\hbar\Big[\big(\partial_x A_y - \partial_y A_x\big)f(x,y) + \big(A_y - A_y + A_x - A_x\big)\partial_y f(x,y)\Big].$$

The second term vanishes and the test function may be removed such that

$$[\pi_i, \pi_j] = -ie\hbar(\partial_{x_i}A_j - \partial_{x_j}A_i)$$

and using $B_i = \epsilon_{ijk}\partial_{x_j}A_k$ with ϵ_{ijk} being the antisymmetric Levi-Civita symbol it is found that

$$[\pi_i, \pi_j] = -ie\hbar\epsilon_{ijk}B_k. \tag{7.21}$$

In particular, using Eqs. (7.15) and (7.21),

$$[\pi_x, \pi_y] = -ie\hbar B.$$

Using this result it is straightforward to confirm that

$$[a, a^\dagger] = 1. \tag{7.22}$$

Eq. (7.22) indicates that the Hilbert space is similar to that of the harmonic oscillator. Any state is constructed out of the groundstate $|0\rangle$ according to

$$|n\rangle = \frac{(a^\dagger)^n}{\sqrt{n!}}|0\rangle$$

and

$$a^\dagger|n\rangle = \sqrt{n+1}\,|n+1\rangle\,, \quad a|n\rangle = \sqrt{n}\,|n-1\rangle\,.$$

The Hamiltonian Eq. (7.19) has the eigenspectrum

$$E_n = \hbar\omega_B(n + \frac{1}{2}), \quad n = 1, 2, 3\ldots, \tag{7.23}$$

see Figure 7.3 (a). For electrons in a magnetic field each eigenstate is evenly spaced and the different levels characterized by n are referred to as *Landau levels*. To see the degeneracy of each Landau level a specific gauge is picked and the wave function is to be found.

The condition for the vector potential Eq. (7.15) is fulfilled by working in the *Landau gauge*

$$\mathbf{A} = xB\hat{y}.$$

With this choice the Hamiltonian Eq. (7.17) becomes

$$H = \frac{1}{2m}(\mathbf{p} + e\mathbf{A})^2 = \frac{1}{2m}(p_x^2 + (p_y + exB)^2).$$

The magnetic field is translation invariant in the xy-plane but the vector potential is only translation invariant in the y-direction. Due to the manifest translation invariance in y-direction the eigenstates of the Hamiltonian should be simultaneous eigenstates of p_y and the following ansatz is made

$$\Psi_k(x,y) = e^{iky}f_k(x).$$

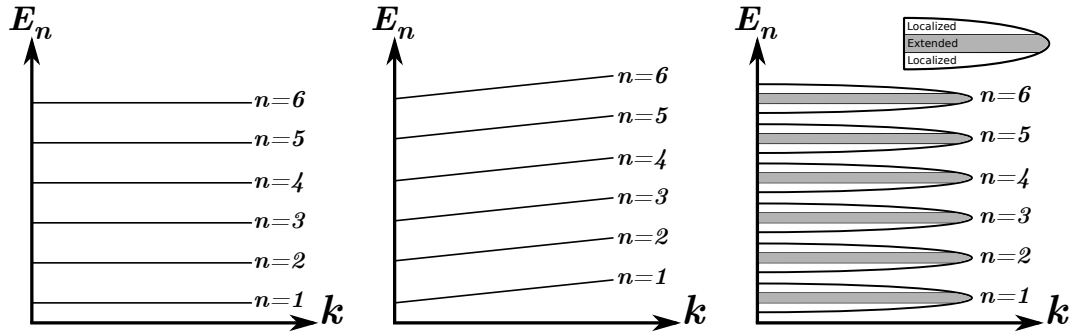

(a) Degenerate Landau levels for electrons in a magnetic field.

(b) Non-degenerate Landau levels for electrons in a magnetic and electric field.

(c) Landau levels split into regions of localized (white) and extended (gray) states in the presence of disorder.

Figure 7.3: Different behaviour of Landau levels for different conditions.

Now

$$H\Psi_k(x,y) = \frac{1}{2m}(p_x^2 + (p_y + exB)^2)\Psi_k(x,y) = \frac{1}{2m}(p_x^2 + (\hbar k + exB)^2)\Psi_k(x,y) \equiv H(k)\Psi_k(x,y).$$

The Hamiltonian $H(k)$ written in terms of the cyclotron frequency and *magnetic length* $l_B = \sqrt{\frac{\hbar}{eB}}$ is

$$H(k) = \frac{1}{2m}p_x^2 + \frac{m\omega_B^2}{2}(x + kl_B^2)^2. \tag{7.24}$$

This is the form of a harmonic oscillator Hamiltonian $H_{ho} = \frac{p^2}{2m} + \frac{m\omega^2}{2}x^2$, for which the corresponding wave function is written in terms of *Hermite polynomials* H_n [40]. The wave function corresponding to Eq. (7.24) is given by [43]

$$\Psi_{n,k}(x,y) \sim e^{iky}H_n(x + kl_B^2)e^{-(x+kl_B^2)^2/2l_B^2}. \tag{7.25}$$

The degeneracy of Landau levels n becomes apparent because the energies Eq. (7.23) depend only on the index n while the wave function Eq. (7.25) depends on momentum k as well. How large is the degeneracy per unit area? Consider sides of length L_x and L_y. In y-direction there is a manifest translation invariance and so momentum is quantized in units of $2\pi/L_y$. For x-direction it is noted that the wave function Eq. (7.25) is located around $x = -kl_B^2$. Therefore $0 \leq x \leq L_x$ implies $-L_x/l_B^2 \leq k \leq 0$. The total number of states in one Landau level is[15]

$$G = \text{allowed momenta per unit } k = \frac{L_y}{2\pi}\int_{-L_x/l_B^2}^{0} dk = \frac{L_xL_y}{2\pi l_B^2} = \frac{eBL_xL_y}{2\pi\hbar}. \tag{7.26}$$

The important thing to notice is that *the degeneracy is dependent on the magnetic field strength.*

In the quantum Hall experiment there is an electric field present which was neglected in the above calculations. It has the effect of making the energies momentum dependent [43] and thus lifting the degeneracy by tilting the energies as seen in Figure 7.3 (b). But more important is the effect that an imperfect sample has on the Landau levels. The imperfection is due to various impurities which can be modelled by a random potential V. If the strength of the disorder is smaller than the energy splitting of the Landau

[15]To understand the factor $L_y/2\pi$ it helps to think of the unit of quantization $2\pi/L_y$ as an area. In this way the total number of allowed states is k divided by this area and per unit of k the number of states is $L_y/2\pi$.

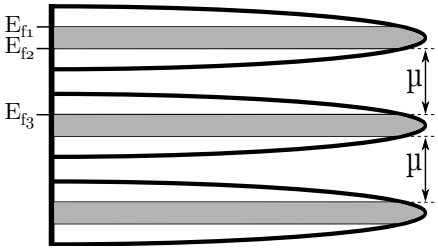

Figure 7.4: Due to disorder the Landau levels exhibit a mobility gap μ between the extended states within which there are no energy levels that contribute to the conductivity.

levels ($V < \hbar\omega_B$) then the energy levels will spread out according to Figure 7.3 (c). The random potential introduces localized states around the impurities which do not contribute to the conductivity. This can be understood semi-classically by the fact that the centre of cyclotron orbits follows equipotentials either around impurities (localized) or in between impurities (extended) [43, 45]. Because the impurities are modelled by local potential minima and maxima the energies of the localized states are the minimum and maximum energies of a given Landau level respectively. This has the effect of surrounding the extended states in the middle of a Landau level with the localized states, as seen in Figure 7.3.

Now the essentials for understanding the stability of the Hall plateaux are introduced. The argument is as follows: When the magnetic field strength is slowly increased the degeneracy of each Landau level increases according to Eq. (7.26) and the Fermi level starts to lower. Suppose that initially the Fermi level E_{f1} lies such that the extended states of the third Landau level is filled, see Figure 7.4. Then the magnetic field is increased such that the Fermi level lowers to E_{f2}. During this process the conductivity has changed because the extended states were emptied. This region of the magnetic field strength correspond to the region in between the plateaux in Figure 7.2 (b). Now, lower the Fermi level further until it reaches E_{f3}. During this deformation the Fermi level lies entirely in the *mobility gap* μ in which there are only localized states. Changing the filling of such states can not affect the conductivity in any way. Therefore this region of the magnetic field corresponds to the Hall plateaux of Figure 7.2 (b). By this it is understood that the higher lying plateaux are labeled by lower Chern numbers.

Recall that the linear response theory derivation of the Hall conductivity (Section 7.2) assumed that the bands (Landau levels) were either full or empty. In essence, it was assumed that all states contribute equally to the conductivity but this is inconsistent with the above arguments. Luckily, the extended states compensate in conductivity in such a way that Eq. (7.13) holds true on the plateaux [43]. The full depth behind why all states of a given Landau level contribute equally to the conductivity was explained by Laughlin [46] in what is now called *Laughlin's gauge argument*. For further discussions on this see also [45].

7.3 Spin Quantum Hall Effect and the $\mathbb{Z}_2$-Invariant

In 2005 [6, 7] discovered another type of topological insulator, called a $\mathbb{Z}_2$*-insulator*, which did not require the presence of a magnetic field to induce topological features. Their model was essentially two copies of a regular quantum Hall insulator with spin-orbit coupling and it features counter-propagating spin-1/2 particles at the boundaries. The counter-propagating modes were dubbed *helical* and are time reversal symmetric. One can show [14] that $\mathcal{F}(k)$ of Eq. (6.2) obeys $\mathcal{F}(-\mathbf{k}) = -\mathcal{F}(\mathbf{k})$ for a time reversal symmetric system and therefore the integral of this odd function over the symmetric Brillouin zone vanishes. The Chern number can not characterize the different topological phases that arise. It turns out that there are only two distinct insulating phases for this system and they are characterized by the topological invariant

$\nu_0 \in \{0,1\} = \mathbb{Z}_2$. The physical interpretation of this topological invariant is discussed in Section 9.2. For now two ways of computing the $\mathbb{Z}_2$ invariant in two dimensions are given without proof.

There exist many equivalent mathematical formulations of the $\mathbb{Z}_2$ invariant [47], all of which are complicated to prove. Assuming that the system is represented by Bloch states, $|u_\alpha(-\mathbf{k})\rangle$, define the matrix elements of the sewing matrix

$$w_{\alpha\beta} = \langle u_\alpha(-\mathbf{k})|T|u_\beta(\mathbf{k})\rangle$$

where T is the time reversal operator. Out of this form

$$\delta_a = \mathrm{Pf}[w(\Lambda_a)]/\sqrt{\mathrm{Det}[w(\Lambda_a)]},$$

where Λ_a are all the points in the Brillouin zone where $k = -k$ and the Pfaffian of an antisymmetric matrix $(A^T = -A)$ is defined by $\big(\mathrm{Pf}(A)\big)^2 = \mathrm{det}A$. The $\mathbb{Z}_2$-invariant ν is defined by

$$(-1)^\nu = \prod_{a=1} \delta_a.$$

Alternatively, if the model conserves perpendicular spin the $\mathbb{Z}_2$-invariant can be written,

$$\nu = n_\sigma \mathrm{mod} 2,\ n_\sigma = (n_+ - n_-)/2,$$

where n_σ is a Chern number. For more mathematical formulations see [47].

8 The 10-Fold Way of Topological Matter

Having talked extensively about topological invariants, now one would like to systematically determine whether or not a system exhibits a topological phase. In a famous paper by Altland and Zirnbauer [48], characterization of non-interacting, fermionic single-particle Hamiltonians leads to ten symmetry classes. Later, Schnyder *et al.* [34] provided a list of possible topological phases for each of those symmetry classes for dimensions $d \leq 3$. It was Kitaev [49] who was able to generalize the result through a K-theory approach and find the possible topological phases for arbitrary dimensions. This discussion justifies a review in its own and therefore only a brief review of the main result and how to obtain it is given.

8.1 Classification of Bloch Hamiltonians

The objective is to classify Bloch Hamiltonians $\mathcal{H}(\mathbf{k})$ with respect to chiral symmetry, time reversal symmetry and particle-hole symmetry. How many possible symmetry classes are there? Recall that time reversal symmetry and particle-hole symmetry can both square to ± 1. In addition, the symmetries may not be present at all (square to 0). This gives a total of nine combinations. In eight of these classes the existence of chiral symmetry is uniquely determined by T and C. However, in the case where the system is neither time reversal, nor particle-hole symmetric, then chiral symmetry may be either present or not [23]. Therefore $T^2 = C^2 = 0$ has two classes with chiral symmetry either present or not. This leads to a total of ten symmetry classes, hence the name *10-fold way*.

Each of these classes possess different restrictions on the Bloch Hamiltonian due to the discrete symmetries, see Chapter 2. In the work of Altland and Zirnbauer [48] the resulting single-particle Hamiltonians is worked out. Each symmetry class is attributed a *Cartan label*. In fact, due to the work of Èlie Cartan in 1926, there exist eleven large families of symmetric spaces. It is possible to group two of these families together and then, there is a *bijection* between the classes of non-interacting, fermionic single-particle Hamiltonians and all symmetric spaces [48]. This is an indication of the fact that the list of symmetry classes that has been found is exhaustive.

The relevant Cartan label is determined from the resulting time evolution operator. Consider a simple example. If all three symmetries are non-existent, then $\mathcal{H}(\mathbf{k})$ is a generic $N \times N$ Hermitian matrix. The time evolution operator $(U(t) = e^{-i\mathcal{H}(\mathbf{k})})$ is therefore a generic unitary matrix and $U(t)$ is an element of the *unitary group* of N dimensional matrices $\mathrm{U}(N)$. The Cartan label for unitary matrices is A. All ten Hamiltonians and corresponding Cartan labels have been worked out in [17] resulting in the classification table given by Table 1. The columns T and C are ± 1 when the square of the operators are ± 1 and zero whenever they are not present. Chiral symmetry is either present $(S = 1)$ or not $(S = 0)$. Note that, whenever two symmetries are present, the third one is automatically present.

8.2 Classification of Topological Phases

Now the task is to determine whether all symmetry classes with a given dimension of the Brillouin zone could possibly host a topological phase. This is done in the famous article by Schnyder *et al.* [34] in dimensions 1 to 3, which are the physically relevant dimension for condensed matter applications. For a classification of topological phases in arbitrary dimensions, see [49]. It turns out that both approaches involve the concept of *homotopy groups* [14]. Here the classification procedure requires that the Hamiltonian is translation invariant. This condition can be relaxed in a more general discussion but it makes the procedure simpler.

As stated before, an equivalence class is made up of the set of all adiabatically connected Bloch Hamiltonians. Thus the equivalence classes are the distinct phases of the system. Following the approach of [14], it is assumed that the spectrum is gapped and that the system is translation invariant. Topological

Cartan label	T	C	S	Group (or coset) of $U(t)$
A	0	0	0	$\mathrm{U}(n)$
AI	+1	0	0	$\mathrm{U}(n)/\mathrm{O}(n)$
AII	-1	0	0	$\mathrm{U}(2n)/\mathrm{Sp}(2n)$
D	0	+1	0	$\mathrm{SO}(2n)$
C	0	-1	0	$\mathrm{Sp}(2n)$
AIII	0	0	1	$\mathrm{U}(n+m)/\mathrm{U}(n)\times\mathrm{U}(m)$
BDI	+1	+1	1	$\mathrm{O}(n+m)/\mathrm{O}(n)\times\mathrm{O}(m)$
CI	+1	-1	1	$\mathrm{Sp}(2n)/\mathrm{U}(n)$
DIII	-1	+1	1	$\mathrm{SO}(2n)/\mathrm{U}(n)$
CII	-1	-1	1	$\mathrm{Sp}(n+m)/\mathrm{Sp}(n)\times\mathrm{Sp}(m)$

Table 1: All ten symmetry classes of a non-interacting, fermionic Bloch Hamiltonian with respect to the three discrete symmetries time reversal symmetry (T), particle-hole symmetry (C) and chiral symmetry (S). The corresponding Cartan label of the group in which the time evolution operator of the Bloch Hamiltonian falls within is given in the first column. If a symmetry is not present its value is zero. When a given symmetry is present it is indicated by the value of the corresponding squared single-particle operator.

classification applies to insulators and to superconductors as well. The superconductors are described by superconducting quasiparticles and the gap to be preserved under deformations is that of the quasiparticles [14]. In such a system the eigenstates are given by Bloch states,

$$\mathcal{H}(\mathbf{k})\left|u_\alpha(\mathbf{k})\right\rangle = E_\alpha(\mathbf{k})\left|u_\alpha(\mathbf{k})\right\rangle,$$

where α is a band index. The Fermi energy is inside the gap such that there is a number n of bands above the Fermi energy and m bands below.

Define the projection operator over filled Bloch states

$$P(\mathbf{k}) = \sum_\alpha^{filled} \left|u_\alpha(\mathbf{k})\right\rangle\left\langle u_\alpha(\mathbf{k})\right|.$$

Out of this, construct the *flatband Hamiltonian*

$$Q(\mathbf{k}) = \mathbb{1} - 2P(\mathbf{k}).$$

The total dimension of the matrix is $n+m$. The degeneracy of the eigenvalues ± 1 shows how many states were above and below the Fermi energy. This is easily understood because the Hamiltonian can be written $H(\mathbf{k}) = \sum_\alpha E_\alpha \left|u_\alpha(\mathbf{k})\right\rangle\left\langle u_\alpha(\mathbf{k})\right|$, where the sum is over all bands. It is straightforward to find that the flatband Hamiltonian has the same eigenstates as H but with eigenvalues ± 1 (hence the name)

$$Q(\mathbf{k}) = \sum_\alpha \lambda_\alpha \left|u_\alpha(\mathbf{k})\right\rangle\left\langle u_\alpha(\mathbf{k})\right|, \quad \lambda_\alpha = \begin{cases} -1, & \alpha = \text{filled} \\ +1, & \alpha = \text{unfilled} \end{cases}.$$

The initially gapped Hamiltonian can always be deformed into the flatband Hamiltonian and therefore they are topologically equivalent but the flatband Hamiltonian is easier to work with. The corresponding *Q-matrix* $\mathcal{Q}(\mathbf{k})$ is the matrix representation of the flatband Hamiltonian,

$$Q(\mathbf{k}) = \sum_k \mathcal{Q}(\mathbf{k})\left|u_\alpha(\mathbf{k})\right\rangle\left\langle u_\alpha(\mathbf{k})\right|.$$

It turns out that in the simplest case where $\mathcal{H}(\mathbf{k})$ is not subjected to any discrete symmetries the $\mathcal{Q}(\mathbf{k})$ is an element of [16] [34],

$$\mathcal{Q}(\mathbf{k}) \in \mathrm{U}(n+m)/(\mathrm{U}(n) \times \mathrm{U}(m)).$$

If the Bloch Hamiltonian is in another class then it is subjected to additional constraints and so is the Q-matrix, making it an element of a new group (or coset). For a complete list of the corresponding flatband Hamiltonians for all symmetry classes see Schnyder *et al.* [34].

The original mission was to find all the equivalence classes of Bloch Hamiltonians. Here is the key idea that allows for this: *if two maps from the Brillouin zone to the flattened spectrum can be continuously deformed into each other, then so can the corresponding Bloch Hamiltonians* [14]. Therefore, one must *find all the unique maps from a d-dimensional torus onto the space of the flatband Hamiltonian.*

Because the band structure is given by a mapping from $\mathbf{k} \in \mathbf{T}^d$ (momentum is defined on a d-dimensional torus) to $\mathcal{H}(\mathbf{k})$ and because every $\mathcal{H}(\mathbf{k})$ corresponds to a unique $\mathcal{Q}(\mathbf{k})$, the band structure can be seen as a mapping from $\mathbf{k} \in \mathbf{T}^d$ to $\mathcal{Q}(\mathbf{k})$. Finding the unique maps $\mathbf{k} \in \mathbf{T}^d \to \mathcal{Q}(\mathbf{k})$ is a simpler way to find the topological phases of the ten classes.

The homotopy group is the group of equivalence classes of maps from a d-dimensional sphere to the target space C_0, denoted $\pi_d(C_0)$. Here C_0 is the group or coset of $\mathcal{Q}(\mathbf{k})$. The fact that homotopy groups regard maps from spheres and not tori turns out to be unimportant in these considerations [23]. Thus, the problem of finding the possible topological phases has been reduced to finding homotopy groups. This is in general, non-trivial. The results are merely given here.

Following this approach, the full classification of existing topological phases for non-interacting, fermionic Bloch Hamiltonians in dimensions $1-3$, is given by table 2, which has been dubbed *the 10-fold way of topological matter* [34]. The table exhibits a periodicity in that it repeats itself every eight dimensions. However, the main focus here will entirely on dimensions $d \leq 3$ because these are of interest in condensed matter applications. It should be noted that dimensions $d \geq 4$ can become important in certain cases where $\mathcal{H}(\mathbf{k})$ admits parameters which can be interpreted as additional momentum components [14]. The system acquires effective extra dimensions. This is not considered in this review. It will just be stated that in total, there are five non-trivial phases in any given dimension, three of which are characterized by $\mathbb{Z}$-invariants and the rest by $\mathbb{Z}_2$-invariants[17].

The $\mathbb{Z}$ quantities are winding numbers (Chapter 4) whenever Chiral symmetry is present, otherwise they are Chern numbers (Chapter 6) [23]. In theory the $\mathbb{Z}$-invariants can take on any integer values, in practice however, further symmetries puts restrictions on the possible values. For example, the SSH model, which is labeled by a one-dimensional winding number, turned out to have only two distinct insulating phases. The $\mathbb{Z}_2$ quantity has different interpretations in different dimensions. In two dimensions, $\mathbb{Z}_2$ is interpreted in terms of the number of Kramers' pairs (see Section 2.2) that cross the Fermi energy, E_f. In particular, the topological invariant ν_0 is one whenever there exists an odd number of Kramers' pairs crossing E_f and zero otherwise and is therefore a $\mathbb{Z}_2 = 0, 1$ invariant. Further discussions on the two-dimensional $\mathbb{Z}_2$-invariant will be held in Chapter 9. In three dimensions there are four topological invariants ν_0, ν_1, ν_2 and ν_3 which take values in $\mathbb{Z}_2$. They are interpreted as the number of Kramers' degenerate band crossings on the surface of the bulk [34]. The one dimensional interpretation of the $\mathbb{Z}_2$ invariant is trickier. An interpretation in one dimension due to Kitaev [13] is reviewed alongside one more interpretation in [50]. Kitaev showed that the topological invariant can be interpreted as the sign of the Pfaffian of the Bloch Hamiltonian written in the basis of Majorana fermions, see Section 9.3.1.

Is the table consistent with results from previous chapters? Recall that the SSH model with real parameters (Section 3.3) was characterized by a winding number. Winding numbers are theoretically allowed to take on any integer value and so the SSH model is characterized by a $\mathbb{Z}$ invariant. The SSH model, with

[16] *The coset $U(n+m)/(U(n) \times U(m))$ is called the complex Grassmanian and denoted $G_{n,n+m}(\mathbb{C})$.*

[17] $\mathbb{Z}_n$ is the group of integers under addition with modulo n.

Cartan label	T	C	S	d=1	d=2	d=3
A	0	0	0	-	$\mathbb{Z}$	-
AI	+1	0	0	-	-	-
AII	-1	0	0	-	$\mathbb{Z}_2$	$\mathbb{Z}_2$
D	0	+1	0	$\mathbb{Z}_2$	$\mathbb{Z}$	-
C	0	-1	0	-	$\mathbb{Z}$	-
AIII	0	0	1	$\mathbb{Z}$	-	$\mathbb{Z}$
BDI	+1	+1	1	$\mathbb{Z}$	-	-
CI	+1	-1	1	-	-	$\mathbb{Z}$
DIII	-1	+1	1	$\mathbb{Z}_2$	$\mathbb{Z}_2$	$\mathbb{Z}$
CII	-1	-1	1	$\mathbb{Z}$	-	$\mathbb{Z}_2$

Table 2: The 10-fold way of topological matter is a list of possible topological phases for non-interacting, fermionic Bloch Hamiltonians in each of Altland's and Zirnbauer's ten symmetry classes. If a symmetry is not present its value is zero. When a given symmetry is present it is indicated by the value of the corresponding squared single-particle operator. The different dimensions d can host only trivial phases, indicated by $-$, a theoretically infinite number of phases labeled by an integer $\mathbb{Z}$ or two phases, labeled by $\mathbb{Z}_2$.

Bloch Hamiltonian

$$\mathcal{H}_{SSH}(k) = \begin{pmatrix} 0 & v + we^{-ik} \\ v + we^{ik} & 0 \end{pmatrix},$$

was found to be chiral symmetric, which is what makes it off-diagonal. Is it time reversal symmetric? The condition on the Bloch Hamiltonian for time reversal symmetric models was found to be Eq. (2.29), $\mathcal{T}\mathcal{H}^*(-k)\mathcal{T}^{-1} = \mathcal{H}(k)$ with $\mathcal{T} = \mathbb{1}$ for spinless fermions. The condition is fulfilled.

Thus, the SSH model has both chiral symmetry and time reversal symmetry, which means that it is also particle-hole symmetric. The three symmetries are related by Eq. (2.37), namely $S = TC$, giving

$$C = T^{-1}S = K\hat{\sigma}_z.$$

The particle-hole operator squares to $+1$. This puts the SSH model into the BDI class, see Table 2. As expected, a one dimensional model, with all symmetries present and $T^2 = C^2 = +1$ (BDI-class) is characterized by a $\mathbb{Z}$-invariant, namely the winding number.

The process of identifying a topological phase of a given gapped non-interacting fermionic model has become very streamlined. First one identifies the symmetries of the model and finds the corresponding symmetry class. By looking at Table 2 the topological invariant which describes the topological phase is found and one can calculate it by means of any of the formulas or interpretations presented in this review. To investigate possible points in parameter space where a topological phase transition could occur, one can look for gap closings.

It should be noted that in some cases the Q-matrix may remain in a subset of the same space by imposing some additional constraint. For example, in the class AI, the corresponding Q-matrix is in the same group but with an additional constraint $\mathcal{Q}^*(\mathbf{k}) = \mathcal{Q}(-\mathbf{k})$. In that case this homotopy group approach is insufficient and one needs to resort to one of the more advanced approaches outlined before. Within the other approaches the Hamiltonians are random matrices, meaning they are not translation invariant [14].

9 Gapless Edge Modes

In this chapter the gapless edge modes which occur for all non-interacting topological systems and the accompanying boundary physics is discussed. First, the existence of gapless edge modes in the SSH model (Section 3.3) will be shown and then the bulk-boundary correspondence which was first encountered in that section will be discussed in more general terms. Lastly, the reason for the robustness of these states is discussed and to finish the developments of this review a brief overview of one of the most promising phenomenon for technological application, namely Majorana zero modes, is given.

9.1 The Gapless Edge Modes of the SSH Model

The open chain SSH model is given by the single-particle Hamiltonian

$$H = \sum_{m=1}^{N} v_m \left|m, B\right\rangle \left\langle m, A\right| + \sum_{m=1}^{N-1} w_m \left|m+1, A\right\rangle \left\langle m, B\right| + h.c.\ . \tag{9.1}$$

The model has been generalized to allow position dependent hopping amplitudes, v_m and w_m. In the end the case $v_m = v$ and $w_m = w,\ \forall m$ will be considered. The coefficients are still real. A general single-particle state can be expanded in terms of the basis kets $\{\left|m, A\right\rangle, \left|m, B\right\rangle\}$, for $m = 1 \ldots N$,

$$\left|\Psi\right\rangle = \sum_{m=1}^{N} (a_m \left|m, A\right\rangle + b_m \left|m, B\right\rangle). \tag{9.2}$$

The aim is to find gapless boundary modes located near the edges of the chain. In Section 3.3 it was argued that the gapless modes have zero energy. Thus, the gapless modes $\left|\Psi_0\right\rangle$ must obey,

$$H \left|\Psi_0\right\rangle = H \sum_{m=1}^{N} (a_m \left|m, A\right\rangle + b_m \left|m, B\right\rangle) = 0.$$

This results in a total of $2N$ equations. In the simple case where $N = 2$ it is found that,

$$H \left|\Psi_0\right\rangle = v_1 b_1 \left|1, A\right\rangle + v_2 a_2 \left|2, B\right\rangle + (v_2 b_2 + w_1 b_1) \left|2, A\right\rangle + (v_1 a_1 + w_1 a_2) \left|1, B\right\rangle = 0.$$

The $2N$ equations are,

$$\begin{aligned} v_2 b_2 + w_1 b_1 = 0, \qquad & v_1 a_1 + w_1 a_2 = 0, \\ v_1 b_1 = 0, \qquad & v_2 a_2 = 0. \end{aligned}$$

The coefficients a_m and b_m never mix due to the chiral symmetry defined by the sublattices A and B of the Hamiltonian. The equations are generalized for arbitrary N,

$$v_m a_m + w_m a_{m+1} = 0, \qquad w_m b_m + v_{m+1} b_{m+1}, \quad m = 1 \ldots N-1, \tag{9.3}$$

with boundary conditions,

$$v_1 b_1 = 0, \qquad v_N a_N = 0. \tag{9.4}$$

Because the equations do not mix one can focus on finding eigenstates of the form,

$$\left|L\right\rangle = \sum_{m=1}^{N} a_m \left|m, A\right\rangle. \tag{9.5}$$

The only limit of interest is the thermodynamic limit where $N \to \infty$. In this case the first of Eqs. (9.3) can be solved in terms of a_1 according to

$$a_2 = -\frac{v_1}{w_1}a_1, \qquad a_3 = \frac{v_1 v_2}{w_1 w_2}a_1, \quad \dots \quad a_N = \frac{v_1 v_2 \dots v_N}{w_1 w_2 \dots w_N}a_1. \tag{9.6}$$

The coefficient a_1 is determined from imposing normalized eigenstates ($|\langle L|L\rangle|^2 = 1$). However, the boundary condition Eq. (9.4) forces $a_N = 0$ which in turn requires a_1 in Eq. (9.6) to be zero, which results in the solution $a_m = 0, \ \forall m$. However, it can be shown [19], that in the thermodynamic limit ($N \to \infty$) and only when $v < w$ then the coefficient $|a_N|$ can be written,

$$|a_N| = |a_1| e^{-(N-1)/\varepsilon}, \tag{9.7}$$

with the localization strength, $\varepsilon = \frac{1}{\overline{\log|w|} - \overline{\log|v|}}$, where $\overline{\log|v|}$ and $\overline{\log|w|}$ are the so called bulk-averages,

$$\overline{\log|v|} = \frac{1}{N-1}\sum_{m=1}^{N-1}\log|v_m|, \qquad \overline{\log|w|} = \frac{1}{N-1}\sum_{m=1}^{N-1}\log|w_m|.$$

Therefore, in the thermodynamic limit (where topological invariants are defined) there is a non-trivial solution for Eq. (9.3). The solutions of Eq. (9.3) for arbitrary N are

$$a_N = |a_1| e^{-(N-1)/\varepsilon}, \qquad a_m = \Big(\prod_{j=1}^{m-1} -\frac{v_j}{w_j}\Big)a_1, \quad m = 1 \dots N-1. \tag{9.8}$$

The gapless, zero energy eigenstates $|L\rangle$ given by Eq. (9.5) has the coefficients (9.8), where a_1 is determined from the normalization condition, becomes

$$|L\rangle = \sum_{m=1}^{N} a_m |m, A\rangle = -\frac{v_1}{w_1}a_1|1,A\rangle + \frac{v_1 v_2}{w_1 w_2}a_1|2,A\rangle + \ldots + \Big(\prod_{j=1}^{1}\frac{-v_j}{w_j}\Big)a_1|N-1,A\rangle + a_N|N,A\rangle.$$

Where is $|L\rangle$ localized? To make a connection with the SSH model introduces in Section 3.3, set $v_m = v$ and $w_m = w, \ \forall m$. The eigenstate Eq. (9.5) becomes,

$$|L\rangle = -\frac{v}{w}a_1|1,A\rangle + \frac{v^2}{w^2}a_1|2,A\rangle + \ldots (-)^{N-1}\frac{v^{N-1}}{w^{N-1}}a_1|N-1,A\rangle + a_N|N,A\rangle. \tag{9.9}$$

From the phase diagram of the SSH model, Figure 3.10 (b), it is known that the topological phase exists for the regime $v < w$. When $v < w$, the eigenstate Eq. (9.9) has ever decreasing amplitude on lattice sites m further away from $m = 1$. In the thermodynamic limit, the amplitude of (9.9) inside the bulk is vanishing. Therefore $|L\rangle$ is seen to be a left boundary mode, or an edge mode. It is possible to solve for b_m in Eqs. (9.3) and (9.4) and obtain another edge mode that is localized at the opposite end of the chain.

It holds in general that, *a topological insulator*[18] *or superconductor has gapless energy states at its boundaries.* This statement is the result of the previously mentioned bulk-boundary correspondence, to be discussed in more detail in the following section.

[18]It should be noted that the term topological insulator often (and here) refers to non-interacting insulators with topological properties that are characterized by their symmetries. This means that, interacting systems which are insulators and have non-trivial topology (by for example *topological order*) are not known as topological insulators. Indeed, topologically ordered insulators do not necessarily have gapless boundary modes.

9.2 Bulk-Boundary Correspondence

In the context of the SSH model it was shown in Section 3.3 that the number of gapless zero-energy modes (now identified as edge modes) at one side of the chain is equal to the winding number of the model. The bulk-boundary correspondence says that there will always be gapless modes at the interface between insulators with non-equal topological invariants. There exists no rigorous, general proof of this theorem that applies to all models at the same time. Instead, it has been shown to hold for specific cases like for example Chern insulators [51], Dirac Hamiltonians [52], *complex classes* of topological insulators [53] and many other. There does however exists a very general, logical proof.

To understand the emergence of gapless modes on the boundaries of topological insulators, consider a chunk of material embedded in a vacuum. The material is in a topological phase, say that it has a non-vanishing Chern number, $C = 1$. The vacuum is gapped and topologically equivalent to any trivial insulator [27], with $C = 0$. The Chern number changes at the interface between the topological insulator and the trivial insulator and it is known that a topological invariant can not change without closing the gap. The conclusion is that the gap must close at the interface between the two materials, see Figure 9.2 (a). As a result, topological insulators will always host gapless edge states in two dimensions and gapless surface states in three dimensions.

This intuitive proof is not without flaws. Intuitively, the topological invariant changes at the interface between the two materials because inside the materials, the topological invariant has its defined value. However, the topological invariants are only well-defined in the bulk, because they rely on translational invariance. The one-dimensional winding number of Chapter 4 was expressed in terms of the determinant of the upper-right block of the Bloch Hamiltonian and the Chern number of Section 6 was expressed in terms of Bloch states, both of which require translation invariance. This means that, as one moves closer to the edge of the sample, the description of the topological invariants falls apart and they are not well-defined in the crucial region where the bulk-boundary correspondence makes predictions. Not to worry, the above argument is merely a way of motivating the bulk-boundary correspondence which is complicated to prove rigorously. For a given Hamiltonian that models a sample the parameters are (if time independent) fixed through out the sample. At the edge however, the parameters take a discontinuous step when leaving the material, even though this is not happening in time, it can be seen as highly unadiabatic and in that sense the topological invariant is allowed to change at the boundary.

There exists a formula statement of the bulk-boundary correspondence which expresses the number of gapless energy modes which arise. The statement is different for $\mathbb{Z}$-topological insulators and $\mathbb{Z}_2$-topological insulators. For $\mathbb{Z}$-systems in two dimensions ($d = 2$) the number of boundary modes that occur on the boundary is determined by the $\mathbb{Z}$ *bulk-boundary correspondence* [27],

Theorem 9.1 (Bulk-boundary correspondence of $\mathbb{Z}$-insulators in $d = 2$) *The difference in number of right-moving modes N_R and left-moving modes N_L at the interface of a topological insulator in $d = 2$ is the difference in Chern number across the surface of the sample*

$$\boxed{\Delta C = N_R - N_L.}$$

Since the difference $N_R - N_L$ (at any particular energy) can not be changed by one edge mode alone, see Figure 9.2, *there must be ΔC gapless edge modes at the boundaries* to fulfill the bulk-boundary correspondence. It should be noted that the theorem is not proven in generality but has been shown for several independent systems. It has also been verified experimentally in for example the quantum Hall effect. The emergence of *chiral modes* (moving in one direction) can be understood semi-classically in terms of cyclotron orbit skipping, see Figure 9.1. A right-moving mode is characterized by a non vanishing group velocity dE/dk_x in x-direction, like the solid line in Figure 9.2 (b). Under a perturbation the difference in right and left moving edge modes can not change. For one and three-dimensional systems the $\mathbb{Z}$-insulator bulk-boundary correspondence is expressed in terms of winding numbers, see [26].

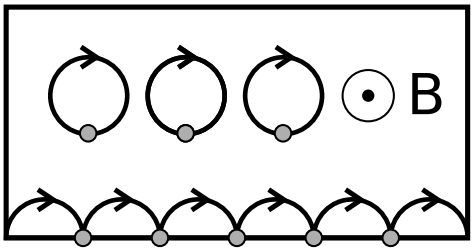

Figure 9.1: Semi-classical description of emergence of chiral edge modes in the quantum Hall effect. The cyclotron orbits of the electrons, induced by the magnetic field, bounces of the edge and causes chiral motion.

The bulk-boundary correspondence of $\mathbb{Z}_2$-insulators is a bit trickier and here the discussion is limited to two-dimensional systems with time reversal symmetry. This means that the symmetry classes under consideration are AII and DIII. For a spinful, time reversal symmetric model in class AII the spin quantum Hall effect may emerge [14]. The spin quantum Hall effect is essentially two copies of the quantum Hall effect which are sorted in spin such that there exists two chiral edge currents with opposite spin and velocity and these are the type of edge modes that appear for $\mathbb{Z}_2$-insulators in two dimensions, see Figure 9.3 (a).

For spin-1/2 particles, the time reversal operator squares to minus one, $T^2 = -1$. By Kramers' theorem (see Section 2.2.2) it is known that the spectrum is at least doubly degenerate. Furthermore, along the edge the one-dimensional momentum k_x exhibits so called time reversal invariant points. In these points ($k = \pm\pi, 0$) the spectrum must be doubly degenerate as discussed in Section 2.2.2. This property of the spectrum is shown in Figure 3.3.

Any edge state must be accompanied by a partner by Kramers' theorem and together the two edge states make up a *Kramers' pair*. There are two possibilities in which Kramers' pairs of edge states can cross the Fermi energy which is taken to lie within the bulk gap, see Figure 9.3 (b)-(c). As discussed and illustrated in [54], when there is an an even number of Kramers' edge pair crossings the edge states can be deformed to close the gap while still preserving time reversal invariant momentum points. Therefore the spectrum is topologically equivalent to that of a trivial insulator. For an odd number of Kramers' pair crossings this is

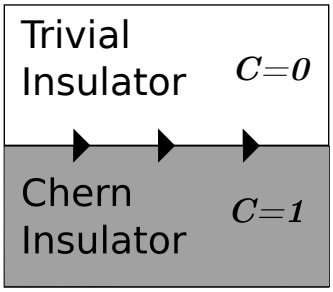

(a) Chiral edge modes exist at the interface between insulators with different Chern numbers.

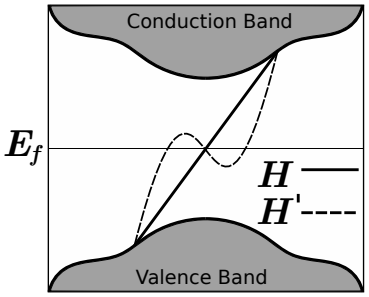

(b) Under a perturbation of the system H to H', the difference in right and left-moving edge modes remains.

Figure 9.2: The characteristics of topological $\mathbb{Z}$-insulators include chiral edge modes, figure (a). The difference in right and left-moving edge modes remains the same under perturbations, figure(b).

not possible and Kramers' theorem enforces the existence of states that traverse the gap. This defines two different topological states which are characterized by a $\mathbb{Z}_2$-invariant. The mathematical statement of the bulk-boundary correspondence for $\mathbb{Z}_2$-insulators becomes [47],

Theorem 9.2 (Bulk-boundary correspondence of $\mathbb{Z}_2$-insulators in $d = 2$) *The number of Kramers' pairs of edge modes N_k which intersect the Fermi energy is the difference in the $\mathbb{Z}_2$-invariant ν across the interface of the sample*

$$\boxed{N_k = \Delta\nu \, mod \, 2.}$$

Due to the existence of Kramers' pairs and the inversion through the energy axis symmetry imposed by time reversal, ν can only change by a multiple of two under adiabatic deformations. Thus the actual topological invariant is the parity of ν.

Because all topological insulators and topological superconductors have gapless edge modes it is sometime taken as the definition. The bulk-boundary correspondence becomes a very powerful tool because one could determine topological invariants by counting the gapless edge modes.

9.3 Robustness

To conclude this review, a brief discussion of a phenomenon with promising technological applications, namely the robustness of the gapless edge modes, is given. As was seen for the SSH model (Figure 3.10 (a)) the gapless states exist throughout the topological phase. This topological protection is enforced by the bulk-boundary correspondences which says that these edge states must exist. Furthermore, the states remain regardless of how the boundary is deformed. This is because the bulk Hamiltonian is independent of the shape of the boundary. Therefore the topological invariants remain well defined. Also, topological insulators are robust against perturbations that destroy the translation invariance of the crystal [14]. This means that a given sample can be reasonably deformed and dirty, that is, have imperfections, yet the gapless edge modes will remain. The edge states are thus said to be topologically protected. This is often the case for samples in the lab and this has tremendous experimental and technological implications.

In the area of quantum computations, the robustness of topological edge states is most welcome. A quantum computer stores information in *quantum bits* or *qubits*, which are quantum systems of two states. For example, a system characterized only by its spin can be in either spin up $|+\rangle$ or spin down $|-\rangle$. The

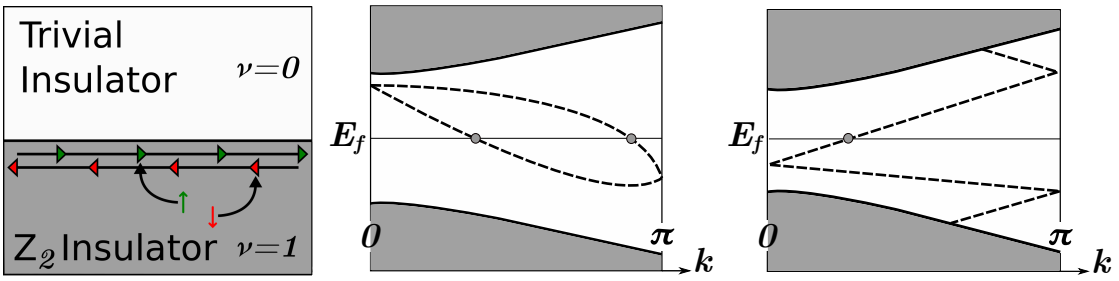

(a) Chiral edge states filtered in terms of spin that arise on the interface of a $\mathbb{Z}_2$-insulator.

(b) A time reversal symmetric $\mathbb{Z}_2$-insulator with an even number of Kramers' pairs crossing the Fermi energy. The spectrum is symmetric by reflection through the energy axis.

(c) A time reversal symmetric $\mathbb{Z}_2$-insulator with an odd number of Kramers' pairs crossing the Fermi energy. The spectrum is symmetric by reflection through the energy axis.

Figure 9.3: The characteristics of topological $\mathbb{Z}_2$-insulators include spin filtered pairs of chiral edge modes, figure (a) and Kramers' pairs crossing the Fermi energy, figure (b)-(c).

advantage that quantum computers bring over classical computations arise from the fact that a given state can also be in a superposition of these states $\alpha_+ |+\rangle + \alpha_- |-\rangle$. Essentially, this allows a quantum computer to solve many tasks at the same time and the computing power grows exponentially with the number of available qubits.

To compute something using qubits, they are transformed by unitary operations. This process may introduce errors. Furthermore, because it is not possible to completely isolate a quantum system, interactions with the environment may also give rise to errors. These errors are known as *quantum noise* or *quantum decoherence*, see [55]. Using topologically protected states, the hope is to achieve highly fault-tolerant quantum computations. One approach to fault-tolerant quantum computation is exploiting *Majorana zero modes*.

Another remarkable property of the edge modes that might have important consequences for transport physics is *ballistic transport*. For a particle occupying a state in the middle of the gap (an edge mode), see Figure 9.2 (b), there is simply no way for that particle to reverse its velocity. There are no states available for backscattering. This means that particles are free to move uninhibited at the boundary and this gives rise to, in theory, ballistic transport, meaning that there is no resistivity. However, an actual sample has finite temperature which allows for inelastic backscattering and therefore a finite conductivity is always measured.

9.3.1 Majorana Zero Modes

In 1937 Ettore Majorana [56] found real wave function solutions to the Dirac equation. These curious solutions, known as *Majorana fermions*, are unlike Dirac fermions, their own antiparticle

$$\gamma = \gamma^\dagger. \tag{9.10}$$

No known elementary particle has this property, with the exception of neutrinos which may fulfill the property. With c_i an ordinary Dirac fermion, the Majorana fermions can be written

$$\gamma_{2i-1} = c_i^\dagger + c_i, \quad \gamma_{2i} = i(c_i^\dagger + c_i)$$

and they obey

$$\{\gamma_i, \gamma_j^\dagger\} = 2\delta_{ij}. \tag{9.11}$$

Another object of fundamental research interest is the *Majorana zero mode* (MZM). In addition to Eqs. (9.10) and (9.11), MZMs obey

$$[\mathscr{H}, \gamma_i] = 0. \tag{9.12}$$

This means that their occurrence is followed by a ground state degeneracy. The groundstate, $|\psi_0\rangle$ obeys

$$\mathscr{H} |\psi_0\rangle = E_0 |\psi_0\rangle$$

and therefore the state $\gamma_i |\psi_0\rangle$ has the same energy

$$\mathscr{H}(\gamma_i |\psi_0\rangle) = \gamma_i(\mathscr{H} |\psi_0\rangle) = E_0(\gamma_i |\psi_0\rangle).$$

MZMs occur theoretically in topological phases of superconductors like the *one-dimensional p-wave superconductor* [57]. The Kitaev Hamiltonian that models such a system is

$$\mathscr{H} = -\mu \sum_{i=1}^{N} c_i^\dagger c_i - \sum_{i=1}^{N-1} (t c_i^\dagger c_{i+1} + \Delta e^{i\phi} c_i c_{i+1} + h.c.). \tag{9.13}$$

The model describes spinless fermions hopping to nearest neighbours on a one-dimensional, open chain. $\Delta e^{i\phi}$ is the p-wave pairing between adjacent sites [57]. The Dirac fermions can be written in terms of Majorana fermions

$$c_i = \frac{e^{-\phi/2}}{2}(\gamma_{i,A} + i\gamma_{i,B}).$$

The Majorana operators $\gamma_{i,A}$ and $\gamma_{i,B}$ are two different types of Majorana operators at lattice site i. The construction of two new Majorana operators at each lattice site is a mathematical trick motivated by the simplicity of the Hamiltonian Eq. (9.13) in the special case $\mu = 0,\ t = \Delta$ where it admits the form

$$\mathscr{H} = -it \sum_{i=1}^{N-1} \gamma_{i,A}\gamma_{i+1,B}. \tag{9.14}$$

The Hamiltonian can be written like this in the region $-2t < \mu < 2t$ [57], as long as the gap does not close. Clearly, $\gamma_{1,B}$ and $\gamma_{N,A}$ are not in the Hamiltonian and therefore they fulfill the MZM condition Eq. (9.12). They are the MZMs of the model and they are located at the opposite ends of the chain. Because the MZMs are not coupled to anything at all it follows that they have zero energy because a given Majorana fermion γ with energy E has a corresponding antiparticle $\gamma^\dagger = \gamma$ with energy $-E$. Because Majoranas are their own antiparticle $E = -E = 0$. The MZMs exist only in the region $-2t < \mu < 2t$ for the special case $\mu = 0,\ t = \Delta$ and disappear when the gap is closed. Therefore the number of MZMs is a topological invariant and this region in parameter space represents a topological phase.

A pair of MZMs, γ_1 and γ_2, can be used as a two level system because they can be used to write Dirac fermions [14] as

$$c = \frac{1}{2}(\gamma_1 + i\gamma_2), \quad c^\dagger = \frac{1}{2}(\gamma_1 - i\gamma_2)$$

which can be either occupied $(cc^\dagger = 1)$ or unoccupied $(cc^\dagger = 0)$. Interestingly, the MZMs can be arbitrarily far apart, meaning that they are stable against local perturbations. This can happen for a long chain, corresponding to a large N in Eq. (9.14).

Experimental confirmations of the existence of MZMs have not been unquestionably established due to a number of difficulties [14]. However, there are strong reasons to believe that they are there. As our knowledge of quantum systems increases and our ability to manipulate them becomes greater, MZMs provide a very promising approach to fault-tolerant quantum computations.

10 Conclusion

To properly conclude this review I would like to give a brief summary in which the various key topics of the review are pointed out and at the same time I present possible elaborations.

In this review I have defined what a topological phase is, how to characterize it and discussed the physical implications that it carries with. This has been done by rigorous derivations and the occasional example. The focus of this review has been on the physical interpretations but care has been taken to hint towards the underlying mathematics.

In Chapter 2 the discrete symmetries chiral symmetry, time reversal symmetry and particle-hole symmetry were presented. I introduced chiral symmetry in terms of non-bonded subsystems which provides a better intuition than how it is normally introduced, namely as a construction out of time reversal and particle-hole operators. Time reversal was introduces in the standard way along with Kramers' theorem. I instead constructed the particle-hole operator out of the other operations. Alternatively particle-hole symmetry could have been discussed in the context of the Bogoliubov–de Gennes Hamiltonian which would further establish its role as a particle-hole operator. The invariance relations for the Bloch Hamiltonian under the above-mentioned symmetries were established and various resulting spectra were examined in Chapter 3.

The concept of topological invariants and topological phases were introduced in a discussion on the SSH model in Chapter 3. The bulk-boundary correspondence came about from the equivalence of the winding number and the number of gapless edge modes (at one side of the chain), which was shown later in Chapter 9. The winding number of the SSH model was generalized in Chapter 4. I provided an alternative interpretation of the one-dimensional winding number in terms of poles and zeros. In three dimensions and in fact, in any odd dimension, there exist a very general expression for the winding number which is properly interpreted as the number of windings of the map from the Brillouin zone defined by the off-diagonal matrix of the flatband Hamiltonian. Although heavily mathematical it is a very powerful result which is outside the scope of an introductory text. The interested reader may refer to [34].

The geometrical phase known as the Berry phase was introduced in the classical sense in Chapter 5 and then interpreted physically as the sum of relative phases of neighbouring eigenstates along the path of deformation. I presented two example calculations of the Berry phase and discussed how it arises in physics for a two-band model, see Section 5.3, and via the Aharonov-Bohm effect, see Section 5.4. Going beyond this review would imply studying the holonomy interpretation and discuss the non-Abelian Berry phase that arises for degenerate systems, see [14].

Out of the Berry phase the Chern number is constructed in Chapter 6 simply by integrating over a closed surface in parameter space, or over all momenta. In this way the Chern number becomes immediately feasible to compute. To understand why it is quantized I presented two alternative interpretations, namely the gauge problem in Section 6.1.1 and enclosed effective magnetic monopoles as sources of Chern number in Section 6.1.2. The monopole method was exploited to find the Chern number for the QWZ model in Section 6.2. Yet a third way to understand the Chern number is in terms of the wrappings parameter space surface around the unit sphere [14]. This approach establishes the similarities between winding numbers and Chern numbers but is outside the scope of this review. Following the description of Chern number quantization I showed how the quantum Hall effect is connected to topology by deriving the Hall conductivity by means of the Kubo formula in Section 7.2 and the stability of the plateaux which was then showed to be a result of the impurities of the sample.

The Altland-Zirnbauer classification of Hamiltonians and the 10-fold way of topological matter was presented in Chapter 8 and the basic procedure for constructing the classification table was introduced. Although often looked up in tables, the relevant homotopy groups can be determined, see [15].

In Chapter 9 the $\mathbb{Z}_2$-invariant which arises in the spin quantum Hall effect is interpreted in terms of Kramers' edge pairs crossing the Fermi energy. I derived explicitly the existence of gapless edge modes of the

SSH model in the topological phase only. The bulk-boundary correspondence was discussed for $\mathbb{Z}$-insulators and $\mathbb{Z}_2$-insulators with time reversal symmetry in two dimensions for both cases. I give an intuitive way of understanding the bulk-boundary correspondence. With the bulk-boundary correspondence taken to hold I explain how the edge states remain robust as a consequence. To end the review, I presented in Section 9.3.1 a brief discussion about topological superconductors and Majorana zero modes and their potential applications in fault-tolerant quantum computations.

For anyone who wishes to continue beyond this review and learn more about the subject of topological phases of matter I could suggest studying the mathematics of topological spaces and differential geometry from the book ”Geometry, topology and physics” by Nakahara [15] and learning more about interacting systems from ”Introduction to topological quantum matter and quantum computation” by Stanescu [14] which presents the subject in the context of quantum computation theory.

A Symmetry Relations of the Hamiltonian Matrix in Position Space

Following the reasoning of Chiu *et al.* [18] the symmetry relations of the Hamiltonian matrix, H (in real space), is to be found from imposing that the symmetries are actual symmetries of the second quantized Hamiltonian, $\mathscr{H}$, meaning

$$[\mathscr{S}, \mathscr{H}] = [\mathscr{T}, \mathscr{H}] = [\mathscr{C}, \mathscr{H}] = 0.$$

For an operation, $\mathscr{U}$, to be regarded as a symmetry of a non-interacting, fermionic system, it must, commute with the Hamiltonian,

$$[\mathscr{H}, \mathscr{U}] = 0 \Leftrightarrow \mathscr{U}\mathscr{H}\mathscr{U}^{-1} = \mathscr{H} \tag{A.1}$$

and preserve the canonical (anti)commutation relation

$$\mathscr{U}\{c_i, c_j^\dagger\}\mathscr{U}^{-1} = \{c_i, c_j^\dagger\}.$$

The second quantized Hamiltonian is written in terms of the Hamiltonian matrix and creation and annihilation operators according to

$$\mathscr{H} = c_i^\dagger \mathcal{H}_{ij} c_j, \tag{A.2}$$

where repeated indices are summed. The operator c_i ($c_i^\dagger$) annihilates (creates) a fermion on lattice site i.

Time reversal symmetry, $\mathscr{T}$, is an antiunitary operation (like its matrix representation) which transforms the creation and annihilation operators according to

$$\mathscr{T} c_i \mathscr{T}^{-1} = \mathcal{T}_{ij} c_j, \quad \mathscr{T} c_i^\dagger \mathscr{T}^{-1} = c_j^\dagger (\mathcal{T}^\dagger)_{ji}, \tag{A.3}$$

where $\mathcal{T}$ is a unitary matrix. By antiunitary, time reversal switches the sign of complex numbers

$$\mathscr{T} i \mathscr{T}^{-1} = -i.$$

To find the effects of time reversal symmetry on the Hamiltonian matrix, evaluate $\mathscr{T}\mathscr{H}\mathscr{T}^{-1}$ and start by applying Eq. (A.2),

$$\mathscr{T}\mathscr{H}\mathscr{T}^{-1} = \mathscr{T} c_i^\dagger \mathcal{H}_{ij} c_j \mathscr{T}^{-1} = (\mathscr{T} c_i^\dagger \mathscr{T}^{-1})(\mathscr{T}\mathcal{H}_{ij}\mathscr{T}^{-1})(\mathscr{T} c_j \mathscr{T}^{-1}).$$

Apply Eq. (A.3) and remember that $\mathcal{H}_{ij}$ is a complex number

$$\mathscr{T}\mathscr{H}\mathscr{T}^{-1} = c_k^\dagger (\mathcal{T}^\dagger)_{ki} (\mathcal{H}^*)_{ij} \mathcal{T}_{jl} c_l.$$

With $\mathscr{T}$ a symmetry of the system, Eq. (A.1) holds, $\mathscr{T}\mathscr{H}\mathscr{T}^{-1} = \mathscr{H}$, implying

$$c_k^\dagger (\mathcal{T}^\dagger)_{ki} (\mathcal{H}^*)_{ij} \mathcal{T}_{jl} c_l = c_k^\dagger \mathcal{H}_{kl} c_l.$$

In matrix form

$$\mathcal{T}^\dagger \mathcal{H}^* \mathcal{T} = \mathcal{H}.$$

Therefore, the single-particle time reversal operator can be implemented by an antiunitary operator $T = \mathcal{T}K$, where K is the complex conjugator (see Section 2.2). It holds that

$$\boxed{T^{-1}\mathcal{H}T = \mathcal{H}.}$$

Time reversal remains a normal symmetry in the matrix representation and it remains antiunitary.

Particle-hole symmetry, $\mathscr{C}$, is a unitary operation (unlike in matrix form) which transforms the creation and annihilation operators according to

$$\mathscr{C} c_i \mathscr{C}^{-1} = (\mathcal{C}^*)_{ij} c_j^\dagger, \quad \mathscr{C} c_i^\dagger \mathscr{C}^{-1} = c_j (\mathcal{C}^T)_{ji}, \tag{A.4}$$

where $\mathcal{C}$ is a unitary matrix. Finding the effects of particle-hole symmetry on the Hamiltonian matrix is done by evaluating $\mathscr{C}\mathscr{H}\mathscr{C}^{-1}$,

$$\mathscr{C}\mathscr{H}\mathscr{C}^{-1} = \mathscr{C} c_i^\dagger \mathcal{H}_{ij} c_j \mathscr{C}^{-1} = (\mathscr{C} c_i^\dagger \mathscr{C}^{-1})(\mathscr{C}\mathcal{H}_{ij}\mathscr{C}^{-1})(\mathscr{C} c_j \mathscr{C}^{-1}) = c_k (\mathcal{C}^T)_{ki} \mathcal{H}_{ij} (\mathcal{C}^*)_{jl} c_l^\dagger.$$

Using the fundamental (anti)commutation relations $\{c_i, c_j^\dagger\} = \delta_{ij}$,

$$\mathscr{C}\mathscr{H}\mathscr{C}^{-1} = (\delta_{kl} - c_l^\dagger c_k)(\mathcal{C}^T)_{ki}\mathcal{H}_{ij}(\mathcal{C}^*)_{jl} = (\mathcal{C}^T)_{li}\mathcal{H}_{ij}(\mathcal{C}^*)_{jl} - c_l^\dagger (\mathcal{C}^T)_{ki}\mathcal{H}_{ij}(\mathcal{C}^*)_{jl} c_k. \tag{A.5}$$

The first term in Eq. (A.5) can be simplified

$$(\mathcal{C}^T)_{li}\mathcal{H}_{ij}(\mathcal{C}^*)_{jl} = (\mathcal{C})_{il}\mathcal{H}_{ij}(\mathcal{C}^\dagger)_{lj} = (\mathcal{C})_{il}(\mathcal{C}^\dagger)_{lj}\mathcal{H}_{ij},$$

by unitarity,

$$(\mathcal{C})_{il}(\mathcal{C}^\dagger)_{lj}\mathcal{H}_{ij} = \delta_{ij}\mathcal{H}_{ij} = \mathcal{H}_{ii} = \mathrm{Tr}\mathcal{H}.$$

Eq. (A.5) becomes

$$\mathscr{C}\mathscr{H}\mathscr{C}^{-1} = \mathrm{Tr}\mathcal{H} - c_l^\dagger (\mathcal{C}^T)_{ki}\mathcal{H}_{ij}(\mathcal{C}^*)_{jl} c_k = \mathrm{Tr}\mathcal{H} - c_l^\dagger (\mathcal{C}^*)_{jl}\mathcal{H}_{ij}(\mathcal{C}^T)_{ki} c_k = \mathrm{Tr}\mathcal{H} - c_l^\dagger (\mathcal{C}^\dagger)_{lj}(\mathcal{H}^T)_{ji}(\mathcal{C})_{ik} c_k.$$

With $\mathscr{C}$ a symmetry of the system, Eq. (A.1) holds, $\mathscr{C}\mathscr{H}\mathscr{C}^{-1} = \mathscr{H}$, implying

$$\mathrm{Tr}\mathcal{H} - c_l^\dagger (\mathcal{C}^\dagger)_{lj}(\mathcal{H}^T)_{ji}(\mathcal{C})_{ik} c_k = c_l^\dagger \mathcal{H}_{lk} c_k.$$

The trace of $\mathcal{H}$ is a constant with no creation or annihilation operator and must vanish for the equality to hold. Thus, by Hermicity of the Hamiltonian,

$$-c_l^\dagger (\mathcal{C}^\dagger)_{lj}(\mathcal{H}^*)_{ji}(\mathcal{C})_{ik} c_k = c_l^\dagger \mathcal{H}_{lk} c_k.$$

In matrix form this becomes

$$\mathcal{C}^\dagger \mathcal{H}^* \mathcal{C} = -\mathcal{H}.$$

Therefore, the single-particle particle-hole operator can be implemented by an antiunitary operator (unlike in second quantization) $C = \mathcal{C}K$. It holds that

$$\boxed{C^{-1}\mathcal{H}C = -\mathcal{H}.}$$

Particle-hole symmetry anticommutes with the Hamiltonian in matrix form and is described by an antiunitary operator, unlike in second quantization.

Chiral symmetry, $\mathscr{S}$, is a antiunitary operation (unlike in matrix representation). It inherits the antiunitary from the time reversal operator because the chiral operator is written $\mathscr{S} = \mathscr{T}\mathscr{C}$. The chiral operator transforms the creation and annihilation operators according to

$$\mathscr{S} c_i \mathscr{S}^{-1} = (\mathcal{S}^*)_{ij} c_j^\dagger, \quad \mathscr{S} c_i^\dagger \mathscr{S}^{-1} = c_j (\mathcal{S}^T)_{ji}, \tag{A.6}$$

where $\mathcal{S} = \mathcal{T}^*\mathcal{S}^*$ is a unitary matrix. Once more, consider $\mathscr{S}\mathscr{H}\mathscr{S}^{-1}$,

$$\mathscr{S}\mathscr{H}\mathscr{S}^{-1} = \mathscr{S} c_i^\dagger \mathcal{H}_{ij} c_j \mathscr{S}^{-1} = (\mathscr{S} c_i^\dagger \mathscr{S}^{-1})(\mathscr{S}\mathcal{H}_{ij}\mathscr{S}^{-1})(\mathscr{S} c_j \mathscr{S}^{-1}) = c_k (\mathcal{S}^T)_{ki}(\mathcal{H}^*)_{ij}(\mathcal{S}^*)_{jl} c_l^\dagger.$$

Using the fundamental (anti)commutation relations

$$\mathscr{S}\mathscr{H}\mathscr{S}^{-1} = (\delta_{kl} - c_l^\dagger c_k)(\mathcal{S}^T)_{ki}(\mathcal{H}^*)_{ij}(\mathcal{S}^*)_{jl}.$$

In exact analogy with particle-hole symmetry, the first term becomes $\mathrm{Tr}\mathcal{H}$, meaning that Eq. (A.6) simplifies to

$$\mathscr{S}\mathscr{H}\mathscr{S}^{-1} = \mathrm{Tr}\mathcal{H} - c_l^\dagger(\mathcal{S}^T)_{ki}(\mathcal{H}^*)_{ij}(\mathcal{S}^*)_{jl}c_k = \mathrm{Tr}\mathcal{H} - c_l^\dagger(\mathcal{S}^*)_{jl}(\mathcal{H}^*)_{ij}(\mathcal{S}^T)_{ki}c_k =$$
$$= \mathrm{Tr}\mathcal{H} - c_l^\dagger(\mathcal{S}^\dagger)_{lj}(\mathcal{H}^\dagger)_{ji}(\mathcal{S})_{ik}c_k.$$

By Hermicity of the Hamiltonian,

$$\mathscr{S}\mathscr{H}\mathscr{S}^{-1} = \mathrm{Tr}\mathcal{H} - c_l^\dagger(\mathcal{S}^\dagger)_{lj}\mathcal{H}_{ji}(\mathcal{S})_{ik}c_k$$

With $\mathscr{S}$ a symmetry of the system, Eq. (A.1) holds, $\mathscr{S}\mathscr{H}\mathscr{S}^{-1} = \mathscr{H}$, implying

$$\mathrm{Tr}\mathcal{H} - c_l^\dagger(\mathcal{S}^\dagger)_{lj}\mathcal{H}_{ji}\mathcal{S}_{ik}c_k = c_l^\dagger\mathcal{H}_{lk}c_k.$$

The trace of the Hamiltonian vanishes as per the same arguments used before,

$$-c_l^\dagger(\mathcal{S}^\dagger)_{lj}\mathcal{H}_{ji}\mathcal{S}_{ik}c_k = c_l^\dagger\mathcal{H}_{lk}c_k.$$

In matrix form this becomes

$$\mathcal{S}^\dagger\mathcal{H}\mathcal{S} = -\mathcal{H}.$$

Therefore, the single-particle chiral operator can be implemented by a unitary operator (unlike in second quantization) $S = \mathcal{S}$. It holds that

$$\boxed{S^{-1}\mathcal{H}S = -\mathcal{H}.}$$

To summarize, it has been shown that the three discrete symmetry operators $\mathscr{T}$ (antiunitary), $\mathscr{C}$ (unitary) and $\mathscr{S}$ (unitary), which commute with a second quantized Hamiltonian, are realized as T (antiunitary and commuting), C (antiunitary and anticommuting) and S (unitary and anticommuting) operators in matrix representation, respectively.

In the paper by Chiu *et al.* [18] it is stated that one can Fourier transform Eq.(A.2) and show that the following invariance relations hold for the Hamiltonian matrices in momentum space

$$T\mathcal{H}(k)T^{-1} = \mathcal{H}(-k), \tag{A.7a}$$
$$C\mathcal{H}(k)C^{-1} = -\mathcal{H}(-k), \tag{A.7b}$$
$$S\mathcal{H}(k)S^{-1} = -\mathcal{H}(k). \tag{A.7c}$$

This is proven in the main text in braket notation in order to better introduce the physical properties of T, C and S.

B Differential Forms

This section follows Kurt Bryan [58] and it is here to familiarize the reader with differential forms and to demonstrate how to integrate them. In general, differential forms allow for a coordinate free way to compute integrals and derivatives. The method is coordinate free in the sense that no metric needs to be defined. Instead, knowledge about the manifold that is being integrated is needed. Ultimately, the goal is to provide enough understanding such that expressions like

$$\gamma_L(t) = \frac{1}{2}\oint_S dR^\mu \wedge dR^\nu \mathbf{\Omega}_{\mu\nu}(\mathbf{R}) \tag{B.1}$$

can be integrated. Note that this is not a complete introduction. Only one example will be given and a reader encountering these objects for the first time might need more examples. For a more complete introduction, see [58].

A *zero-form* is merely a function, which everyone is familiar with. The simplest *one-form* is $\omega^{(1)} = dx_i$. The most general one-form is

$$\omega^{(1)} = F_1(\mathbf{x})dx_1 + F_2(\mathbf{x})dx_2 + \ldots + F_n(\mathbf{x})dx_n, \quad \mathbf{x} \in \mathbb{R}^n = (x_1, x_2 \ldots x_n).$$

Any form, is said to "act" on vectors [58]. In particular, a general one-form acts on one input vector according to

$$\omega^{(1)}(\mathbf{v}) = F_1(\mathbf{x})v_1 + F_2(\mathbf{x})v_2 + \ldots + F_n(\mathbf{x})v_n. \tag{B.2}$$

Equation Eq. (B.1) is an example of a *two-from*. The simplest two-form is given by $\omega^{(2)} = dx_i \wedge dx_j$. The operation $\wedge$ is known as the *wedge product* or *exterior product*. It is known as an antisymmetric tensor product [14]. It has the property

$$dx_i \wedge dx_j = dx_i \otimes dx_j - dx_j \otimes dx_i = -dx_j \wedge dx_i.$$

And as a trivial result

$$dx_i \wedge dx_i = 0.$$

A two-form acts on two input vectors. the simplest two-form acts on two vectors according to

$$\omega^{(2)}(\mathbf{v}_1, \mathbf{v}_2) = dx_i \wedge dx_j(\mathbf{v}_1, \mathbf{v}_2) = \det \begin{pmatrix} dx_i(\mathbf{v}_1) & dx_i(\mathbf{v}_2) \\ dx_j(\mathbf{v}_1) & dx_j(\mathbf{v}_2) \end{pmatrix}.$$

The most general two-form is

$$\omega^{(2)} = \sum_{1 \le i < j \le n} F_{ij}(\mathbf{x}) dx_i \wedge dx_j.$$

Note that the sum can be taken such that $i < j$ because whenever $i > j$, that contribution can be defined into the term $i \leftrightarrow j$ with a minus sign because $dx_i \wedge dx_j = -dx_j \wedge dx_i$. A general two-form acts on two input vectors according to

$$\begin{aligned} \omega^{(2)}(\mathbf{v}_1, \mathbf{v}_2) &= \sum_{1 \le i < j \le n} F_{ij}(\mathbf{x}) dx_i \wedge dx_j(\mathbf{v}_1, \mathbf{v}_2) = \\ &= \sum_{i,j>i} F_{ij}(\mathbf{x}) \det \begin{pmatrix} dx_i(\mathbf{v}_1) & dx_i(\mathbf{v}_2) \\ dx_j(\mathbf{v}_1) & dx_j(\mathbf{v}_2) \end{pmatrix}. \end{aligned} \tag{B.3}$$

The matrix consists of very simple one-forms. Such one-forms act on one vector and takes out one component of them

$$dx_i(\mathbf{v}) = v_i.$$

Now that differential forms are better understood, it is time to show what it means to integrate them.

B.1 Integrating Differential Forms

Take the example of the one-form $\omega^{(1)} = F_1(\mathbf{x})dx_1 + F_2(\mathbf{x})dx_2 + \ldots + F_n(\mathbf{x})dx_n$. It is to be integrated over a one-dimensional manifold that is embedded into n dimensions. The manifold M, is parameterized by $\mathbf{X}(t) = (x_1(t), x_2(t) \ldots x_n(t))$ and $t \in [a, b]$. The integral of this one-form over the manifold M is given by

$$\int_M \omega^{(1)} = \int_a^b \big(F_1(\mathbf{x})dx_1 + F_2(\mathbf{x})dx_2 + \ldots + F_n(\mathbf{x})dx_n\big)\big(\mathbf{X}'(t)\big)dt. \tag{B.4}$$

There is an important lesson here. *When integrating differential forms, they "act" on the derivative of the vectors that parameterize the manifold.* That is, in Eq. (B.1) the two-form acts on the derivatives of the vectors that parameterize the surface S. Furthermore, because differential forms in integrals always act on vectors which are defined from the manifold being integrated over, the integrals are often written with a suppressed notation

$$\int_M \big(F_1(\mathbf{x})dx_1 + F_2(\mathbf{x})dx_2 + \ldots + F_n(\mathbf{x})dx_n\big). \tag{B.5}$$

Everything in equation Eq. (B.4) can be inferred from Eq. (B.5) by knowledge of the manifold. This is why the hern number can be written in the simple way in the simple way of Eq. (6.2). A one-form acts on vectors according to Eq. (B.2), such that the integral becomes

$$\int_M \omega^{(1)} = \int_a^b \big(F_1(\mathbf{x})\frac{\partial x_1}{\partial t} + F_2(\mathbf{x})\frac{\partial x_2}{\partial t} + \ldots + F_n(\mathbf{x})\frac{\partial x_n}{\partial t}\big)dt.$$

This is integrable using ordinary calculus and this was the goal of this section. To be able to understand what it means to integrate differential forms.

Note that all of these notions can be extended to any dimension k by discussing *k-forms*.

B.2 Example Calculation

As a last example, consider the two dimensional manifold, M, parameterized by

$$\mathbf{X}(\mathbf{u}) = (u_1, u_1 - u_2, 3 - u_1 + u_1u_2, -3u - 2), \quad u_1^2 + u_2^2 < 1.$$

Here $\mathbf{u} = (u_1, u_2) \in D$ where D is a region in $\mathbb{R}^2$ and the manifold is embedded in $\mathbb{R}^4$. Note that now the manifold is two dimensional such that two variables are needed to describe it. The two-form to be integrated is

$$\omega^{(2)} = x_2dx_1 \wedge dx_3 - x_4dx_3 \wedge dx_4. \tag{B.6}$$

The integral is again defined such that the form acts on the derivative of the vectors that parameterize the manifold

$$\int_M \omega^{(2)} = \int_D \omega^{(2)}\big((\frac{\partial \mathbf{X}}{\partial u_1}, \frac{\partial \mathbf{X}}{\partial u_2})\big)du_1du_2 =$$

$$= \int_D (x_2dx_1 \wedge dx_3 - x_4dx_3 \wedge dx_4)\big((\frac{\partial \mathbf{X}}{\partial u_1}, \frac{\partial \mathbf{X}}{\partial u_2})\big)du_1du_2.$$

The two derivatives become

$$\frac{\partial \mathbf{X}}{\partial u_1} = (1, 1, u_2 - 1, 0), \quad \frac{\partial \mathbf{X}}{\partial u_2} = (0, -1, u_1, -3).$$

The two-form Eq. (B.6) acts on these vectors according to Eq. (B.3),

$$\omega^{(2)}\big(\frac{\partial \mathbf{X}}{\partial u_1},\frac{\partial \mathbf{X}}{\partial u_2}\big)=\sum_{i,j>i}F_{ij}(\mathbf{x})\text{det}\begin{pmatrix} dx_i(\frac{\partial \mathbf{X}}{\partial u_1}) & dx_i(\frac{\partial \mathbf{X}}{\partial u_2}) \\ dx_j(\frac{\partial \mathbf{X}}{\partial u_1}) & dx_j(\frac{\partial \mathbf{X}}{\partial u_2})\end{pmatrix}.$$

In this particular example, the function $F_{ij}(\mathbf{x})$ which characterizes the two-form is given by

$$F_{ij}(\mathbf{x})=\begin{cases}0 & ij\neq 13 \text{ or } 34\\ x_2 & ij=13\\ -x_4 & ij=34\end{cases}.$$

Consequently

$$\omega^{(2)}\big(\frac{\partial \mathbf{X}}{\partial u_1},\frac{\partial \mathbf{X}}{\partial u_2}\big)=x_2\text{det}\begin{pmatrix} dx_1(\frac{\partial \mathbf{X}}{\partial u_1}) & dx_1(\frac{\partial \mathbf{X}}{\partial u_2}) \\ dx_3(\frac{\partial \mathbf{X}}{\partial u_1}) & dx_3(\frac{\partial \mathbf{X}}{\partial u_2})\end{pmatrix}-x_4\text{det}\begin{pmatrix} dx_3(\frac{\partial \mathbf{X}}{\partial u_1}) & dx_3(\frac{\partial \mathbf{X}}{\partial u_2}) \\ dx_4(\frac{\partial \mathbf{X}}{\partial u_1}) & dx_4(\frac{\partial \mathbf{X}}{\partial u_2})\end{pmatrix}=$$

$$=x_2\text{det}\begin{pmatrix}1 & 0\\ u_2-1 & u_1\end{pmatrix}-x_4\text{det}\begin{pmatrix}u_2-1 & u_1\\ 0 & -3\end{pmatrix}=u_1^2-u_1u_2-9u_2^2+9u_2.$$

The integral becomes

$$\int_D\big(u_1^2-u_1u_2-9u_2^2+9u_2\big)du_1du_2=$$

$$=\int_{-1}^{1}\int_{-\sqrt{1-u_1^2}}^{\sqrt{1-u_1^2}}(u_1^2-u_1u_2-9u_2^2+9u_2)du_1du_2=-2\pi.$$

C Characterizing Topological Phases of Interacting Models

The 10-fold way of non-interacting systems (Chapter 8) is based on the homotopy groups of the Q-matrix which is uniquely defined by the Bloch Hamiltonian. Clearly it becomes impossible to define a Bloch Hamiltonian that characterizes the whole system due to the appearance of four operators in the two-body processes of an interacting Hamiltonian

$$\mathscr{H} = \sum_{i,j} a_i^j c_i^\dagger c_j + \sum_{i,j,k,l} b_{i,j}^{k,l} c_i^\dagger c_j^\dagger c_k c_l.$$

Although there exists no general classification of topological phases of interacting systems some progress has been made with methods of tensor categories [59] and group cohomology theory [60]. For the rest of the review the focus has been on symmetry protected topological phases. Symmetry protection holds for some interacting systems as well, however other systems require the concept of *quantum entanglement* to be topologically classified. That is, even without symmetry constraints there exists topologically distinct phases. The phases exhibit what is called *topological order*.

There are different methods of approaching entanglement within a system [61]. Here a short introduction to one such approach, based on topological *entanglement entropy* [62] is given. The goal is to determine the degree of entanglement within a system. Formally, an entangled state is a state which can not be written as a product of one-particle states. As an example

$$\frac{1}{\sqrt{2}}(|+,-\rangle + |-,+\rangle)$$

does not admit the form $|\alpha\rangle \otimes |\beta\rangle$ and is therefore an entangled state.

To understand entanglement entropy, consider an arbitrary partitioning of a system, in real space, into two subsystems A and B. The density operator of the pure ground state $|\Psi\rangle$ is

$$\rho = |\Psi\rangle \langle\Psi| .$$

Taking the partial trace over the B subsystem defines the operator

$$\rho_A = \mathrm{Tr}_B |\Psi\rangle \langle\Psi| . \tag{C.1}$$

As an example, consider the entangled state

$$|\Psi\rangle = |+_1,+_2\rangle + |+_1,-_2\rangle + |-_1,+_2\rangle + |-_1,-_2\rangle .$$

The index labels particle one or two which can have either spin up $(+)$ or down $(-)$. If the two subsystems is defined by two different particles, then the partially traced density operator Eq. (C.1) becomes

$$\begin{aligned}
\mathrm{Tr}_B |\Psi\rangle \langle\Psi| &= \mathrm{Tr}_B\big(|+_1,+_2\rangle \langle+_1,+_2| + |+_1,+_2\rangle \langle+_1,-_2| + \dots \big) = \\
&= \mathrm{Tr}_B\big(|+_1\rangle \langle+_1| \otimes |+_2\rangle \langle+_2| + |+_1\rangle \langle+_1| \otimes |+_2\rangle \langle-_2| + \dots \big) = \\
&= \sum_{\sigma\in\{+,-\}} \big(|+_1\rangle \langle+_1| \otimes \langle\sigma| \left(|+_2\rangle \langle+_2|\right) |\sigma\rangle + |+_1\rangle \langle+_1| \otimes \langle\sigma| \left(|+_2\rangle \langle-_2|\right) |\sigma\rangle + \dots \big) = \\
&= 2\big(|+_1\rangle \langle+_1| + |+_1\rangle \langle-_1| + |-_1\rangle \langle+_1| + |-_1\rangle \langle-_1| \big).
\end{aligned}$$

For a more general partitioning of the system, the *von Neumann entropy* S is given by

$$S = -\mathrm{Tr}_A(\rho_A \log \rho_A).$$

It has the form [62]

$$S = \alpha L - \gamma + \mathcal{O}(L^{-1})$$

where L is the length of the boundary that separates the systems, α is a constant and γ is the *topological entanglement entropy*. γ is a constant which is independent of the specifics of how the two subsystems were defined and therefore it is a topological property of the system. When $\gamma \neq 0$ the system exhibits *long-range entanglement*. Long-range entangled states are said to be *topologically ordered*. Topologically ordered states are characterized by different topological invariants from those of the main text. Examples include the entanglement entropy and the ground state degeneracy for systems defined on topologically non-trivial manifolds [14]. Two well-known systems which exhibit topological order are the Toric code and the fractional quantum Hall liquid [14].

For further developments regarding topologically non-trivial interacting systems see [63, 64, 65].

References

[1] K v Klitzing, Gerhard Dorda, and Michael Pepper. "New method for high-accuracy determination of the fine-structure constant based on quantized Hall resistance". In: *Physical Review Letters* 45.6 (1980), p. 494.

[2] Klaus von Klitzing. "Developments in the quantum Hall effect". In: *Philosophical Transactions of the Royal Society of London A: Mathematical, Physical and Engineering Sciences* 363.1834 (2005), pp. 2203–2219.

[3] Tsuneya Ando and Yasutada Uemura. "Theory of quantum transport in a two-dimensional electron system under magnetic fields. I. Characteristics of level broadening and transport under strong fields". In: *Journal of the Physical Society of Japan* 36.4 (1974), pp. 959–967.

[4] Bertrand I Halperin. "Quantized Hall conductance, current-carrying edge states, and the existence of extended states in a two-dimensional disordered potential". In: *Physical Review B* 25.4 (1982), p. 2185.

[5] Nobelprize.org. Nobel Media AB 2014. *The Nobel Prize in Physics 2016 - Scientific background: Topological phase transitions and topological phases of matter.* 2016. URL: https://www.nobelprize.org/nobel_prizes/physics/laureates/2016/advanced.html (visited on 04/02/2018).

[6] Charles L Kane and Eugene J Mele. "Z 2 topological order and the quantum spin Hall effect". In: *Physical review letters* 95.14 (2005), p. 146802.

[7] Charles L Kane and Eugene J Mele. "Quantum spin Hall effect in graphene". In: *Physical review letters* 95.22 (2005), p. 226801.

[8] B Andrei Bernevig, Taylor L Hughes, and Shou-Cheng Zhang. "Quantum spin Hall effect and topological phase transition in HgTe quantum wells". In: *Science* 314.5806 (2006), pp. 1757–1761.

[9] Markus König et al. "Quantum spin Hall insulator state in HgTe quantum wells". In: *Science* 318.5851 (2007), pp. 766–770.

[10] Liang Fu and Charles L Kane. "Topological insulators with inversion symmetry". In: *Physical Review B* 76.4 (2007), p. 045302.

[11] David Hsieh et al. "A topological Dirac insulator in a quantum spin Hall phase". In: *Nature* 452.7190 (2008), p. 970.

[12] Nicholas Read and Dmitry Green. "Paired states of fermions in two dimensions with breaking of parity and time-reversal symmetries and the fractional quantum Hall effect". In: *Physical Review B* 61.15 (2000), p. 10267.

[13] A Yu Kitaev. "Unpaired Majorana fermions in quantum wires". In: *Physics-Uspekhi* 44.10S (2001), p. 131.

[14] Tudor D Stanescu. *Introduction to Topological Quantum Matter & Quantum Computation*. CRC Press, 2016.

[15] Mikio Nakahara. *Geometry, topology and physics*. CRC Press, 2003.

[16] Mark Anthony Armstrong. *Basic topology*. Springer Science & Business Media, 2013.

[17] Shinsei Ryu et al. "Topological insulators and superconductors: tenfold way and dimensional hierarchy". In: *New Journal of Physics* 12.6 (2010), p. 065010.

[18] Ching-Kai Chiu et al. "Classification of topological quantum matter with symmetries". In: *Reviews of Modern Physics* 88.3 (2016), p. 035005.

[19] János K Asbóth, László Oroszlány, and András Pályi. "A Short Course on Topological Insulators". In: *Lecture Notes in Physics* 919 (2016).

[20] Bryan W Roberts. "Three myths about time reversal in quantum theory". In: *Philosophy of Science* 84.2 (2017), pp. 315–334.

[21] R Simon et al. "Two elementary proofs of the Wigner theorem on symmetry in quantum mechanics". In: *Physics Letters A* 372.46 (2008), pp. 6847–6852.

[22] B Andrei Bernevig and Taylor L Hughes. *Topological insulators and topological superconductors*. Princeton university press, 2013.

[23] Andrei Bernevig and Titus Neupert. "Topological superconductors and category theory". In: *Topological Aspects of Condensed Matter Physics: Lecture Notes of the Les Houches Summer School: Volume 103, August 2014* 103 (2017), p. 63.

[24] Immanuel Bloch. "Ultracold quantum gases in optical lattices". In: *Nature Physics* 1.1 (2005), p. 23.

[25] Charles Kittel, Paul McEuen, and Paul McEuen. *Introduction to solid state physics*. Vol. 8. Wiley New York, 1996.

[26] Bo-Hung Chen and Dah-Wei Chiou. "A detailed proof of bulk-boundary correspondence in the generalized Su-Schrieffer-Heeger model". In: *arXiv preprint arXiv:1705.06913* (2017).

[27] M Zahid Hasan and Charles L Kane. "Colloquium: topological insulators". In: *Reviews of Modern Physics* 82.4 (2010), p. 3045.

[28] Jun-Won Rhim, Jens H Bardarson, and Robert-Jan Slager. "Unified bulk-boundary correspondence for band insulators". In: *Physical Review B* 97.11 (2018), p. 115143.

[29] Andrew M Essin and Victor Gurarie. "Bulk-boundary correspondence of topological insulators from their respective Green's functions". In: *Physical Review B* 84.12 (2011), p. 125132.

[30] Margaret McIntyre and Grant Cairns. "A new formula for winding number". In: *Geometriae Dedicata* 46.2 (1993), pp. 149–159.

[31] TO Puel, PD Sacramento, and MA Continentino. "Effect of hybridization symmetry on topological phases of odd-parity multiband superconductors". In: *arXiv preprint arXiv:1601.07609* (2016).

[32] Rolf Nevanlinna and Veikko Paatero. "Introduction to complex analysis". In: (1969).

[33] George B Arfken, Hans J Weber, and Frank E Harris. *Mathematical methods for physicists: a comprehensive guide*. Academic press, 2011.

[34] Andreas P Schnyder et al. "Classification of topological insulators and superconductors in three spatial dimensions". In: *Physical Review B* 78.19 (2008), p. 195125.

[35] David J Griffiths. *Introduction to quantum mechanics*. Cambridge University Press, 2016.

[36] Jan Carl Budich and Björn Trauzettel. "From the adiabatic theorem of quantum mechanics to topological states of matter". In: *physica status solidi (RRL)-Rapid Research Letters* 7.1-2 (2013), pp. 109–129.

[37] Michael V Berry. "Quantal phase factors accompanying adiabatic changes". In: *Proceedings of the Royal Society of London. A. Mathematical and Physical Sciences* 392.1802 (1984), pp. 45–57.

[38] Barry Simon. "Holonomy, the quantum adiabatic theorem, and Berry's phase". In: *Physical Review Letters* 51.24 (1983), p. 2167.

[39] Yvonne Choquet-Bruhat, Cécile DeWitt-Morette, and Margaret Dillard-Bleick. *Analysis, manifolds, and physics*. Gulf Professional Publishing, 1982.

[40] Jun John Sakurai and Jim Napolitano. *Modern quantum mechanics*. Cambridge University Press, 2017.

[41] Akira Tonomura et al. "Observation of Aharonov-Bohm effect by electron holography". In: *Physical Review Letters* 48.21 (1982), p. 1443.

[42] J Zak. "Berry's phase for energy bands in solids". In: *Physical review letters* 62.23 (1989), p. 2747.

[43] David Tong. "Lectures on the quantum Hall effect". In: *arXiv preprint arXiv:1606.06687* (2016).

[44] David Tong. "Lectures on kinetic theory". In: *Lecture notes available at http://www. damtp. cam. ac. uk/user/tong/kinetic. html* (2012).

[45] Jainendra K Jain. *Composite fermions*. Cambridge University Press, 2007.

[46] Robert B Laughlin. "Quantized Hall conductivity in two dimensions". In: *Physical Review B* 23.10 (1981), p. 5632.

[47] CL Kane and Chapter Outline Head. "Topological Band Theory and the Z2 invariant". In: *Topological Insulators* 6 (2013), p. 1.

[48] Alexander Altland and Martin R Zirnbauer. "Nonstandard symmetry classes in mesoscopic normal-superconducting hybrid structures". In: *Physical Review B* 55.2 (1997), p. 1142.

[49] Alexei Kitaev. "Periodic table for topological insulators and superconductors". In: *AIP Conference Proceedings*. Vol. 1134. 1. AIP. 2009, pp. 22–30.

[50] Jan Carl Budich and Eddy Ardonne. "Equivalent topological invariants for one-dimensional Majorana wires in symmetry class D". In: *Physical Review B* 88.7 (2013), p. 075419.

[51] Takahiro Fukui et al. "Bulk-edge correspondence for Chern topological phases: A viewpoint from a generalized index theorem". In: *Journal of the Physical Society of Japan* 81.11 (2012), p. 114602.

[52] Roger SK Mong and Vasudha Shivamoggi. "Edge states and the bulk-boundary correspondence in Dirac Hamiltonians". In: *Physical Review B* 83.12 (2011), p. 125109.

[53] Emil Prodan and Hermann Schulz-Baldes. "Bulk and boundary invariants for complex topological insulators". In: *K* (2016).

[54] Anders Ström. *Interaction and disorder in helical conductors*. 2012.

[55] Michael A Nielsen and Isaac L Chuang. *Quantum computation and quantum information*. Cambridge university press, 2010.

[56] Ettore Majorana. "Teoria simmetrica dell'elettrone e del positrone". In: *Il Nuovo Cimento (1924-1942)* 14.4 (1937), p. 171.

[57] Hoi Yin Hui. "Majorana zero modes in solid state systems". PhD thesis. University of Maryland, College Park, 2015.

[58] Kurt Bryan. "Differential Forms". In: *Lecture notes, MA 305* (2016).

[59] Vladimir G Turaev. *Quantum invariants of knots and 3-manifolds*. Vol. 18. Walter de Gruyter GmbH & Co KG, 2016.

[60] Xie Chen et al. "Symmetry protected topological orders and the group cohomology of their symmetry group". In: *Physical Review B* 87.15 (2013), p. 155114.

[61] Ryszard Horodecki et al. "Quantum entanglement". In: *Reviews of modern physics* 81.2 (2009), p. 865.

[62] Alexei Kitaev and John Preskill. "Topological entanglement entropy". In: *Physical review letters* 96.11 (2006), p. 110404.

[63] Bei Zeng et al. "Quantum Information Meets Quantum Matter–From Quantum Entanglement to Topological Phase in Many-Body Systems". In: *arXiv preprint arXiv:1508.02595* (2015).

[64] Eduardo Fradkin. *Field theories of condensed matter physics*. Cambridge University Press, 2013.

[65] Shinsei Ryu. “Interacting topological phases and quantum anomalies”. In: *Physica Scripta* 2015.T164 (2015), p. 014009.